Thesis

Coherence of single and many-particle states in mesoscopic systems

HAACK, Géraldine

Abstract

Cette thèse est consacrée à l'étude des propriétés de cohérence d'états à électron unique ou à plusieurs électrons dans des systèmes mésoscopiques. Nous avons tout d'abord utiliser les propriétés de cohérence d'électrons émis par une source dc pour proposer une mesure de parité à l'aide d'un interféromètre de Mach-Zehnder qui crée de l'intrication entre deux qubits. Nous nous sommes ensuite intéressés aux électrons émis par une source qui permet d'injecter des états à particule unique de manière quasi-déterministe. Nous avons caractérisé leurs propriétés de cohérence à l'aide de leur fonction de corrélation au 1er ordre, dérivée à partir de la matrice de diffusion de la source. Enfin, nous avons développé une théorie quantique de la distribution des temps d'attente entre deux électrons consécutifs dans un conducteur mésoscopique. Contrairement à la mesure des fluctuations du courant moyen à travers un canal quantique parfait, cela a permis de mettre en évidence, entre autres, le fait que les électrons ne sont pas séparés en temps de manière uniforme du fait des [...]

UNIVERSITÉ DE GENÈVE
Département de physique théorique

FACULTÉ DES SCIENCES
Professeur M. Büttiker

Coherence of single and many-particle states in mesoscopic systems

THÈSE

présentée à la Faculté des Sciences de l'Université de Genève
pour obtenir le grade de Docteur ès sciences, mention physique

par

Géraldine Haack

Née à Cannes, France

Thèse N° 4434

GENÈVE
Atelier de reproduction de la Section de physique
2012

Soutenue le 15 juin 2012 devant le jury composé de :

M. Piet W. Brouwer	Examinateur
M. Markus Büttiker	Directeur de thèse
M. Christian Glattli	Examinateur
M. Atac Imamoglu	Examinateur
M. Michael V. Moskalets	Examinateur
M. Eugene Sukhorukov	Examinateur

Remerciements

Mes remerciements vont en tout premier lieu à Markus Büttiker qui m'a guidé et accompagné pendant ces quatre années d'apprentissage du métier de chercheur. Je le remercie pour sa grande disponibilité ainsi que pour sa patience à faire partager ses grandes connaissances et son intuition dans de multiples domaines de la physique. Je voudrais tout particulièrement souligner l'attention qu'il a toujours portée à la formulation des problèmes rencontrés ainsi qu'à mes interrogations lors de nos diverses discussions. Cela m'a permis de découvrir et de me familiariser petit à petit avec le monde passionnant de la physique mésoscopique. Tout en m'ayant laissé une grande liberté, ce qui m'a valu de longs mois laborieux surtout en début de thèse, il a su me réorienter sur les bonnes questions à des moments décisifs. Avec maintenant plus de recul, je peux mesurer toute la confiance qu'il m'a accordée. J'ai ainsi pu consacrer du temps à des questions qui me tenaient à coeur, ce qui a, pour ma part, beaucoup contribué à développer mon esprit critique quant à différents sujets de recherche et à me donner envie de poursuivre dans la filière académique. Je le remercie énormément pour tout cela.

Le plaisir que j'ai eu à faire partie du groupe de Markus pendant quatre années réside également dans les nombreux moments passés avec les différents membres de l'équipe, que ce soit au coffee break (rituel auquel l'on ne peut pas et ensuite auquel l'on ne veut plus se soustraire), à la délicieuse cafet de Sciences II ou encore à l'Echalotte. Pour tous les bons moments, je voudrais ici remercier, dans l'ordre chronologique de départ du groupe, Janine Splettstoesser, Mathias Lunde, Simon Nigg, Geneviève Fleury, Rafael Sanchez, Mathias Albert et ceux qui sont encore présents, Jian Li, Christian Flindt, Dania Kambly, Pierre Delpace, Konrad Müller et Bjorn Sötheman. Pour toutes les discussions qui permettent de satisfaire, tout en la maintenant, une curiosité pour des questions allant de l'électrodynamique aux fonctions de Wannier, de la condensation de Bose-Einstein à la Full Counting Statistics, et des quantum dots aux matrices aléatoires, je voudrais en particulier remercier Simon Nigg, Pierre Delplace, Mathias Albert, Christian Flindt et Rafael Sanchez. Ces moments sont extrêmement importants pour moi et ont contribué à ma décision de continuer dans la recherche en soutenant ma motivation dans les moments difficiles. Un grand merci à vous tous.

Un merci tout particulier va à Michael Moskalets qui a joué un grand rôle tout

au long de cette thèse. J'ai eu la chance de pouvoir travailler avec lui directement, et je voudrais le remercier pour sa constante présence pour discuter et répondre à mes multiples questions. Même loin, Misha s'est toujours rendu disponible (en des temps records !) pour discuter de physique et cela a été un immense plaisir et privilège que de l'avoir comme collaborateur. Diakuiu !

De manière plus générale, je tiens à remercier l'ensemble du département de physique de l'Université de Genève pour sa bonne et chaleureuse ambiance. En particulier, je remercie Francine Gennai-Nicole et Cécile Jaggi pour leur bonne humeur et leur prompt dévouement à nous faciliter constamment les démarches administratives, ainsi que Eugene Sukhorukov, Philippe Jacquod, Corinna Kollath, Alberto Morpurgo et Martin Kunz, avec qui j'ai eu le plaisir de partager diverses discussions ou de travailler à travers les tâches d'assistanat. Je tiens enfin à remercier Marc Vonlanthen, mon compagnon de bureau pendant 4 années et ami.

Je remercie également Piet W. Brouwer, Christian Glattli, Atac Imamoglu, Michael V. Moskalets et Eugene Sukhorukov, qui ont tous accepté spontanément de faire parti de mon jury de thèse. Je les remercie de l'intérêt qu'ils ont porté à mon travail et des discussions qui s'en sont suivies. Pour la (les) relecture(s) du manuscrit et leurs précieuses remarques, je tiens à remercier tout spécialement Mathias, Pierre, Christian, Misha, Markus et Augustin.

Finalement, je tiens à remercier les nombreux membres de ma famille et belle-famille ainsi que mes amis qui ont accepté d'assister à ma soutenance. Je remercie en particulier mes grands-parents ainsi que ma grande-tante Friderun de faire le déplacement. C'est un grand plaisir que de vous avoir tous à mes côtés pour clôturer ces années de labeur. Je tiens aussi à remercier mes parents pour leur soutien et leur intérêt pour un domaine et une filière qui leur étaient (au passé !) étrangers. Un merci tout spécial va à ma soeur Maya et Augustin, qui ont été constamment présents sur place, en toutes circonstances.

à Augustin.

Contents

Introduction

Motivations

Mesoscopic physics aims at investigating quantum phenomena that arise from coherence properties of electron motion in conductors. Although samples usually consist of a huge number of atoms (typically of the order of 10^{10}), they are small enough to permit the coherent propagation of electrons. These conductors are characterized by a dephasing length l_φ longer than the geometrical size of the sample L and smaller than or of the order of the inelastic scattering length l_{in},

$$L \lesssim l_\varphi \leqslant l_{in} \,.$$

The dephasing length l_φ is defined as the distance an electron travels through the conductor before suffering a random phase change of 2π. This dephasing length is generally due to smooth or quasi-elastic interaction processes. In contrast, the inelastic dephasing length l_{in} is the distance an electron travels before loosing an energy $k_B T$, where k_B is the Boltzmann constant and T is the temperature. These inelastic processes are due to a coupling of the conductor with the environment and due to electron-electron interactions and the corresponding dephasing processes are usually irreversible.

The quantum-mechanical phase coherence of electrons in mesoscopic samples has enabled the observation of interference effects such as persistent currents [Büttiker 83, Lévy 90, Chandrasekhar 91, Bleszynski-Jayich 09], Aharonov-Bohm oscillations in mesoscopic rings threaded by a magnetic flux [Aharonov 59, Büttiker 84, Gefen 84, Webb 85] and the measurements of universal conductance fluctuations in diffusive samples [Umbach 84, Altshuler 85, Lee 85, Beenakker 91, Baranger 94, Jalabert 94]. Diffusive samples are for instance disordered metals. They are characterized by an elastic scattering length l_e which is smaller than the dephasing length l_φ. The elastic scattering processes are due to presence of impurities in the sample and importantly, they do not destroy phase coherence. In this thesis, we investigate the transport properties in a different regime, namely the ballistic regime. It is characterized by an elastic scattering length l_e of the order of or larger than the sample,

$$L \lesssim l_e \lesssim l_\varphi \lesssim l_{in} \,.$$

Ballistic samples are made of semiconductor nanostructures which contain a layer where the motion is quantized in the direction perpendicular to the layer. Electrons are then forced to move in the plane of the layer, this forms a two-dimensional electron gas (2DEG). A 2DEG is characterized by a low electronic density inducing a large Fermi wave-length compared to the inter-atomic distance (typically of the order of 40 nm for GaAs). In the ballistic regime, scattering with impurities can be neglected and the description of single and many-particle states necessitates a quantum-mechanical treatment. Then, by varying the geometry of the sample with voltage gates for instance, the transport properties of the electrons can be controlled and the conductor can be seen as a wave guide with several modes or channels for the electrons. The quantization of the conductance of a quantum point contact, which is a short and narrow constriction in a 2DEG, belongs to the most famous quantum transport properties [Van Wees 88, Wharam 88]; it depends on the integer number of propagating modes through the constriction.

The observation of these phenomena is a remarkable signature of the coherence properties of the mesoscopic conductors and of the particles emitted by mesoscopic sources, which are set by the dephasing length l_φ and the inelastic scattering length l_{in} introduced above. Since the early days of mesoscopic physics, a huge technical development has taken place which now enables a detailed exploration of quantum-mechanical properties of mesoscopic conductors. Among impressive realizations during the last decade, we can cite the fabrication of semiconductor nanowires (which are promising candidates for the first experimental proof of the existence of the Majorana fermions) [Lutchyn 10, Oreg 10, Mourik 12], the coupling of quantum dots with microwave resonators which combines the field of mesoscopic physics and circuit quantum electrodynamics [Delbecq 11, Frey 12], the realization of on-demand single-electron sources (SES) [Fève 07] and the realization of electronic Mach-Zehnder interferometers (MZI) [Ji 03].

The two latter experiments stimulated most of the work described in this thesis. Indeed, the on-demand SES generates single-particle states at a controlled time, which constitutes an analog of the single-atom or single-photon sources. The principle of this source consists in applying a periodic potential onto a cavity with quantized energy levels in order to shift one energy level above and below the Fermi sea. Under specific conditions which we will present in the introduction of the chapter 2, one single electron and one single hole are emitted on average per period at a time controlled by the driving potential. In order to manipulate the single-electron states emitted by the source for quantum information processes or for investigating fundamental quantum phenomena like the anti-bunching of fermions, it is necessary to characterize the coherence properties of these single-electron quantum states, and in particular their first-order coherence length Λ. This length Λ is of fundamental importance as it sets the distance over which a single-particle state is able to interfere with itself at the output of an interferometer [Loudon].

This length is accessible by measuring the first-order correlation function $G^{(1)}$ with an interferometer. Such experiments have already been performed with single-photon sources for example [Yamamoto 99, Santori 02, Flagg 10]. The decay of $G^{(1)}$ as a function of the time delay between the arms of the interferometer gives access to the coherence time of the single-particle states, usually referred to as the T_2 time. This coherence time is set by the linewidth of the pulse (generally called the lifetime of the pulse or the relaxation time T_1) and by the phase coherence length (T_φ or T_2^* in the literature). The coherence length Λ is related to the coherence time T_2 by the light velocity. With the realization of the on-demand SES in mesoscopic physics, such a characterization of the first-order coherence properties of the single-electron states is crucial. This is one of the main questions that we answer in this thesis by using the electronic MZI.

The coherence properties of the electronic MZI make it an outstanding device to investigate and to manipulate coherent quantum states. It will be used to determine the coherence length of different existing sources in mesoscopic physics but also as a parity detector to create entanglement between two charge qubits. In an electronic MZI, electrons traveling in the arms conserve their coherence properties over a large distance on a mesoscopic scale, of the order of 10 μm. This follows from the fact that the MZI is built in the quantum Hall regime where a high magnetic field is applied perpendicularly to the 2DEG. In this regime, electrons propagate along the edges of the sample without being reflected, in edge states. Each edge state is characterized by a particular velocity. The transport is unidirectional and the elastic and inelastic scattering lengths exceed the size of the sample. The dephasing length l_φ depends predominantly on the electronic temperature, on the applied bias, on the size of the interferometer and on the interaction between carriers in nearby edge states [Neder 06, Roulleau 08, Litvin 08, Bieri 09, Huynh 12]. It has been shown to be sufficiently large to enable for instance the realization of an Hanbury-Brown and Twiss experiment where two-particle Aharonov-Bohm interferences have been observed [Neder 07].

The coherence properties of single and many-particle states are characterized by transport features which are measured at the output of mesoscopic conductors. Due to the indistinguishability and due to the large number of particles, the transport in mesoscopic samples is in its essence a stochastic process. Since the beginnings of mesoscopic physics, the measured quantities have been typically the average charge or average current and the noise which are the first two moments of the distribution of the transferred charge. The noise stems from the charge fluctuations in the mesoscopic conductor. At low temperature, charge fluctuations originate both from the discreteness of the charge [Schottky 18] and from the probabilistic nature of the quantum transport (quantum shot noise) [Khlus 87, Lesovik 89, Büttiker 90]. The quantum shot noise arises from the quantum mechanical uncertainty when particles are scattered by a potential : the particles are transmitted or reflected in a com-

pletely random and unpredictable way. Therefore fluctuations in a non-equilibrium transport experiment can be used to gain insight about the quantum statistical properties of the system. For example the observation of the anti-bunching of fermions [Oberholzer 00] and the determination of the effective charge in the fractional quantum Hall regime [Saminadayar 97, Picciotto 97] have been rendered possible through noise measurements.

Importantly, however, the average current and the zero-frequency noise only provide partial information about the stochastic quantum transport process. A significant example in the context of this thesis is the case of a QPC characterized by a transmission probability T, connected to two reservoirs via one-dimensional single channels. The quantum shot noise measured in such a setup is proportional to $T(1-T)$ [Reznikov 95, Kumar 96]. As a consequence, when there is no scatterer, $T = 0$ (all the electrons are reflected) or $T = 1$ (all the electrons are transmitted), there is no quantum shot noise [Büttiker 90, Blanter 00]. To fully characterize the quantum transport properties through a mesoscopic sample, the investigation of the full probability distribution of the transferred charge and/or the investigation of other statistical tools like the distribution of waiting times are necessary. By definition the waiting time is the interval between the arrival times of two successive carriers. It therefore provides information about the short-time physics properties.

Reconstructing the probability distribution function of the transferred charge implies the determination of the higher-order moments of the distribution, known as Full Counting Statistics (FCS) [Levitov 93, Levitov 96, Nazarov 03]. FCS investigates long-time physics as it considers the distribution of the transferred charge through a mesoscopic conductor over a long time compared to all other time scales of the system. It constitutes a very efficient statistical tool which enabled for instance a more accurate description of the properties of a QPC used as a quantum detector of a quantum state [Averin 05]. Much efforts have been put into experiments in the last decade so that today, up to several cumulants (between 3 and 5) of the transferred charge have been measured in different systems (tunneling process though a quantum dot [Gustavsson 06, Ubbelohde 12] or avalanche-type transport [Gabelli 09] for instance). However the average current in these experiments is so small (of the order of few nA) that quantum effects are almost unperceivable.

Recently the distribution of waiting times (WTD) in mesoscopic conductors has attracted much interest as it provides different informations on the stochastic quantum transport process [Koch 05, Brandes 08, Welack 08, Welack 09, Albert 11]. It probes short-time physics compared to the transferred charge over a long time investigated in FCS. Up to now, the WTD has been derived using a master equation approach which takes into account single-particle tunneling processes through a mesoscopic conductor. Within this approach, various mesoscopic issues have been investigated such as avalanche-type transport through molecules [Koch 05] or the on-demand single-electron source to characterize the accuracy of the emission of single

particles [Albert 11]. In this thesis, we have developed a full quantum approach of the WTD. When considering for instance the transport experiment through a QPC mentioned above, we have shown in particular that the WTD provides exciting informations about the statistics and the coherence properties of the many-body incoming state, even for a fully open or nearly pinched-off QPC.

Organization of the thesis

In Chapter 1, we investigate the electronic MZI as a parity detector for two double quantum dots playing the role of charge qubits. Together with single-particle sources and single-qubit operations, parity measurements enable efficient quantum information processing by generating entanglement between the qubits. A parity meter projects the state of two qubits onto two subspaces with different parities, the states in each parity class being indistinguishable, therefore producing entanglement between the qubits. In this chapter, we give the conditions under which the MZI operates as a parity detector and interestingly we show that its efficiency is maximal. This means that the quantum systems are dephased only as fast as the detector acquires information. This property has remarkable consequences when considering the probability to generate entangled states.

In Chapter 2, we characterize the coherence properties of single-electron states emitted by a new type of electron sources in mesoscopic physics, the on-demand SES. For this, we calculate the first-order coherence function $G^{(1)}$ from the current at the output of the MZI. Importantly, we derive it in terms of the scattering matrix of the source. As a function of the imbalance of the interferometer, $G^{(1)}$ decays with a characteristic time which is, by definition, the coherence time T_2. This is done for single-particle states emitted by the source in the adiabatic and in the non-adiabatic regimes, where these two regimes depend on the shape of the driving potential applied to the cavity. We show that, in both regimes, the source emits single-particle states which are Fourier-transform limited, i.e their coherence time is only set by their relaxation time. The on-demand SES is therefore promising for generating single-electron states suitable, for instance, for manipulating quantum information.

In Chapter 3, we develop a quantum theory of electron waiting times between charge carriers in mesoscopic conductors. The distribution of waiting times provides a complementary view on charge transport compared to the more traditional investigations of the mean current and the fluctuations of the current. This statistical approach yields information about the quantum statistics and therefore on the coherence properties of the incoming many-particle state. We illustrate our methodology by calculating the waiting time distribution for a biased QPC, where the incoming many-particle state is described by a Slater determinant. Surprisingly, we find a cross-over from Wigner–Dyson statistics at full transmission to Poisson statistics

close to pinch-off. Even when the low-frequency transport is noiseless, the electrons are not equally spaced in time due to their inherent wave nature. The WTD proves to be a powerful tool to investigate the coherence properties of many-particle states.

Throughout this work, we have investigated the coherence properties of single and many particle states using a scattering matrix approach. This formalism has been proven to be very efficient to characterize the transport features in coherent mesoscopic samples considering non-interacting particles. In Appendix 4.1, we therefore briefly present the formalism by recalling the main properties of the scattering matrix as well as the expression of the measurable observables like the current operator.

Every chapter is self-contained such that a reader interested in only a part of the thesis may start right at the beginning of the corresponding chapter.

Chapter 1

The electronic Mach-Zehnder interferometer as parity detector

Contents

1.1 Introduction

Quantum information processing (QIP) relies on the ability to implement two-qubit gates like the CNOT gate, which create entanglement. Combined with single-qubit operations, they form a set of universal operations, sufficient for quantum computing [Barenco 95]. *Efficient* QIP is achieved when the complexity of the resources required for the implementation of quantum algorithms is polynomial.With photon-based qubits, efficient two-qubit gates have been realized by making use of interactions between the qubits produced with non-linear optical elements which couple the optical modes together. However this is experimentally very demanding [Turchette 95]. For solid-state qubits which are subject to the Coulomb interaction, the implementation of efficient gates is also difficult as it requires a precise control of the strength of this Coulomb interaction.

A decade ago, E. Knill, R. Laflamme and G. J. Milburn have shown that nearly deterministic two-qubit gates can be efficiently implemented without any qubit-qubit interactions but only with linear operations [Knill 01]; this opened the field of "linear optics quantum computation" (LOQC) [Kok 07, Kiraz 04]. Three years later, the field of "free-electrons quantum computation" (FEQC) was opened by C. W. Beenakker, D. P. Vincenzo, C. Emary and M. Kindermann [Beenakker 04]. These proposals for QIP require single-particle sources, single-qubit operations and parity measurements. LOCQ and FECQ are measurement-based proposals, i.e it is the parity-measurement process that creates the entanglement resource necessary for the implementation of quantum algorithms. A parity meter couples two qubits and allows to measure whether the qubits are in the even subspace spanned by the even states $\{|\uparrow\uparrow\rangle, |\downarrow\downarrow\rangle\}$ or in the odd subspace spanned by the odd states $\{|\uparrow\downarrow\rangle, |\downarrow\uparrow\rangle\}$. A particular basis for these two subspaces are the four Bell states, which are the maximally entangled states for two qubits. As these Bell states are also eigenstates of the parity operator for two qubits, a parity measurement drives the qubits into a Bell state and constitutes a source of entanglement. This is shown in more details in the next subsection.

In mesoscopic physics, several realizations of parity meters have been discussed, considering a QPC as detector. In the different setups, the QPC is weakly coupled to the quantum systems, which are either spin [Engel 05, Coish 06, Zilberberg 08] or charge qubits [Trauzettel 06]. The purpose of our work is to investigate parity detection of charge qubits with the help of a Mach-Zehnder interferometer (MZI). Compared to the previous proposals with a QPC, the MZI coupled to qubits in its arms has the advantage that the two qubits are on the mesoscopic scale far away from each other. Therefore they are not subject to mutual Coulomb interaction. Another advantage of this setup lies in the tunability of the MZI through a variation in the applied magnetic field and through side-gate voltages which change the length of the upper and lower arms of the MZI. We provide below more details on the experimental realization of such an electronic MZI. In this work, we present the conditions under

which a MZI can be operated as parity detector with maximal efficiency (ideal parity detectors). This is of interest for QIP as such ideal detectors dephase the qubits only as fast as they measure it when one looks at the time-averaged evolution of the qubits. We also investigate the creation of entanglement between the qubits and derive a class of initial states for which the MZI acts as a nearly deterministic source of entanglement for mesoscopic qubits.

1.1.1 Entanglement generation through a parity measurement

Let us consider a two-level system characterized by an "up-state" $|\uparrow\rangle$ and a "down-state" $|\downarrow\rangle$. The computational basis for two qubits is spanned by the states $\{|\uparrow\uparrow\rangle, |\uparrow\downarrow\rangle, |\downarrow\uparrow\rangle, |\downarrow\downarrow\rangle\}$. By definition, the parity operator $\hat{P}$ is [Messiah]:

$$\hat{P} = \hat{\sigma}_z^1 \otimes \hat{\sigma}_z^2 \,, \tag{1.1}$$

where $\hat{\sigma}_z^i$ are the $\hat{z}$-Pauli matrices for the first and second qubits, $i = 1, 2$:

$$\hat{\sigma}_z^i = \begin{pmatrix} 1 & 0 \\ 0 & -1 \end{pmatrix} \tag{1.2}$$

This parity operator has 2 eigenvalues which are twice degenerate, 1 and -1.

The eigenvalue 1 corresponds to the even parity class whose subspace is spanned by the two Bell states $\{|\psi_e^+\rangle, |\psi_e^-\rangle\}$. These *even* Bell states are a superposition of the even states of the computational basis:

$$|\psi_e^+\rangle \;=\; \frac{1}{\sqrt{2}}\left(|\uparrow\uparrow\rangle + |\downarrow\downarrow\rangle\right), \quad |\psi_e^-\rangle = \frac{1}{\sqrt{2}}\left(|\uparrow\uparrow\rangle - |\downarrow\downarrow\rangle\right) . \tag{1.3}$$

The lower indices indicate the parity class and the upper indices ($\pm$) indicate whether the sum or difference of the computational states is taken. In contrast, the eigenvalue -1 corresponds to the odd parity class, whose subspace is spanned by the two odd Bell states $\{|\psi_o^+\rangle, |\psi_o^-\rangle\}$:

$$|\psi_o^+\rangle \;=\; \frac{1}{\sqrt{2}}\left(|\uparrow\downarrow\rangle + |\downarrow\uparrow\rangle\right), \quad |\psi_o^-\rangle = \frac{1}{\sqrt{2}}\left(|\uparrow\downarrow\rangle - |\downarrow\uparrow\rangle\right). \tag{1.4}$$

These Bell states are of fundamental importance as they share the property to be the maximal entangled states for two qubits. This can be shown by looking at the Shannon entropy S [Nielsen 00]:

$$S = -\sum_i \lambda_i \log_2 \lambda_i \,,$$

The λ_i's are the coefficients in the Schmidt expansion of a state $|\Psi_{12}\rangle$ made up of two subsystems 1 and 2:

$$|\Psi_{12}\rangle = \sum_i \sqrt{\lambda_i} |i_1\rangle \otimes |i_2\rangle \,,$$

where $|i_1\rangle$ and $|i_2\rangle$ are the eigenstates of the reduced density matrices of the subsystems 1 and 2. A separable state $|\Psi_s\rangle = |\Psi_1\rangle \otimes |\Psi_2\rangle$ is characterized by a Schmidt expansion with coefficients $\lambda_i = 1$. Its Shannon entropy is minimal meaning that all the information about the reduced density matrices ρ_1 and ρ_2 is available. To the contrary, a Bell state, for instance $|\psi_e^+\rangle$, has a Schmidt decomposition which reads:

$$|\psi_e^+\rangle = \frac{1}{\sqrt{2}}|\uparrow\rangle_1 \otimes |\uparrow\rangle_2 + \frac{1}{\sqrt{2}}|\downarrow\rangle_1 \otimes |\downarrow\rangle_2 \,.$$

The coefficients λ_i are equal to $1/2$ and the Shannon entropy is equal to 1. The disorder being maximum, there is no information left concerning the reduced density matrices ρ_1 and ρ_2, these states are *maximally entangled*.

A parity measurement therefore projects the qubits onto the even and odd subspaces, driving the qubits into a superposition of the even and odd Bell states respectively. As we show in our work, when both qubits are initially in a superposition state $|\Psi_i\rangle = 1/2(|\uparrow\rangle + |\downarrow\rangle) \otimes (|\uparrow\rangle + |\downarrow\rangle)$, the MZI acts as a source of entanglement for the odd subspace with maximal probability $1/2$ by putting the qubits in the odd Bell state $|\psi_o^+\rangle$.

1.1.2 Weak coupling regime

Our analysis of the parity detection is based on a formulation which takes into account that the detector is *weakly* coupled to the system: the average current measured at the output of the detector is assumed to be very large compared to the difference in the current produced by the state of the qubits. As a consequence many electrons have to pass through the detector before one can distinguish the two parity subspaces in the case of a parity detector. In other words, the measurement takes a finite time. Such a weakly responding detector is characterized by its measurement rate Γ_m defined as the signal-to-noise ratio. Considering a parity meter which distinguishes only the even current I_e from the odd current I_o, this measurement rate is defined as [Korotkov 99]:

$$\Gamma_m = \frac{(I_o - I_e)^2}{4\, S_{II}},$$

where S_{II} is the zero-frequency current fluctuation spectrum of the detector. Such weakly coupled detectors are typical for on chip detectors in mesoscopic physics and have led to a strong theoretical development in the last 15 years. A non-exhaustive list includes the works of [Korotkov 99, Martin 00, Korotkov 01, Pilgram 02, Clerk 03, Averin 05, Clerk 10]. The efficiency of these detectors is characterized by the ratio of the measurement rate with the dephasing rate Γ_d of the qubits. In the section 1.3 and 1.4, we have derived these rates for the MZI operating as a parity meter and show that it can be operarted in the ideal regime, where the detector acquires information as fast as it dephases the qubits.

1.1.3 The electronic Mach-Zehnder interferometer

The electronic Mach-Zehnder interferometer (MZI) and its extrinsic coherence properties are at the heart of this project. It is an analog solid state device of the optical Mach-Zehnder interferometer that allows for electron waves to interfere. A scheme of an optical interferometer is shown in Fig. 1.1 a). The particles are injected in the MZI via a source S connected to one of the inputs. At the left beam splitter $BS1$, the wave-packets are split into the upper and lower arms. Depending on the lengths of the two arms, the particles acquire a different phase which leads to an interference pattern in the intensity measured in $D1$ or $D2$. In the electronic version, the MZI is built in the quantum Hall regime in which a strong magnetic field is applied. The phase difference between the two arms is the Aharonov-Bohm phase which originates in the magnetic flux enclosed by the arms. Electrons on the arm i acquires a phase θ_i which depends on the vector potential $\vec{A}$ [Aharonov 59]:

$$\theta_i = \frac{e}{\hbar} \int_{\mathcal{C}_i} \vec{dl} \vec{A}\,, \tag{1.5}$$

where $\mathcal{C}_i$ is the length of the upper or lower arm. When the wave-packets recombine at the right QPC, the interference term exhibits oscillations which depend on the phase difference between the upper and lower arms:

$$\theta_u - \theta_d = \frac{e}{\hbar} \oint_{\mathcal{C}} \vec{dl} \vec{A} = \frac{e}{\hbar} \int_{\mathcal{S}} \vec{dS} \vec{B} = 2\pi\Phi/\Phi_0\,. \tag{1.6}$$

Here $\mathcal{C}$ is the closed contour defined by the upper and lower arms and the Stokes theorem converts the path integral into an integral over the area enclosed by the arms $\mathcal{S}$. The magnetic flux Φ is expressed in units of the flux quantum for a single particle, $\Phi_0 = h/e$. This interference pattern is manifest for instance in the electrical current measured at the outputs of the MZI.

The experimental realization of the electronic MZI is very challenging, a pioneering experiment was performed by Ji et al. [Ji 03]. A scanning microscope image is shown in Fig. 1.1 b). It consists of a four-terminal conductor built in a quantum Hall bar with two QPCs made of metallic gates. These two QPCs play the role of beam splitters for the electrons, they are labelled $QPC1$ and $QPC2$ in Fig. 1.1 c). Their transmission probabilities are controlled through gate voltages. In the quantum Hall regime, the transport takes place along the edges of the sample. These edge states act as wave-guides for the electrons. The transport is chiral due to suppressed backscattering [Halperin 82, Büttiker 88]. The non-linear behavior of the MZI has received much experimental [Neder 06, Roulleau 08, Litvin 08, Bieri 09] and theoretical attention [Sukhorukov 07, Levkivskyi 08, Kovrizhin 09a, Kovrizhin 09b] in the past years. Throughout this thesis, we assume that the applied voltages are small and that the MZI is operated within its linear response regime.

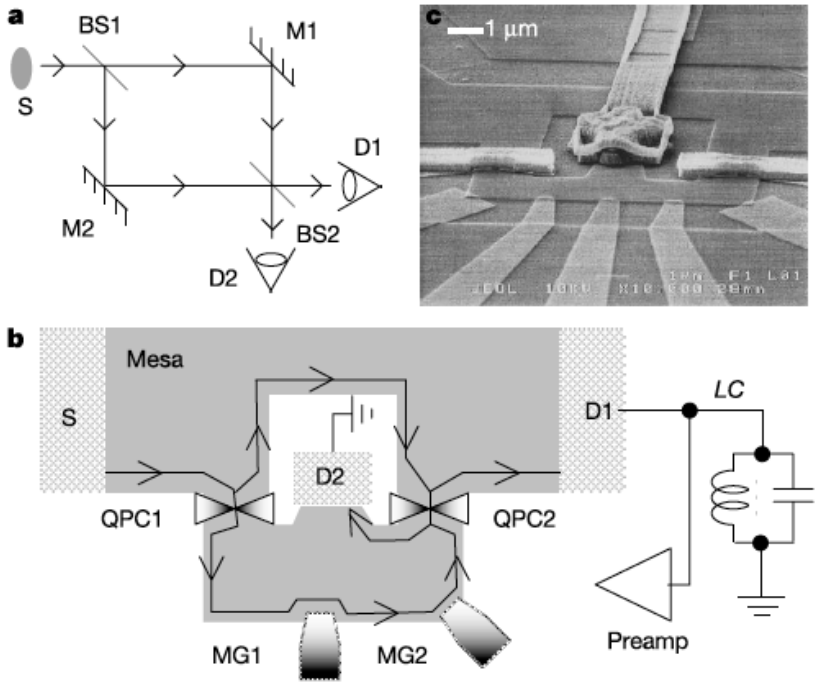

Figure 1.1: Experimental setup of the MZI taken from Ref. [Ji 03]. a) Optical version of the MZI. The incident beam emitted by the source S is split onto the left beam splitter $BS1$ and recombined by the second beam splitter $BS2$. The lengths of the upper and lower arms is controlled by changing the position of the mirrors $M1$ and $M2$. The detectors $D1$ and $D2$ measure the intensity which exhibits an interference pattern. b) Electronic version of the MZI. The sample is built in the quantum Hall regime. The motion of electrons takes place along edge states which play the role of wave-guides for the carriers (thin black curves). Quantum point contacts ($QPC1$ and $QPC2$) act as beam splitters for the electrons. The current measured at the output $D1$ exhibits Aharonov-Bohm oscillations. By applying side metallic gates ($MG1$ and $MG2$), they control the length of the upper and lower arms, which define the enclosed area. c) Scanning electron micrograph of the sample.

At the output labelled $D2$ in Fig. 1.1 b), the conductance is measured and exhibits AB oscillations as a function of the magnetic field and of a side-gate voltage as shown in Fig. 1.2 a). These two tunable parameters control the magnetic flux enclosed by the arms of the interferometer. Experimentally to vary the magnetic field, they use the natural drift with respect to time of a magnetic field produced by a current in a superconducting magnet. In the first experiment of [Ji 03], the AB oscillations measured in the conductance exhibit a visibility of 60%, where the visibility is defined as $(I_{\max} - I_{\min})/(I_{\max} + I_{\min})$. The maximal and minimal current are respectively $I_{\max}$ and $I_{\min}$. More recent experiments with MZIs at filling factor $\nu = 2$ have been able to reach a visibility of 90% by reducing for instance the coupling between the two edge states [Neder 07, Huynh 12]. Figure 1.2 b) shows that the MZI exhibits a maximal visibility for half-transmitting QPCs. The transmission and

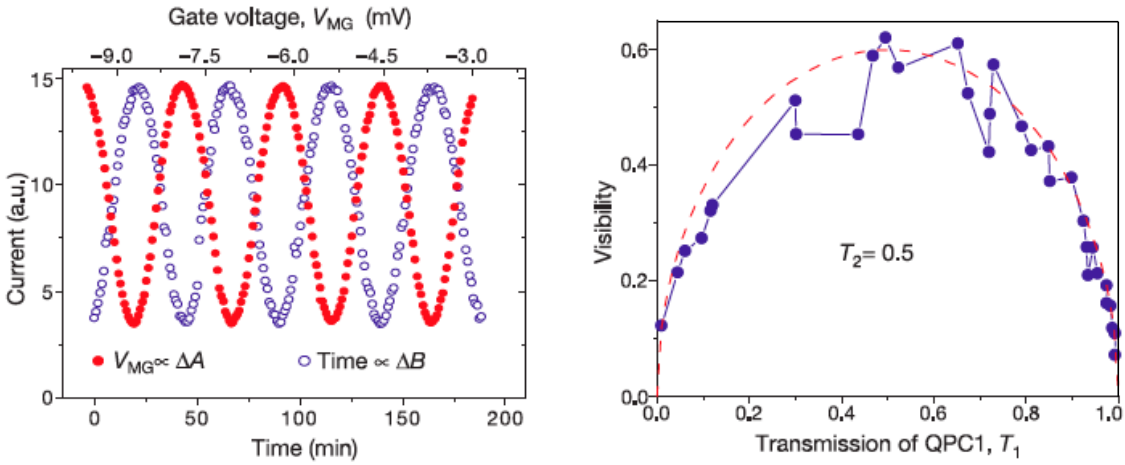

Figure 1.2: Left: Aharonov-Bohm (AB) oscillations measured in the current at the output of the electronic MZI. These oscillations are controlled through two tunable parameters, the change in the magnetic field (blue empty dots) and the length of the arms which defines the enclosed area (red full dots). Right: The visibility of the AB oscillations is measured as a function of the transmission probabilities T of the two QPCs playing the role of beam splitters for the electrons. It exhibits a maximum for a symmetric configuration, $T_1 = T_2 = 1/2$. Figure taken from Ref. [Ji 03].

reflection probabilities are equal to 1/2 for the left and right QPCs ($QPC1$ and $QPC2$ on the figure). In this thesis, we will therefore always consider the MZI with symmetric QPCs to measure the maximal visibility of the AB oscillations.

1.2 The electronic MZI as parity meter

1.2.1 Model

The electronic MZI is built in a quantum Hall bar by using two QPCs as beam splitters. The qubits are coupled to each arm of the MZI as shown in Fig. 1.3. They are spatially separated so that they do not interact directly with each other. The interaction takes place between each qubit and the charges of the corresponding arm and is described with the help of geometrical capacitance coefficients: C_1 determines the coupling of the charge on the DQD to the charge on the arm, C_i determines the coupling between the dots, and C_2 is the capacitance of the upper (lower) dot of qubit 1 (qubit 2) to the ground. For simplicity, here, the capacitances are assumed to be the same for each qubit. The regime of weak coupling between the detector and the DQDs is defined by $C_1, C_2 \ll C_\mathrm{i}$. Additionally, to control the system, we can tune the Aharonov-Bohm flux through the length of the arms and the magnetic field, and the transmission and reflection probabilities of the QPCs. The Hamiltonian of this model is :

$$\hat{H} = \hat{H}_\mathrm{qb} + \hat{H}_\mathrm{int} + \hat{H}_\mathrm{det}\,, \tag{1.7}$$

where $\hat{H}_\mathrm{qb}$ is the Hamiltonian of the DQDs, $\hat{H}_\mathrm{int}$ is the interaction Hamiltonian and $\hat{H}_\mathrm{det}$ is the Hamiltonian of the MZI which acts as detector. A DQD characterized by its tunneling Δ and its energy bias ϵ plays the role of a charge qubit described by the Hamiltonian $(\epsilon/2)\,\hat{\sigma}_z + (\Delta/2)\,\hat{\sigma}_x$.

As mentioned in the introduction, we want to operate the MZI coupled to the two qubits as ideal parity meter. To reach this regime, the Hamiltonians of the qubits and of the interaction have to preserve the parity classes. This can be achieved if these two Hamiltonians commute with the parity operator. They are then diagonalizable in the same basis, i.e the $\hat{\sigma}_z$-basis. We assume therefore that there is no tunneling in each DQD. In addition, for simplicity we assume that the two qubits have the same energy bias ϵ :

$$\hat{H}_\mathrm{qb} = \frac{\epsilon}{2}(\hat{\sigma}_z^1 + \hat{\sigma}_z^2)\,. \tag{1.8}$$

The Pauli matrices for the upper and lower qubits are $\hat{\sigma}_z^1$ and $\hat{\sigma}_z^2$. With such an Hamiltonian for the qubits, the commutation relation reads $[\hat{H}_\mathrm{qb}, \hat{P}] = 0$. This means that the free evolution of the qubits does not mix the parity subspaces. This is an important assumption to operate the MZI as an ideal parity detector as we show in more details below.

The interaction Hamiltonian is derived by writing down the Coulomb energy of the electronic circuit corresponding to the double quantum dot coupled to the charge

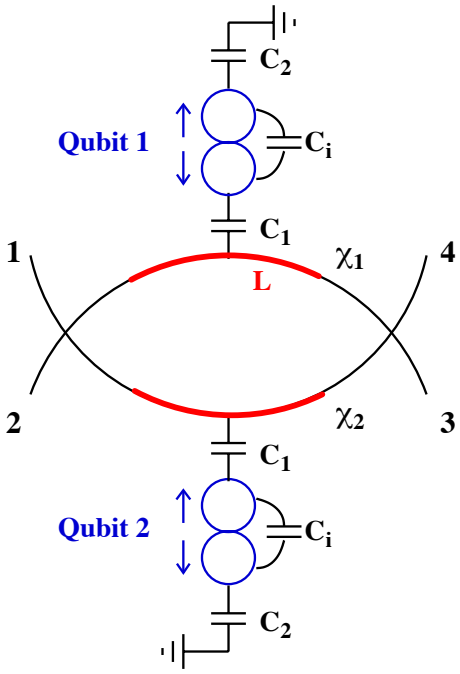

Figure 1.3: Mach-Zehnder interferometer (MZI) coupled capacitively to two qubits. $\chi_1(\chi_2)$ is the phase accumulated by the electrons passing through the upper (lower) arm of the MZI over a length L (red curve). These phases depend on the state of the qubits. C_1, C_2 and C_i are the capacitances characterizing the double quantum dots (DQDs).

in the arm of the interferometer. The interaction Hamiltonian between the arms of the MZI and the corresponding DQDs reads [Pilgram 02, Aleiner 02] :

$$\begin{aligned} \hat{H}_{\mathrm{int}} &= \frac{\hat{Q}_{up}\hat{Q}_1}{C_i} + \frac{\hat{Q}_d\hat{Q}_2}{C_i} \\ &= e\left(\frac{1-\hat{\sigma}_z^1}{2}\right)\hat{U}_1 + e\left(\frac{1+\hat{\sigma}_z^2}{2}\right)\hat{U}_2\,. \end{aligned} \tag{1.9}$$

The expressions $\hat{Q}_{up} = e(1-\hat{\sigma}_z^1)/2$ and $\hat{Q}_d = e(1+\hat{\sigma}_z^2)/2$ are the charge operators of the qubits which couple to the potential operators on the arms of the interferometer. The Mach-Zehnder detector considered here is a linear detector in the sense that qubits couple linearly to the charge in the arms of the MZI through the $\hat{\sigma}_z$ operator. The operators $\hat{U}_{1,2} = \hat{Q}_{1,2}/C_i$ are the potential operators on the upper and lower arms respectively. They depend on the bare charge and on the screening charge on the arms due to the presence of the DQDs. They are derived self-consistently from the density-of-states in the arms calculated from the Wigner-Smith time-delay matrix [Büttiker 00a, Büttiker 00b]. This derivation is given in the Appendix 4.2.With this interaction Hamiltonian, the electrons transiting in the arms of the MZI are sensitive to the charge in the DQDs only if this charge is in the dot close to the arm. For instance, if the charge of the qubit 1 is in the upper dot, the matrix elements of the

operator $(1-\hat{\sigma}_z^1)/2$ are zero whereas if the charge in qubit 2 is in the lower dot, the matrix elements of $(1+\hat{\sigma}_z^1)/2$ are zero. The phase χ_i that electrons on arm $i=1,2$ acquire during their transfer is the sum of a dynamical phase, of a phase due to the magnetic field and a phase due to the state of the DQDs:

$$\chi_1 = k_F(d-L)+\theta_{up}+\Delta\chi_1\frac{1-\hat{\sigma}_z^1}{2}, \tag{1.10}$$

$$\chi_2 = k_F(d-L)+\theta_d+\Delta\chi_2\frac{1+\hat{\sigma}_z^2}{2}. \tag{1.11}$$

Here we consider both arms having the same length d and the electrons are sensitive to the DQDs over a length L (see Fig. 1.3). The wave vector k_F is evaluated at the Fermi energy E_F and the phases due to the magnetic field verify $\theta_{up}-\theta_d = 2\pi\Phi/\Phi_0$, where Φ is the magnetic flux and Φ_0 is the flux quantum. The additional phases $\Delta\chi_i$ depend on the state of the DQDs through the charge operator of the DQDs in the $\hat{\sigma}_z$-basis.

Equations (1.10) and (1.11) should be viewed only as abbreviations, since in reality the phases and the transmission amplitude probability S_{31} to be given in the next section are complex numbers depending on the state of the qubits. Thus instead of writing operators in Eqs. (1.10) and (1.11) we should index these quantities with the corresponding qubit states. Here we avoid such a heavy notation and keep operators.

Given that both the Hamiltonian of the qubits and the interaction Hamiltonian commute with the parity operator $\hat{P}$ given in Eq.(1.1), there is no relaxation process for the DQDs due to the coupling with the detector. Here relaxation refers to the decay of the population terms in the density matrix. This is important as it implies that, in this configuration, the Mach-Zehnder detector is a quantum non demolition detector (QND-detector) of the parity classes [Caves 80, Braginsky 92, Haroche 06]. This is to say that repeated measurements will find the qubits in the same parity class, the MZI detects only two stationary currents. This is an important distinction between previous works on entanglement generation [Ruskov 03, Mao 04, Ruskov 06, Trauzettel 06, Williams 08] and the investigation presented here. In the previous works, they use a qubit Hamiltonian formulated in the $\hat{\sigma}_x$-basis which mixes the parity subspaces. With such a setup the detector distinguishes three states [Trauzettel 06], two states which are detectable in repeated measurements belonging to the two parity classes and a time-dependent state which oscillates between the parity classes. Although this configuration creates entanglement between the two qubits, the detector can not be operated as an ideal parity meter.

In the next sections, we derive the conditions under which the MZI coupled to DQDs allows their parity detection and operates as ideal detector in this regime. We then investigate the creation of entanglement through the parity measurement.

1.2.2 Parity meter

The observable we measure is the average current in lead 3 (see Fig. 1.3). Assuming that the electrons are injected in lead 1, within a scattering-matrix approach, the average current is given by :

$$I = \frac{2e^2V}{h}T_{31}\,, \tag{1.12}$$

where T_{31} is the transmission probability from lead 1 to lead 3,

$$\begin{aligned} T_{31} &= |S_{31}|^2 \\ &= \big(T_{\rm L}R_{\rm R} + T_{\rm R}R_{\rm L} + 2\sqrt{T_{\rm R}R_{\rm L}T_{\rm L}R_{\rm R}}\cos\tilde{\Phi}\big). \end{aligned} \tag{1.13}$$

It can be calculated with the help of the scattering matrix S of this model: $T_{31} = |S_{31}|^2$, where S_{31} is one element of the S-matrix. It corresponds to the amplitude probability of going from lead 1 to lead 3,

$$S_{31} = \sqrt{R_{\rm L}T_{\rm R}}e^{i\chi_1} + \sqrt{T_{\rm L}R_{\rm R}}e^{i\chi_2}\,. \tag{1.14}$$

We introduce the phase $\tilde{\Phi} = \chi_1 - \chi_2$ where χ_1 and χ_2 are given in Eqs. (1.10) and (1.11). Depending on the four possible states of the qubits $\{|\uparrow\uparrow\rangle, |\uparrow\downarrow\rangle, |\downarrow\uparrow\rangle, |\downarrow\downarrow\rangle\}$, $\tilde{\Phi}$ can take four different values :

$$\tilde{\Phi}_{\uparrow\uparrow} = 2\pi\Phi/\Phi_0 - \Delta\chi_2, \tag{1.15a}$$
$$\tilde{\Phi}_{\uparrow\downarrow} = 2\pi\Phi/\Phi_0, \tag{1.15b}$$
$$\tilde{\Phi}_{\downarrow\uparrow} = 2\pi\Phi/\Phi_0 + \Delta\chi_1 - \Delta\chi_2, \tag{1.15c}$$
$$\tilde{\Phi}_{\downarrow\downarrow} = 2\pi\Phi/\Phi_0 + \Delta\chi_1. \tag{1.15d}$$

The MZI can detect the four different states in which the two qubits can be. The principle of the parity meter relies on the choice to not measure all the information which is available about the qubits' states. This increases the Shannon entropy and the qubits become entangled. Below we derive the conditions under which only two currents are distinguishable, the currents corresponding to the even and odd subspaces.

Conditions for a parity measurement

To operate the MZI as parity meter, only two currents have to be distinguishable, corresponding to the two parity classes:

- I_o corresponding to the odd states $\big\{|\uparrow\downarrow\rangle, |\downarrow\uparrow\rangle\big\}$.
- I_e corresponding to the even states $\big\{|\uparrow\uparrow\rangle, |\downarrow\downarrow\rangle\big\}$.

Considering Eqs. (1.15b-1.15c), only one current I_o for the odd states is measurable if the incremental phases $\Delta\chi_i$ for electrons in upper and lower arms are the same :

$$\Delta\chi_1 = \Delta\chi_2 = \Delta\chi. \tag{1.16}$$

This condition is fulfilled if the upper and lower DQDs are described by the same set of capacitances. Then the internal potentials in the upper and lower arms are equal, $U_1 = U_2 \equiv U$. The self-consistent derivation of U is in Appendix 4.2. If we assume that the potential U is constant over the traversal time of the electrons in the region L of the arm of the MZI, the phase $\Delta\chi$ only depends on the capacitances :

$$\Delta\chi \;=\; \frac{e}{\hbar}\int_0^\tau dt' U(t') = \frac{e}{\hbar} U\,\tau = 2\pi\frac{C_\mu}{C_i}\,. \tag{1.17}$$

The electrochemical capacitance C_μ is expressed as the sum in series of the geometrical capacitances and of the quantum capacitance $C_q = 1/(e^2 N)$:

$$\frac{1}{C_\mu} = \frac{1}{C_1} + \frac{1}{C_2} + \frac{1}{C_i} + \frac{1}{e^2\,N}\,. \tag{1.18}$$

Here N is the density-of-states in the arm. Assuming Eq. (1.16) and measuring the output current as a function of the magnetic flux, three currents will be in general distinguishable: one for the odd states I_o and two for the even states $I_{\uparrow\uparrow}$ and $I_{\downarrow\downarrow}$ as shown on Fig. 1.4 a. Although this measurement is not a true parity measurement in the sense that more than two currents are distinguishable, it already allows entanglement between the qubits. Measuring the odd current would mean that the qubits have been driven into the odd subspace and are therefore in a superposition state of the two odd Bell states. However if $I_{\uparrow\uparrow}$ or $I_{\downarrow\downarrow}$ are measured, no entanglement has been generated. In our work we want a true parity meter with advantages for the entanglement probabilities in the even and odd subspaces as discussed in more details in the next section.

Equations (1.15a) and (1.15d) and Fig. 1.4 b show that measuring only one current I_e for the even states is possible if the magnetic flux is set to :

$$2\pi\Phi/\Phi_0 = 0 \quad \text{modulo} \quad \pi, \tag{1.19}$$

providing a maximum or minimal transmission. To be at the maximum of the transmission we choose $2\pi\Phi/\Phi_0 = 2\pi$ in the rest of the work.

Equations (1.16) and (1.19) are the two conditions required for the MZI to act as parity meter. When expanding the transmission probability T_{31} around $2\pi\Phi/\Phi_0 = 2\pi$ up to second order in $\Delta\chi$, the transmission probability is expressed only in terms of the parity operator introduced before, $\hat{P} = \hat{\sigma}_z^1 \otimes \hat{\sigma}_z^2$:

$$\begin{aligned} T_{31} &= T_{\rm L}R_{\rm R} + T_{\rm R}R_{\rm L} + 2\sqrt{T_{\rm R}R_{\rm L}T_{\rm L}R_{\rm R}}\cos\left(\Delta\chi\left(\frac{1-\hat{\sigma}_z^1}{2}\right)\left(\frac{1+\hat{\sigma}_z^2}{2}\right)\right) \\ &= T_{\rm L}R_{\rm R} + T_{\rm R}R_{\rm L} + 2\sqrt{T_{\rm R}R_{\rm L}T_{\rm L}R_{\rm R}}\left(1 - \frac{\Delta\chi^2}{4}(1+\hat{\sigma}_z^1\otimes\hat{\sigma}_z^2)\right). \end{aligned} \tag{1.20}$$

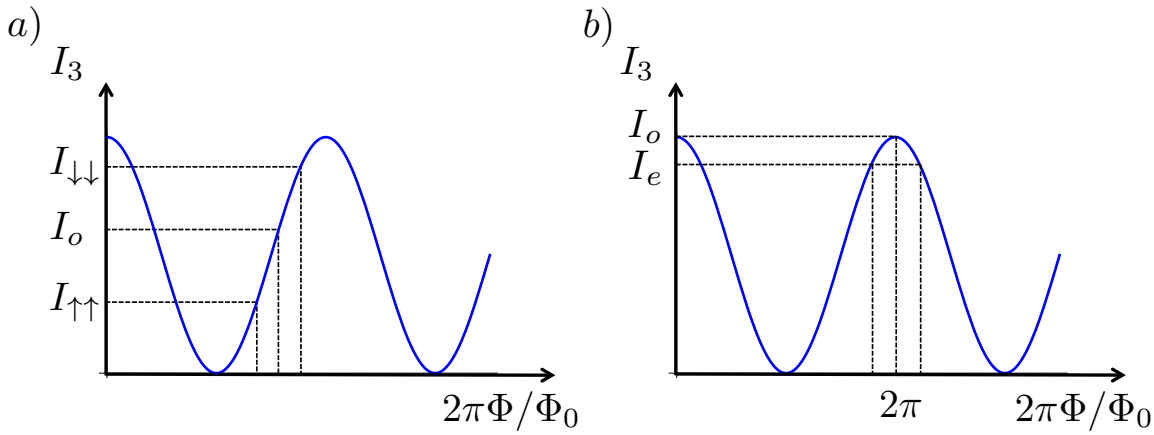

Figure 1.4: Current measured at lead 3 as a function of the magnetic flux between the arms of the MZI. a) At an arbitrary flux three currents $I_o, I_{\uparrow\uparrow}$ and $I_{\downarrow\downarrow}$ are distinguishable even if the incremental phases are identical: $\Delta\chi_1 = \Delta\chi_2 = \Delta\chi$. b) To measure only two currents corresponding to the parity classes, I_o and I_e, we set the flux to $2\pi\Phi/\Phi_0 = 0 \mod \pi$. A maximum of the current is reached at $2\pi\Phi/\Phi_0 = 2\pi$.

The parity operator $\hat{P}$ has two eigenvalues ± 1 of degeneracy 2, corresponding respectively to the even parity class and to the odd parity class. Its four eigenstates are the Bell states defined above, $|\psi_e^+\rangle, |\psi_e^-\rangle, |\psi_o^+\rangle, |\psi_o^-\rangle$. A key property of the qubit Hamiltonian $\hat{H}_{\rm qb}$ considered in this work is that its dynamics conserves the parity of the Bell states:

$$\hat{H}_{\rm qb}|\psi_e^\pm\rangle = \epsilon|\psi_e^\mp\rangle \quad \text{and} \quad \hat{H}_{\rm qb}|\psi_o^\pm\rangle = 0|\psi_o^\pm\rangle\,. \tag{1.21}$$

This shows that the MZI can be operated as a true parity meter in the sense that each measurement will project the states of the qubits in a parity subspace. It is the parity measurement in the $\hat{\sigma}_z$-basis combined with the qubit Hamiltonian $\hat{H}_{\rm qb}$ and the coupling in this $\hat{\sigma}_z$-basis (no relaxation process) that allows the MZI to act as parity meter for the DQDs during the entire measurement process. In this sense, this weak measurement procedure is the analog of a QND measurement of parity classes.

Having demonstrated that the MZI can be operated as a parity detector during the entire measurement process, we investigate its efficiency in the next section to show that it acts as an ideal detector. The efficiency η is defined as the ratio of the dephasing time over the measurement time, $0 < \eta \leq 1$. If $\eta = 1$, the quantum detector is an ideal detector: it extracts information on the quantum system as fast as it dephases it. In other words the measurement process is the only dephasing source and this is crucial for efficient QIP: the ideality of the detector constitutes a key property for the success of entanglement generation as shown in a next section.

1.3 Efficiency

The quantum efficiency η is defined as :

$$\eta = \frac{\Gamma_{\rm m}}{\Gamma_{\rm deph}}\,, \tag{1.22}$$

where $\Gamma_{\rm deph}$ is the dephasing (or decoherence) rate of the measured quantum system and $\Gamma_{\rm m}$ is the measurement rate of the detector. The most efficient quantum detector one can implement is a quantum-limited detector, $\eta = 1$. It acquires the information about the measured system as fast as the quantum system loses its quantum coherence. $\Gamma_{\rm deph}$ is the inverse of the dephasing time T_2 of the measured quantum system. This rate can be extracted from the off-diagonal elements of the reduced density-matrix of the qubits or from a charge fluctuations approach. In this work we have considered both methods.

1.3.1 The measurement rate

The measurement rate $\Gamma_{\rm m}$ is defined as the inverse of the time needed by the detector to distinguish the signal from the output noise [Korotkov 99] :

$$\Gamma_{\rm m} = \frac{(\Delta I)^2}{4S_{II}}\,. \tag{1.23}$$

S_{II} is the zero-frequency noise spectrum [Büttiker 92a] and $\Delta I = I_o - I_e$ is the difference between the even and odd average currents measured in lead 3 (see Fig. 1.4 b). Given that we look at the linear response in the weak coupling regime this current difference is much smaller than the even or odd currents, $\Delta I \ll I_o, I_e$. We can therefore assume that the shot noise is independent of the qubits' states :

$$S_{II} = \frac{S^e + S^o}{2}\,, \tag{1.24}$$

where $S^{e,o}$ are the zero-frequency shot noise produced by the even and odd configurations:

$$\begin{aligned} S^{e,o} &= \frac{2e^3V}{h} T_{31}^{e,o}\,(1 - T_{31}^{e,o})\,, \\ T_{31}^{e} &= T_{\rm L}R_{\rm R} + T_{\rm R}R_{\rm L} + 2\sqrt{T_{\rm R}R_{\rm L}T_{\rm L}R_{\rm R}}\,\left(1 - \frac{\Delta\chi^2}{2}\right)\,, \\ T_{31}^{o} &= T_{\rm L}R_{\rm R} + T_{\rm R}R_{\rm L} + 2\sqrt{T_{\rm R}R_{\rm L}T_{\rm L}R_{\rm R}}\,. \end{aligned}$$

Using Eq. (1.12), the current difference up to the second order in the small parameter $\Delta\chi$ is :

$$\Delta I = \frac{2e^2V}{h}\sqrt{R_{\rm R}T_{\rm R}R_{\rm L}T_{\rm L}}\,\Delta\chi^2 \tag{1.25}$$

The MZI has a maximum visibility for symmetric QPCs, so the maximum value of $\Gamma_{\rm m}$ is reached for $T_{\rm L} = T_{\rm R} = 1/2$:

$$\Gamma_{\rm m} = \frac{1}{8}\frac{eV}{h}\Delta\chi^2 = \frac{\pi}{4}\frac{eV}{\hbar}\left(\frac{C_\mu}{C_{\rm i}}\right)^2 . \tag{1.26}$$

Here the additional phase $\Delta\chi$ is expressed as a function of the capacitances of the system, $\Delta\chi = 2\pi C_\mu/C_{\rm i}$. In the next section, we calculate the dephasing rates to investigate the efficiency of the MZI as parity meter.

1.4 The dephasing rates

In general, for two qubits, there are six dephasing rates describing the coherence between the states $\{|\uparrow\uparrow\rangle, |\uparrow\downarrow\rangle, |\downarrow\uparrow\rangle, |\downarrow\downarrow\rangle\}$. To calculate them, two approaches are possible: the entanglement approach or the charge fluctuations approach. The entanglement approach [Hackenbroich 00, Clerk 03, Averin 05, Khym 06] aims at writing the reduced density matrix for the qubits; the dephasing terms are extracted from the off-diagonal elements which are also called the coherence terms of the system. The charge fluctuations approach [Büttiker 00a, Pilgram 02, Young 10] consists in investigating the effect of the transit of many electrons through the arms. This transport is stochastic and gives rise to fluctuating potentials in the arms also seen by the DQDs through the coupling. As a consequence the DQDs exhibit a fluctuating phase which leads to dephasing.

1.4.1 Entanglement approach

To extract the dephasing rates within this approach, we have to write the reduced density matrix of the two DQDs at time t, after the transit of N electrons. For this, we first consider the transit of one electron (one scattering event) in a time $\tau \ll t$, τ being the traversal time of one electron in the MZI. We assume that all consecutive scattering events are independent. This is justified by doing a simple estimation of this traversal time. By assuming that the electrons are sensitive to the qubits over a region $L \sim 2\,\mu$m and have a drift velocity $\sim 10^4$ m/s, the traversal time is of the order of 0.2 ns. The dc-bias V between the leads 1 and 3 of the MZI sets the average rate at which electrons are emitted, eV/h. Considering a bias of the order of $20\,\mu$V, this rate is of the order of the traversal time. As a consequence the entanglement generated by the measurement will be the product of the entanglement generated by each independent electron that transfers through the MZI during the measurement time, $t = N\tau = Nh/eV$. Initially the MZI and the two DQDs are completely disentangled :

$$\begin{aligned} |\Psi_0\rangle &= |\Psi_{\rm det}\rangle \otimes |\Psi^{qb}(0)\rangle \\ &= |\Psi_{\rm det}\rangle \otimes \big(\alpha|\uparrow\rangle + \beta|\downarrow\rangle\big) \otimes \big(\gamma|\uparrow\rangle + \delta|\downarrow\rangle\big), \end{aligned} \tag{1.27}$$

where $|\Psi_{\rm det}\rangle$ is the state of the detector before the experiment starts. The complex numbers $\alpha, \beta, \gamma, \delta$ verify $|\alpha|^2 + |\beta|^2 = 1 = |\gamma|^2 + |\delta|^2$. When one electron transits through the arms of the MZI, it interacts with the DQD and the state of the detector and the state of the qubits become entangled. This interaction is used to acquire information about the state of the DQDs. Assuming that the electron can go out in lead 3 and 4 of the MZI, the entangled state of the MZI and the qubits at time τ reads [Averin 05]:

$$\begin{aligned} |\Psi(\tau)\rangle &= \alpha\gamma\, e^{-i\epsilon\tau/\hbar}\,(S_{41}^{\uparrow\uparrow}|4\rangle + S_{31}^{\uparrow\uparrow}|3\rangle) \otimes |\uparrow\uparrow\rangle \\ &+ \beta\delta\, e^{i\epsilon\tau/\hbar}\,(S_{41}^{\downarrow\downarrow}|4\rangle + S_{31}^{\downarrow\downarrow}|3\rangle) \otimes |\downarrow\downarrow\rangle \\ &+ \alpha\delta\,(S_{41}^{\uparrow\downarrow}|4\rangle + S_{31}^{\uparrow\downarrow}|3\rangle) \otimes |\uparrow\downarrow\rangle \\ &+ \beta\gamma\,(S_{41}^{\downarrow\uparrow}|4\rangle + S_{31}^{\downarrow\uparrow}|3\rangle) \otimes |\downarrow\uparrow\rangle. \end{aligned} \tag{1.28}$$

The kets $|3\rangle$ and $|4\rangle$ are the output detector states and S_{ij} are the amplitudes of probabilities to go from input j to output i. These amplitudes depend on the state of the DQDs through the phases χ_1 and χ_2 (see Eq. (1.14) for the expression of S_{31} for instance). The phase factor depending on the qubit bias ϵ describes the free evolution of the qubits during the time τ. The reduced density matrix for the DQDs at time τ is given by :

$$\rho^{qb}(\tau) = \langle 3|\Psi(\tau)\rangle\langle\Psi(\tau)|3\rangle + \langle 4|\Psi(\tau)\rangle\langle\Psi(\tau)|4\rangle. \tag{1.29}$$

The elements of this reduced density matrix can be expressed in the form [Hackenbroich 00]:

$$\rho_{ij}^{qb}(\tau) = \rho_{ij}^{qb}(0) e^{-i\omega_{ij}\tau} A_{ij}. \tag{1.30}$$

For simplicity the density matrix is written in the computational basis $\{|\uparrow\uparrow\rangle, |\uparrow\downarrow\rangle, |\downarrow\uparrow\rangle, |\downarrow\downarrow\rangle\}$ and $\rho^{qb}(0)$ is given by $|\Psi^{qb}(0)\rangle\langle\Psi^{qb}(0)|$. The factor A_{ij} depends on the state of the DQDs through $\Delta\chi_1$ and $\Delta\chi_2$ and on the reflection and transmission probabilities of the left QPC, $R_{\rm L}$ and $T_{\rm L}$. The frequency ω_{ij} depends on ϵ and describes the free evolution corresponding to the matrix element ρ_{ij}. Then at time t, assuming that the N electrons are independent, the reduced density matrix's elements are given by:

$$\rho_{ij}^{qb}(t) = \rho_{ij}^{qb}(0) e^{-i\omega_{ij}t} A_{ij}^{N}. \tag{1.31}$$

By comparing this expression for the off-diagonal elements with the standard expression of the coherence terms, $\rho_{ij}^{qb}(t) = \rho_{ij}^{qb}(0) e^{-i\omega_{ij}t} e^{-\Gamma_{{\rm deph},ij}t}$, we deduce the expressions of the dephasing rates:

$$\Gamma_{{\rm deph},ij} = -\frac{1}{t}\log\left|A_{ij}\right|^{N}. \tag{1.32}$$

At this stage, we obtain 6 different rates as expected for a 4×4 density matrix. As shown below, the parity assumptions reduce the number of dephasing rates to 3, corresponding to the dephasing rates between the parity subspaces. Let us specify that in the entanglement approach, two or more scattering matrices are used, depending

on the number of qubits in the setup. In our case we deal with 4 scattering matrices namely depending on the charge state $\sigma\sigma'$ of the qubits, $S^{\sigma\sigma'}$. In contrast, in the charge fluctuations approach presented below, the scattering properties are expressed in terms of a reference scattering matrix S (scattering matrix in the absence of the qubits) and in terms of functional derivatives with regards to potential variations. The two approaches are connected by :

$$S^{\sigma\sigma'} = S + \frac{\partial S}{\partial U}\delta U^{\sigma\sigma'} + \dots , \tag{1.33}$$

where $\delta U^{\sigma\sigma'}$ is calculated self-consistently [Büttiker 00a, Büttiker 00b, Pilgram 02]. This provides the capacitance fraction in the entanglement approach. In our case the different scattering matrices differ only through phases, i.e $\Delta\chi = 2\pi C_\mu/C_i$.

Dephasing rates under the parity measurement assumptions

With the entanglement approach we obtain six different dephasing rates which reduce to three rates when taking into account the parity assumptions, Eqs. (1.16) and (1.19):

$$\Gamma_{eo} = \pi R_{\rm L} T_{\rm L} \frac{eV}{\hbar}\left(\frac{C_\mu}{C_{\rm i}}\right)^2 , \tag{1.34a}$$

$$\Gamma_{ee} = 4\pi R_{\rm L} T_{\rm L} \frac{eV}{\hbar}\left(\frac{C_\mu}{C_{\rm i}}\right)^2 , \tag{1.34b}$$

$$\Gamma_{oo} = 0. \tag{1.34c}$$

Γ_{ij} is the dephasing rate between the parity classes i and j, where i and j are either e for the even class or o for the odd class. These results reflect the perfect anticorrelation between the events on the upper and lower arms of the MZI due to current conservation in the system [Seelig 01].

Importantly, these rates show that the odd subspace is not subject to dephasing during the parity measurement process. If the qubits are driven in an odd Bell state during the measurement, this entangled state will not decohere within our model. To the contrary, the parity measurement induces dephasing in the even subspace. This can be understood when looking at Fig. 1.4b). Even if the two even states $|\uparrow\uparrow\rangle$ and $|\downarrow\downarrow\rangle$ produce the same current I_e under the parity assumptions, the wave-functions of these two states differ by a phase, namely $2\Delta\chi$. It is this phase difference which leads to the non-zero dephasing rate in the even subspace Γ_{ee}. As long as the wave-functions are different, this dephasing process is unavoidable.

1.4.2 Charge fluctuations approach

This approach investigates the fluctuating potentials in the arms of the MZI and in the DQDs, arising from the quantum statistical nature of electron transport. For

clarity, we first present the method for the case of a single qubit coupled to a detector before presenting the results for our setup which consists in two qubits coupled to the detector.

Case of one qubit coupled to a detector

In the simple case of one two-level system coupled to a detector, the dephasing rate is given by [Levinson 97, Büttiker 00a, Pilgram 02, Young 10] :

$$e^{-\Gamma_{\rm deph}t} = \langle e^{i\delta\phi(t)}\rangle_U, \tag{1.35}$$

where U is the fluctuating potential of the detector and $\delta\phi(t)$ is the fluctuating phase acquired by the two-level system as a consequence of U. Assuming that the phase $\delta\phi(t)$ is Gaussian distributed, the dephasing rate can be written as [Young 10]:

$$e^{-\Gamma_{\rm deph}t} = \langle e^{i\delta\phi(t)}\rangle_U = e^{-\frac{1}{2}\langle\delta\phi(t)^2\rangle_U}, \tag{1.36}$$

with

$$\langle\delta\phi(t)^2\rangle_U = \left(\frac{e}{\hbar}\right)^2 S_{UU}(0)\, t \tag{1.37}$$

Here $S_{UU}(0)$ is the spectral density of the voltage fluctuations at zero frequency. This spectral density can be expressed in terms of a non-equilibrium charge relaxation resistance R_v [Büttiker 00a, Martin 00, Pilgram 02] :

$$S_{UU}(0) = \left(\frac{C_\mu}{C_i}\right)^2 R_v|eV|\,.$$

If spatial variations of the potential can be neglected, only a single potential U counts and the non-equilibrium charge relaxation resistance is given by:

$$R_v = \frac{h}{e^2}\frac{\mathrm{Tr}[\mathcal{N}_{12}\mathcal{N}_{12}^*]}{N^2}\,. \tag{1.38}$$

$\mathcal{N}$ is the Wigner-Smith time delay matrix (a density-of-states matrix) from which the density of states N can be calculated by taking the trace of $\mathcal{N}$. This density-of-states matrix is determined by the region inside the detector where the potential U is non zero [Martin 00]:

$$\mathcal{N}_{\alpha\beta}(E) = \frac{-1}{2\pi i}\sum_\nu S^\dagger_{\nu\alpha}(E,U)\frac{\partial S_{\nu\beta}(E,U)}{e\partial U}\,. \tag{1.39}$$

In Appendix 4.2, we show how to derive self-consistently the potential U from the density-of-state matrix $\mathcal{N}$ of the upper arm of the MZI coupled to a charge. This illustrates these definitions.

Case of two qubits coupled to the detector

Adapting this method to the case of two DQDs coupled to the MZI, we assume two fluctuating potentials induced by the transfer of the electrons, $U_1(t)$ on the upper arm and $U_2(t)$ on the lower arm. Through the coupling capacitances C_1, both DQDs will acquire a fluctuating phase on top of their free evolution phase, $\delta\phi_1(t)$ for the upper DQD and $\delta\phi_2(t)$ for the lower DQD, which will depend on the state of the DQDs. As in the simple case presented above, the correlators $\langle\delta\phi_i(t)\delta\phi_j(t)\rangle_U$ are proportional to the voltage fluctuations $S_{U_iU_j}(0)$ which are themselves proportional to the non-equilibrium charge relaxation resistance $R_v^{(ij)}$ given by:

$$R_v^{(ij)}=\frac{h}{e^2}\frac{\mathrm{Tr}[\mathcal{N}_{12}^{(i)}\mathcal{N}_{12}^{(j)*}]}{N^{(i)}N^{(j)}},\quad \mathcal{N}_{\alpha\beta}^{(i)}=\frac{1}{2\pi i}\sum_\nu S_{\nu\alpha}^{(i)\dagger}\frac{dS_{\nu\beta}^{(i)}}{d\chi_i}\frac{d\chi_i}{dE_i}. \tag{1.40}$$

The indices $(i,j)=1,2$ stand for the upper and lower arms. The phases χ_1 and χ_2 are those defined by Eqs. (1.10) and (1.11) and the Wigner-Smith matrix can be calculated from the scattering matrix given by Eq. (1.14).

We find the following expressions for the correlators:

$$\langle\delta\phi_1(t)\delta\phi_2(t)\rangle_U=-2\pi R_\mathrm{L}T_\mathrm{L}\frac{eVt}{\hbar}\left(\frac{C_\mu}{C_\mathrm{i}}\right)^2, \tag{1.41}$$

$$\langle\delta\phi_1(t)^2\rangle_U=\langle\delta\phi_2(t)^2\rangle_U=2\pi R_\mathrm{L}T_\mathrm{L}\frac{eVt}{\hbar}\left(\frac{C_\mu}{C_\mathrm{i}}\right)^2. \tag{1.42}$$

These correlators show that the events on the upper arm and lower arm are perfectly anticorrelated as expected from the conservation of the current. Due to this perfect anticorrelation, one finds by calculating the six dephasing rates that they reduce to three when taking into account the parity assumptions, Eqs. (1.16) and (1.19) :

$$\Gamma_{eo} = \frac{1}{2t}\left\langle\delta\phi_{1,2}(t)^2\right\rangle_U=\pi R_\mathrm{L}T_\mathrm{L}\frac{eV}{\hbar}\left(\frac{C_\mu}{C_\mathrm{i}}\right)^2, \tag{1.43}$$

$$\Gamma_{ee} = \frac{1}{2t}\left\langle\left(\delta\phi_1(t)-\delta\phi_2(t)\right)^2\right\rangle_U=4\pi R_\mathrm{L}T_\mathrm{L}\frac{eV}{\hbar}\left(\frac{C_\mu}{C_\mathrm{i}}\right)^2, \tag{1.44}$$

$$\Gamma_{oo} = \frac{1}{2t}\left\langle\left(\delta\phi_1(t)+\delta\phi_2(t)\right)^2\right\rangle_U=0. \tag{1.45}$$

It is interesting to notice that the assumption $\Delta\chi_1=\Delta\chi_2=\Delta\chi$ to measure only one current in the odd subspace is equivalent to assume a perfect anticorrelation between $\delta\phi_1(t)$ and $\delta\phi_2(t)$, $\Gamma_{oo}=0$. These dephasing rates are exactly those obtained with the entanglement approach. By comparing them to the measurement rate, we can now characterize the MZI as parity detector by its efficiency.

1.4.3 Efficiency of the MZI as parity detector

The ideality of a detector depends only on the information that this detector is able to measure. Under the parity assumptions, the MZI operates as a parity

detector during the entire measurement process and therefore the dephasing rate that has to be taken into account for the efficiency η is Γ_{eo}, i.e the dephasing rate between the even and odd classes. For half-transmitting QPCs ($R_{\rm L}=R_{\rm R}=1/2$) for which the measurement rate is maximal, the MZI is an ideal parity detector :

$$\eta_{\max}=\frac{\Gamma_{\rm m}(R_{\rm L}=R_{\rm R}=1/2)}{\Gamma_{eo}(R_{\rm L}=1/2)}=1\,. \tag{1.46}$$

For symmetric QPCs, the MZI acquires information on the parity of the qubits as fast as it dephases them. The ideality of the MZI reduces the possible sources of decoherence during the measurement process, enhancing thus the probabilities to get entangled states. Importantly the dephasing rates in the two parity subspaces differ and in particular the dephasing rate in the odd subspace is zero. We show in the next section that this makes the MZI a deterministic source of entanglement when the odd current is measured. By initializing both DQDs in a given state, they end in a determined odd Bell state if the odd current is measured. The probability of entanglement is 1/2 and this Bell state does not dephase. To the contrary, the measurement of an even current at the output of the MZI puts the qubits in a superposition of the even Bell states $|\Psi_e^+\rangle$ and $|\Psi_e^-\rangle$ which dephases with the characteristic rate Γ_{ee}. The probabilities for the qubits to be in a given Bell states is extracted from the density operator, calculated by solving a stochastic differential equation for the evolution of the qubits.

1.5 Creation of entanglement

The entanglement of the DQDs through the measurement process is investigated by solving the differential stochastic equation governing the evolution of the DQDs [Korotkov 99, Korotkov 02, Jordan 06]:

$$\begin{aligned}\dot{\rho}_{ij} &= -\frac{i}{\hbar}[\hat{H}_{\rm qb},\rho]_{ij}-\Big(\frac{(I_i-I_j)^2}{4S_{II}}+\gamma_{ij}\Big)\rho_{ij}\\ &\quad+\xi(t)\Big(I_i+I_j-2\sum_{k=1}^{4}\rho_{kk}I_k\Big)\frac{\rho_{ij}}{S_{II}}.\end{aligned} \tag{1.47}$$

In the weak coupling regime, the current is the sum of an average current $\bar{I}$ and a noisy term $\xi(t)$ which is the random white noise of the output characterized by $\langle\xi(t)\xi(0)\rangle=2S_{II}\delta(t)$. Here S_{II} is the zero-frequency noise spectrum of the MZI (see Eq. (1.24)). In the stochastic differential equation, the average current is expressed in terms of the diagonal elements of the density matrix:

$$\bar{I}=\sum_k \rho_{kk}I_k$$

where ρ_{kk} is the density matrix's element associated with the state $|\psi_k\rangle$. The indices $k=1,2,3,4$ correspond to the four Bell states $\{|\psi_e^+\rangle,|\psi_e^-\rangle,|\psi_o^+\rangle,|\psi_o^-\rangle\}$ defined

in Eqs. (1.3) and (1.4). I_i corresponds to the average current the state $|\psi_i\rangle$ would produce. Given that the MZI acts as parity meter, $I_1 = I_2 = I_e$ and $I_3 = I_4 = I_o$, where I_e and I_o are the even and odd currents.

The differential equation Eq. (1.47) can be decomposed into three terms. The first term describes the standard Schrödinger evolution due to the qubit Hamiltonian $\hat{H}_{\mathrm{qb}}$. The possible sources of decoherence for the qubits are considered in the second term of this equation. They consist of the term $(I_i - I_j)^2/(4S_{II})$ corresponding to the measurement rate (compare to Eq. (1.23)) and a term γ_{ij} which takes into account additional sources of dephasing. The last term describes the backaction of the measurement result on the qubits evolution through the noise $\xi(t)$ of the current. In this work, we are not interested in the entanglement genesis [Williams 08] so we look at the time-average corresponding equation:

$$\dot{\rho}_{ij} = -\frac{i}{\hbar}[\hat{H}_{\mathrm{qb}}, \rho]_{ij} - \Big(\frac{(I_i - I_j)^2}{4S_{II}} + \gamma_{ij}\Big)\rho_{ij}. \tag{1.48}$$

For the different parity subspaces we have to take into account the following dephasing terms:

- In the odd subspace, the measurement rate is zero, $I_3 = I_4 = I_o$, and $\Gamma_{oo} = 0$ as shown in the previous section. The odd subspace does not experience any dephasing processes.

- In the even subspace, $I_1 = I_2 = I_e$ so that the measurement rate is also zero. However $\Gamma_{ee} \neq 0$ and has to be taken into account in the stochastic differential equation.

- Between the odd and even subspaces, the only dephasing term that counts is the measurement rate as the MZI acts as ideal parity detector, $\Gamma_m = \Gamma_{eo}$.

The linear differential equation Eq. (1.48) can be solved analytically to find the elements of the density operator ρ. By definition, the diagonal elements $\rho_{ii}(t)$ determine the probabilities to be in the state $|\psi_i\rangle$ at time t: the probability $P_i(t)$ to be in the Bell state $|\psi_i\rangle$ is given by $\rho_{ii}(t)$. For the parity subspaces, the probability to be in the even subspace is given by $P_e(t) = \rho_{11}(t) + \rho_{22}(t)$ and the probability to be in the odd subspace is given by $P_o(t) = \rho_{33}(t) + \rho_{44}(t)$. These probabilities depend in general on the initial state of the two qubits given below by Eq. (1.49). In our setup, considering a qubit Hamiltonian without tunneling, a classical initial state (a fully mixed state) will remain classical. Therefore we consider an initial state in which the individual qubits are in superposition states,

$$|\Psi_{qb}\rangle = (\alpha|\uparrow\rangle + \beta|\downarrow\rangle) \otimes (\gamma|\uparrow\rangle + \delta|\downarrow\rangle)\,, \tag{1.49}$$

where $\alpha, \beta, \gamma, \delta$ are complex numbers such that $|\alpha|^2 + |\beta|^2 = |\gamma|^2 + |\delta|^2 = 1$.

From Eq. (1.48), we find the probabilities to measure outcomes in the different parity subspaces:

$$P_e = |\alpha|^2|\gamma|^2 + |\beta|^2|\delta|^2, \tag{1.50}$$
$$P_o = |\alpha|^2|\delta|^2 + |\beta|^2|\gamma|^2. \tag{1.51}$$

As expected from a qubit Hamiltonian that does not mix the parity classes, Eqs. (1.50) and (1.51) do not depend on time. The electronic MZI in this setup works as perfect parity meter during the entire measurement process. Each time an electron transits through the arms, the DQDs are weakly projected onto a subspace with a definite parity. In our QND-limit (see Section III), we can approximate the weak measurement with many projective measurements as the backaction does not take place.

The probabilities for the qubits to be in one of the Bell states are given by:

$$P_e^+(t) = \frac{1}{2}\Big(|\alpha|^2|\gamma|^2 + |\beta|^2|\delta|^2 + 2\mathrm{Re}\big\{\alpha\gamma\beta^*\delta^* e^{-i2\epsilon t/\hbar}\big\}e^{-\Gamma_{ee}t}\Big) \tag{1.52}$$
$$P_e^-(t) = \frac{1}{2}\Big(|\alpha|^2|\gamma|^2 + |\beta|^2|\delta|^2 - 2\mathrm{Re}\big\{\alpha\gamma\beta^*\delta^* e^{-i2\epsilon t/\hbar}\big\}e^{-\Gamma_{ee}t}\Big) \tag{1.53}$$
$$P_o^+ = \frac{|\alpha\delta+\beta\gamma|^2}{2}, \tag{1.54}$$
$$P_o^- = \frac{|\alpha\delta-\beta\gamma|^2}{2}. \tag{1.55}$$

In the odd subspace the probabilities to entangle the qubits depend only on the initial state via the complex coefficients α, β, γ and δ. This result is again expected from the qubits' dynamics which induces no evolution in the odd subspace, the odd Bell states being eigenstates of $\hat{H}_{\mathrm{qb}}$ (see Eq. (1.21)). As a consequence, by choosing specific complex coefficients for the initial state, one can know with probability one in which odd Bell state the qubits are if the odd current is measured. Furthermore there is no dephasing in this odd parity subspace. This shows that the MZI works as a deterministic source of entanglement in the odd subspace.

In the even subspace, the evolution is more complex. Although the qubit Hamiltonian conserves parity, it induces an evolution between the two even Bell states due to the bias ϵ:

$$\hat{H}_{\mathrm{qb}}|\psi_e^+\rangle = \epsilon|\psi_e^-\rangle \tag{1.56}$$
$$\hat{H}_{\mathrm{qb}}|\psi_e^-\rangle = \epsilon|\psi_e^+\rangle. \tag{1.57}$$

If the measurement outcome is the even current, the qubits will remain in the even parity subspace during the entire measurement process but they will undergo oscillations between the even Bell states with a frequency $2\epsilon/\hbar$, whatever the complex coefficients $\alpha, \beta, \gamma, \delta$ are. It is not possible to determine in which even Bell state the

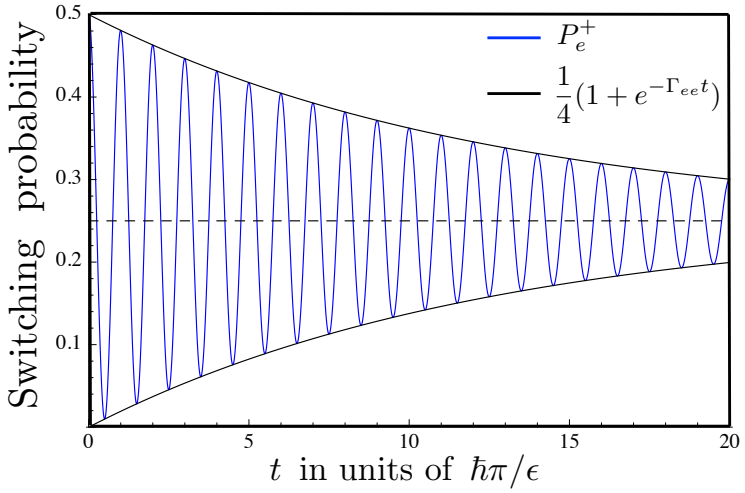

Figure 1.5: Probability to be in the even Bell state $|\psi_e^+\rangle$ as a function of time (blue curve) (in units of $\hbar\pi/\epsilon$). The qubits undergo oscillations with frequency $2\epsilon/\hbar$ between the two even Bell states. Due to the finite dephasing rate Γ_{ee}, the amplitude of these oscillations decay with time. As an illustration, we choose $\Gamma_{ee} = 0.08\epsilon/\hbar\pi$. The envelope is the thin black line. At long times, the probability tends to the value of 0.25 (thin dashed line). The qubits are not entangled anymore, they are either in the upper state $|\uparrow\uparrow\rangle$ or in the down state $|\downarrow\downarrow\rangle$.

DQDs are entangled, they will be in a superposition state of $|\psi_e^+\rangle$ and $|\psi_e^-\rangle$. Due to the dephasing term Γ_{ee}, this superposition decays with time [1]. To illustrate these properties, we consider below the explicit case of two initial states and we compare the probabilities of getting the different Bell states in the odd and even subspaces.

1.5.1 Illustration of the entanglement properties of the MZI

We consider two product states as initial states defined by $\alpha, \beta, \gamma, \delta = \pm 1/\sqrt{2}$ and we compare their probabilities. These states present the strong advantage to be implementable with the experimental state-of-the-art of solid-state quantum dots by applying external gate voltages to the DQDs [Hayashi 03]. The first state corresponds to $\alpha = \beta = \gamma = \delta = 1/\sqrt{2}$ whereas the second one corresponds to $\alpha = \beta = \gamma = -\delta = 1/\sqrt{2}$:

$$|\Psi_1\rangle = \frac{1}{2}\left(|\uparrow\rangle + |\downarrow\rangle\right) \otimes \left(|\uparrow\rangle + |\downarrow\rangle\right), \tag{1.58}$$

$$|\Psi_2\rangle = \frac{1}{2}\left(|\uparrow\rangle + |\downarrow\rangle\right) \otimes \left(|\uparrow\rangle - |\downarrow\rangle\right) \tag{1.59}$$

It is straightforward to see that $P_e = P_o = 1/2$ in both cases. As expected the even probabilities exhibit an oscillating behavior between the two even Bell states which

[1] In Ref.[Haack 10], this decay is omitted.

decays at the rate Γ_{ee}. The probabilities for $|\Psi_1\rangle$ are:

$$P_e^+(t) = \frac{1}{4}\big(1+\cos(2\epsilon t/\hbar)e^{-\Gamma_{ee}t}\big), \tag{1.60}$$

$$P_e^-(t) = \frac{1}{4}\big(1-\cos(2\epsilon t/\hbar)e^{-\Gamma_{ee}t}\big)\,. \tag{1.61}$$

Figure 1.5 shows $P_e^+(t)$ as a function of time. The probabilities for $|\Psi_2\rangle$ only differ by a $\pi/2$-phase. In contrast the probabilities in the odd subspace are time independent and allow to distinguish between the two odd Bell states. Starting with $|\Psi_1\rangle$, one finds:

$$P_o^+ = 1/2, \quad P_o^- = 0, \tag{1.62}$$

whereas starting with $|\Psi_2\rangle$, one gets:

$$P_o^+ = 0, \quad P_o^- = 1/2. \tag{1.63}$$

This example clearly shows that the electronic MZI acting as parity meter entangles the qubits with probability one ($P_e + P_o = 1$) and allows to know exactly in which odd Bell state the qubits are if the current I_o is measured. In a more general way, if one writes the initial coherent superposed state for both qubits as

$$|\Psi_{\text{in}}\rangle = \frac{1}{2}\left(|\uparrow\rangle + e^{i\eta_1}|\downarrow\rangle\right) \otimes \left(|\uparrow\rangle + e^{i\eta_2}|\downarrow\rangle\right), \tag{1.64}$$

where η_1 and η_2 are phases specific to the upper and lower qubit respectively, then the class of states that allows deterministic generation of odd Bell states is defined by:

$$\eta_2 - \eta_1 = 0 \quad \text{modulo} \quad \pi. \tag{1.65}$$

This property makes it a very interesting quantum detector and entangler for further experiments.

1.6 Conclusion

With this work, we have presented an investigation of the MZI as quantum detector of two DQDs characterized by a bias energy and no tunneling between the states. Thanks to the control of the flux and of the transparency of the QPCs that can be tuned to specific values, the MZI can be operated as an ideal parity detector. In this regime, only two currents are distinguishable at the output of the interferometer, one corresponding to the even parity class and the other one for the odd parity class. Such a measurement is crucial to generate the source of entanglement required for efficient quantum information processing.

Compared to previous works on parity detection, we have considered an Hamiltonian for the qubits which commutes with the parity operator. In this situation, the free evolution of the qubits conserves the parity classes and the measurement is an analog to a QND measurement of the parity classes. To characterize the efficiency of such a detector, we have calculated its measurement rate and the dephasing rates in the different parity subspaces using two distinct approaches. One approach follows the qubit's point of view by extracting the dephasing rates from the reduced density matrix of the qubits. The other approach is from the detector's point of view, we investigated the charge fluctuations in the arms of the MZI which induce a fluctuating phase for the qubits. When looking at the time-average evolution of the qubits, this fluctuating phase leads to dephasing. Importantly we have found that the odd subspace does not undergo any dephasing processes. If the odd current is measured, our MZI acts as a deterministic source of entanglement for the qubits.

In this work, we have focused on the time-average evolution of the qubits and this set of results encourages the implementation of such a setup in mesoscopic physics. The regime of weak coupling between the detector and the qubits that we consider here motivates a further investigation. In particular, the stochastic differential equation describing the evolution of the qubits in this regime allows to take into account the measurement outcome in the evolution of the qubits: the noise spectrum of the current is correlated with the fluctuating phase of the qubits. By implementing feed-back loops to reconstruct this phase, it could therefore be possible to avoid measurement-induced dephasing. Such proposals are of strong interest for instance to generate steady entangled states.

Chapter 2

Coherence length of single-electron sources from Mach-Zehnder interferometry

Contents

2.1 Introduction

Recently high-frequency on-demand single-electron sources have been realized experimentally, a step that presumably constitutes one of the main achievements in the field of mesoscopic physics, both theoretically and experimentally. These sources can be operated in a regime in which they emit single charges at a controlled time, heralding a new field in low temperature electron physics. Tunable multiparticle exchange, two-particle interference effects and entanglement [Ol'khovskaya 08, Splettstoesser 09] have already been proposed as promising avenues towards quantum information processing [Bennett 00]. However, for further key advances in quantum electronics, the characterization of the emitted single-electron quantum state by its coherence properties is crucial. In particular, the coherence length of a single particle sets the distance over which this particle is able to interfere with itself at the output of an interferometer: it is therefore at the origin of quantum single-particle interferences. This coherence length is experimentally accessible by measuring the first-order correlation function in an interferometry setup. It probes the correlation between the amplitudes at two distinct points in time-space.

More generally, to characterize the coherence properties of a state, Glauber introduced the correlations functions of order n, $G^{(n)}$ [Glauber 63a, Glauber 63b, Glauber 63c]. The first-order correlation function $G^{(1)}$ is the one that characterizes the spatial or temporal coherence of a field or a state (it does not distinguish between a classical field and a quantum field), whereas the second-order correlation function $G^{(2)}$ tests the quantum statistics of the particles, visible in the antibunching of bosons or of fermions in an Hanbury-Brown and Twiss experiment for instance. In quantum optics [Mandel 99] and atom optics, the coherence length of single-photon sources [Lounis 05, Michler 00, Santori 02, Kiraz 04, Flagg 10] and single-atoms sources [Cronin 09] has been experimentally measurable and controllable for a long time. When using the new on-demand single-electron source (SES) of Fève *et al.* realized at the Laboratoire Pierre Aigrain in Paris [Fève 07], it becomes now possible to address experimentally in mesoscopics this fundamental property of a single-particle state, its coherence length.

To determine this length, we proposed to couple this on-demand SES to one of the inputs of an electronic Mach-Zehnder interferometer (MZI). This interferometer is built in the quantum Hall regime and the output current exhibits Aharonov-Bohm (AB) oscillations as a function of the magnetic flux enclosed by the arms. The interference part of the current corresponds to the first-order correlation function $G^{(1)}$. By measuring the decrease of the amplitude of these AB oscillations as a function of the asymmetry of the interferometer, we extract the coherence time and equivalently the coherence length of the emitted single electrons. Importantly we derive an analytical expression of the temporal first-order correlation function of the emitted particles in terms of the scattering matrix of the source.

This chapter is organized as follows. Below, we review the different proposals for single-charge emitters and in particular the SES realized at the Laboratoire Pierre Aigrain [Fève 07]. This source consists of a quantum capacitor driven by a time-periodic voltage. To take into account this periodic driving, we make use of a Floquet scattering matrix approach to describe the source. We therefore introduce the Floquet theorem and then we define the correlation functions introduced by Glauber to characterize the coherence properties of single particles. In the second section, we present our results for the first-order correlation function $G^{(1)}$ in terms of the scattering matrix of the source. From the $G^{(1)}$ function, we extract the analytical expression of the coherence length of the single particles emitted by the SES. Importantly these analytical calculations have been done in the two regimes in which the quantum capacitor can be operated as presented below, the adiabatic regime and non-adiabatic regimes. The $G^{(1)}$ function and the coherence length are experimentally accessible in a time-resolved measurement of the current at the output of the MZI. Given that these sources work in the GHz frequency domain, we propose to measure average quantities such as the charge and the mean of the squared current to overcome experimental difficulties related to a measurement resolved in time.

2.1.1 Single-charge emitters

Thus far, most of the electronic sources in mesoscopic experiments have consisted of metallic contacts or superconducting contacts [Imry 02, Nazarov 03]. These sources allow the injection of a quasi-regular train of single particles on top of the Fermi sea. When considering a dc-source biased by a voltage V, the particles are emitted *on average* each h/eV. The energy window of the particles is given by the energy bias eV which can be quite large depending on the potential V. Dc-sources have enabled the investigation of fundamental quantum mechanical effects or principles such as the complementary principle in an AB interferometer [Chang 08]. To go further in the quantum regime, a source that injects single particles at a controlled time and within a finite energy range is required. Such sources work in the GHz frequency domain and have been extensively investigated in the past years. In this introduction, we review some of the existing experiments for which a quantized current has been measured.

Quantum dots in the strong Coulomb blockade regime

The first proposals to inject on-demand single particles rely on a metallic island in the strong Coulomb blockage regime [Averin 91, Pothier 92, Keller 96]. Such a mesoscopic device is characterized by two energy scales : the level spacing Δ originating from the quantization of the orbital motion inside the dot and the Coulomb charging energy $E_C = e^2/C$, where C is the total geometrical capacitance of the dot,

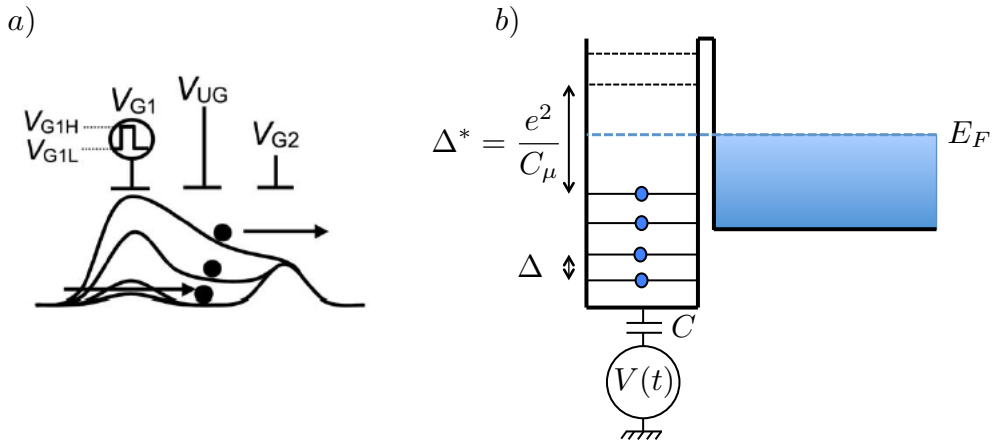

Figure 2.1: a) Quantized pumps for single electrons. Two gate voltages V_{G1} and V_{G2} allow to trap a single electron and to release it at a given time by changing the height of the potential V_{G1} to its higher and lower values $V_{\mathrm{G1,H/L}}$. The upper gate voltage V_{UG} controls the number of transferred charges. Figure taken from Ref [Fujiwara 08]. b) Quantum dot in the strong Coulomb blockade regime driven by a time-dependent potential $V(t)$. The energy Δ^* required to add or remove an electron is given by the electrochemical capacitance C_μ which takes into account the Coulomb blockade energy $E_C = e^2/C$ and the level spacing energy Δ.

see Fig. 2.1b. This Coulomb charging energy reflects the Coulomb repulsion between the electrons. To add one electron to the quantum dot, an energy $\Delta^* = \Delta + E_C$ has to be provided. This energy Δ^* can be written as:

$$\Delta^* = \frac{e^2}{C_\mu} = \Delta + \frac{e^2}{C}\,. \tag{2.1}$$

The electrochemical capacitance C_μ results from the addition in series of the geometrical capacitance C and the quantum capacitance $C_q = e^2/\Delta$:

$$\frac{1}{C_\mu} = \frac{1}{C} + \frac{1}{C_q}\,. \tag{2.2}$$

In a metallic island, the level spacing Δ is much smaller than the charging energy so the quantum capacitance C_q tends to infinity and the energy that has to be supplied to promote one level of the dot above the Fermi sea is equal to the charging energy. This energy E_C can be supplied for instance by applying a time-dependent gate voltage $V(t)$ on the quantum dot. At a given time several levels of the dot are shifted above the Fermi sea with roughly the same energy E_C. Consequently the Pauli principle ensures that only one single particle tunnels outside the dot and a quantized current has been measured experimentally as long as the temperature of the system remains below the charging energy, $k_B T \ll E_C$. These metallic quantum dots allow the emission of single electrons but in a large energy window corresponding to E_C. This statistical distribution in energy smears out the coherent properties

of the single particles, making difficult a manipulation of single particle states for quantum information.

Charge pumps

Other proposals consist in quantized charge pumps working at a GHz frequency [Kouwenhoven 91, Blumenthal 07, Fujiwara 08, Maire 08]. Single electrons are trapped and released by a time-dependent potential created by three gates applied directly on a quantum wire, as shown in Fig. 2.1. The two outer gates (V_{G1} and V_{G2}) define a quantum dot whereas the middle gate (V_{UG}) permits the control of the potential of the dot. By increasing gradually the left and middle potentials, a populated quantum dot is formed and pumping of single charges is achieved. Trapped electrons are emitted to the right of the asymmetric potential. With such a charge pump, a quantized current has been measured.

The "Lorentzian" source

Two different proposals allow the injection of single particles at a given time and within a finite energy range which is narrow compared to the charging energy E_C of a quantum dot or compared to the energy window eV of a dc-source. One of them consists in exciting the Fermi sea by applying a time-dependent potential $V(t)$ which fulfills an "area quantization condition":

$$\frac{e}{\hbar}\int V dt = n\,,$$

where n corresponds to the number of charges per pulse. This leads to the emission of single particles when $n = 1$ but also to the emission of additional neutral particles, electron-hole (e-h) pairs, which randomize the number of emitted single particles [Ivanov 93, Levitov 96, Keeling 06]. To avoid these additional excitations, Keeling *et al.* have shown that choosing a Lorentzian shape for the potential does not create the spurious excitations in absence of interactions [Keeling 06]. The first experimental results confirm these predictions [Dubois 12]: different potentials have been applied to the Fermi sea : a sinusoidal, a square and a Lorentzian potential. It is only with the latter one that no e-h pairs are emitted when the average charge per pulse is quantized. With these Lorentzian pulses, single particles are emitted within a time range determined by the width of the Lorentzian pulse. This makes this source an important candidate for single-electron sources for future experiments in mesoscopic physics.

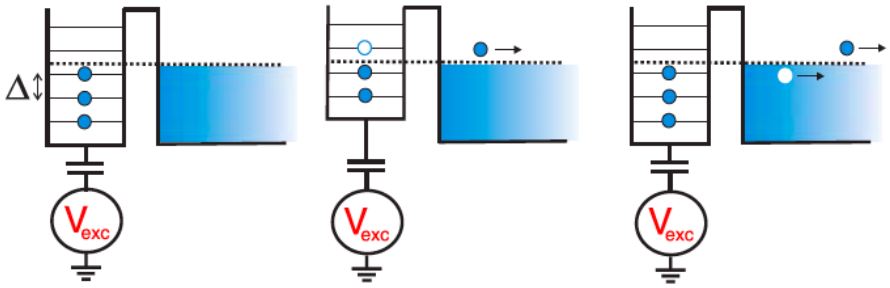

Figure 2.2: Experimental setup of the single-electron source based on the mesoscopic capacitor. By applying a top gate, this semiconductor quantum dot has a charging energy much smaller than the level spacing Δ. By applying a periodic potential V_{exc} which provides an energy Δ, the energy levels are promoted periodically above and below the Fermi energy. On average on electron and a hole are emitted per period of the potential. Figure taken from Ref. [Fève 07].

The mesoscopic capacitor

A second proposal is based on a mesoscopic capacitor [Büttiker 94] driven by a periodic potential which has been experimentally realized at the LPA in Paris [Gabelli 06, Fève 07, Mahé 10]. The mesoscopic capacitor consists in a quantum dot on which a top-gate is applied as shown in Fig. 2.2. This gate screens the charges, making the charging energy E_C of the dot comparable or smaller than the level spacing Δ. By modulating this top-gate with a time-periodic potential, the energy levels of the dot are shifted above and below the Fermi sea one by one. In this situation, the energy uncertainty of the emitted particle state corresponds to the energy width of the promoted level and the single-particle state is closer to the Heisenberg uncertainty equality. The single particles tunnel into an edge state through a quantum point contact (QPC) characterized by its transmission probability T_{SES}. This source is operated in two regimes which depend on the shape of the potential. If the potential changes smoothly in time compared to the dwell time of the particle $\tau_D = h/(T_{\mathrm{SES}}\Delta)$, the potential is constant over the time spent by a particle inside the cavity. This corresponds to the *adiabatic* regime and can be reached for instance by applying a sinusoidal potential. To the contrary, when the potential varies much faster than the time spent by a particle inside the cavity, the capacitor is operated in the *non-adiabatic* regime. This is for example the case with a square potential. Experimentally a quantized current has been measured in both regimes and current-current correlations exhibit sub-poissonian statistics [Fève 07, Mahé 10, Albert 10]. An Hanbury-Brown and Twiss experiment was also realized very recently to better characterize the resolution in energy of the emitted quantum state [Bocquillon 12].

One important difference between the Lorentzian source and the mesoscopic capacitor has to be pointed out when looking at the charges that are emitted: the mesoscopic capacitor emits on average one electron *and* one hole per period of the

potential whereas the Lorentzian potential can be considered as a *pure* single-electron source. The mesoscopic capacitor is therefore a pure ac-source, the dc-component of the average current is zero.

For further experiments like the orbital entanglement of two of these emitted particles, an additional characterization of the emitted quantum state has to be done through its coherence length. Investigating the temporal first-order correlation function of these single particles emitted on demand has been the subject of the work presented in this chapter done in collaboration with M. Moskalets, J. Splettstoesser and M. Büttiker. We consider explicitly charges emitted by the mesoscopic capacitor and by the Lorentzian potential.

2.1.2 The Floquet theorem

Currently the on-demand single electron sources are driven by a periodic potential that shifts the levels of the cavity above and below the Fermi sea or that shakes directly the Fermi sea. Analytical expressions of the current emitted by these sources have been obtained by using a Floquet formalism, which allows to take into account the time-periodic potential of the system. In this paragraph, we recall the Floquet theorem which is the analog of the Bloch theorem, but for Hamiltonians which are periodic *in time*. According to the Floquet theorem, the solution of the Schrödinger equation with a time-periodic Hamiltonian $\mathcal{H}(t) = \mathcal{H}(t+\mathcal{T})$ can be written as a plane wave which multiplies a function having the periodicity of the Hamiltonian :

$$\begin{aligned} \Psi(t) &= e^{-iEt/\hbar}\phi(t) \quad \text{with} && \text{(2.3a)} \\ \phi(t) &= \phi(t+\mathcal{T})\,, && \text{(2.3b)} \end{aligned}$$

where $\mathcal{T}$ is the period of the Hamiltonian. The proof of the theorem is similar to the proof of the Bloch theorem [Ashcroft] and we outline it here. Given the periodicity in time of the Hamiltonian, we can define a translation operator in time $\theta_{\mathcal{T}}$ such that $\theta_{\mathcal{T}}\Psi(t) = \Psi(t+\mathcal{T})$. This operator and the Hamiltonian commute, $[\mathcal{H}(t), \theta_{\mathcal{T}}] = 0$, which implies that they are diagonalizable in the same basis :

$$\begin{aligned} \mathcal{H}(t)\Psi(t) &= i\hbar\partial_t\Psi(t) \\ \theta_{\mathcal{T}}\Psi(t) &= C_{\mathcal{T}}\Psi(t) = \Psi(t+\mathcal{T})\,, && \text{(2.4)} \end{aligned}$$

The factor $C_{\mathcal{T}}$ is a constant which depends on the period $\mathcal{T}$. Furthermore if we apply twice the translation operator to the solution Ψ, we get :

$$\theta_{\mathcal{T}}\theta_{\mathcal{T}'}\Psi(t) = \Psi(t+\mathcal{T}+\mathcal{T}') = \theta_{\mathcal{T}+\mathcal{T}'}\Psi(t)$$

which implies

$$C_{\mathcal{T}}C_{\mathcal{T}'} = C_{\mathcal{T}+\mathcal{T}'}\,.$$

The constant C is therefore an exponential factor. From the normalization condition of the wave-function, we obtain $C_{\mathcal{T}} = e^{-iE\mathcal{T}/\hbar}$ where E has the dimension of an energy. The Floquet theorem reads:

$$\Psi(t+\mathcal{T}) \;=\; e^{-iE\mathcal{T}/\hbar}\Psi(t)\,. \tag{2.5}$$

The states $\Psi(t)$ can be expressed as $\Psi(t) = e^{-iEt/\hbar}\phi(t)$, where the functions $\phi(t)$ have the periodicity $\mathcal{T}$. The energy E, called the Floquet quasi-energy, is the eigenvalue of the Floquet operator $\mathcal{H}_F = \mathcal{H}(t) - i\hbar\partial_t$:

$$\begin{aligned} & \mathcal{H}(t)\Psi(t) = \mathcal{H}(t)e^{-iEt/\hbar}\phi(t) = i\hbar\partial_t\big(e^{-iEt/\hbar}\phi(t)\big) \\ \Leftrightarrow\quad & \Big(\mathcal{H}(t) - i\hbar\partial_t\Big)\phi(t) = E\phi(t) \\ \Leftrightarrow\quad & \mathcal{H}_F\phi(t) = E\phi(t)\,. \end{aligned}$$

Unlike energies which are uniquely determined, Floquet quasi-energies are defined up to integer multiples of $2\pi/\mathcal{T}$. Given that the functions $\phi(t)$ are periodic, the solutions of the time-dependent Schrödinger equation can be expanded in a Fourier series :

$$\Psi(t) = e^{-iEt/\hbar}\sum_{n=-\infty}^{\infty} e^{-in\Omega t}c_n\,, \tag{2.6}$$

with the frequency $\Omega = 2\pi/\mathcal{T}$ and c_n being the n-th Fourier component of the function $\phi(t)$. When considering scattering through a time-periodic potential, the Floquet scattering matrix relates the incoming and outgoing wave-functions, whose general form is given by Eq. (2.6) [Li 99, Moskalets 11].The on-demand single source presented in the previous section is driven by a periodic voltage. In the next section we derive its Floquet scattering matrix. The goal is then to characterize the emitted state by its temporal first-order correlation function. We therefore introduce below the correlations functions $G^{(n)}$ defined by Glauber and in particular the first-order correlation function $G^{(1)}$ which allows the determination of the coherence length of the emitted single-particle state.

2.1.3 First-order correlation function

To describe quantitatively the coherence properties of a field, Glauber introduced the correlation functions $G^{(n)}(x_1 \dots x_n, x_{n+1} \dots x_{2n})$ in a series of articles in 1963 [Glauber 63a, Glauber 63b, Glauber 63c]. The function $G^{(n)}$ characterizes the n-th order correlations between the fluctuations of a field at separated positions and times $x_i = (\vec{r}_i, t_i), i = 1, \dots, 2n$. In particular the first-order correlation function $G^{(1)}(x, x')$ is a two-point correlation function. It probes the correlations between the fluctuations of the field at the space-time positions $(\vec{r}, t)$ and $(\vec{r}', t')$. Integrated over space, the $G^{(1)}$ function provides information about the time during which the

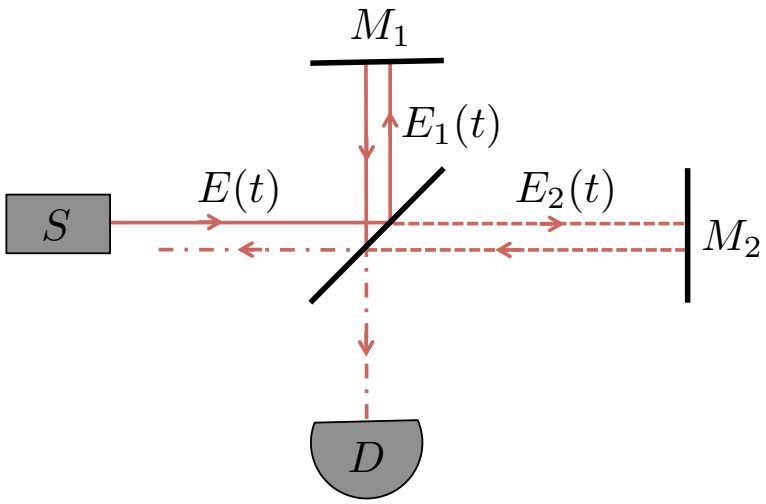

Figure 2.3: A Michelson interferometer. A monochromatic field $E(t)$ is emitted by the source labelled S. It is split into two components $E_1(t)$ and $E_2(t)$ at a half-transmitting beam splitter represented by an oblique thick line. After being reflected by the mirrors M_1 and M_2, the fields are recombined at the oblique mirror and are measured by the detector D. Interferences fringes are observed in the mean intensity measured in D as a function of the length difference between the arms 1 and 2 of the interferometer.

incoming field is able to interfere with itself at the output of the interferometer with a time delay between its arms. By definition, this time is called the coherence time T_2 of the field, where the name T_2 comes from earlier works on the relaxation times of nuclear magnetic resonance spins [Abragam 85]. Experimentally, the coherence time is the characteristic time over which the first-order correlation function decreases as a function of the time delay of the interferometer.

To illustrate this definition, let us consider the case of a Michelson interferometer as shown in Fig. 2.3. The source S emits a monochromatic electromagnetic field $E(t) = A(t)e^{i(\omega t+\phi(t))}$ where $A(t)$ is the complex amplitude, ω is the frequency of the optical mode and $\phi(t)$ is a fluctuating phase. The path difference between the two arms of the interferometer is characterized by the delay time $\Delta\tau$. The mean intensity I_{out} in the detector D is given by :

$$\begin{aligned} I_{\text{out}} &= \frac{\varepsilon c}{4}\left\langle \frac{1}{2}|E_1(t) - iE_2(t+\Delta\tau)|^2 \right\rangle \\ &= \frac{\varepsilon c}{8}\Big(\left\langle |A_1(t)|^2 \right\rangle + \left\langle |A_2(t+\Delta\tau)|^2 \right\rangle \\ &\quad +2\,\mathrm{Re}\left\langle A_1(t)A_2^*(t+\Delta\tau)e^{-i\omega\Delta\tau}e^{i(\phi_1(t)-\phi_2(t+\Delta\tau))}\right\rangle \Big), \end{aligned} \tag{2.7}$$

where $E_{1,2}(t)$ are the components of the field $E(t)$ having travelled in the arms 1 and 2. The coefficients ε and c are respectively the electrical permittivity and the velocity of light. The first two terms correspond to the mean intensity measured in arm 1 and

in arm 2. The interference term $\langle E_1^*(t)E_2(t+\Delta\tau)\rangle$ corresponds to the correlation of the component E_1 in arm 1 with the component E_2 in arm 2 with a time delay $\Delta\tau$. The brackets $\langle\ldots\rangle$ stand for the average over time, where the integration time is assumed to be much longer than $1/\omega$. It is generally set by the measurement apparatus. In general, the temporal first-order correlation function $G^{(1)}$ depends on time t and on the time delay $\Delta\tau$:

$$G_{12}^{(1)}(t,\Delta\tau) = \langle E_1(t)E_2^*(t+\Delta\tau)\rangle = \langle A_1(t)A_2^*(t+\Delta\tau)e^{-i\omega\Delta\tau}e^{i(\phi_1(t)-\phi_2(t+\Delta\tau))}\rangle\,. \quad (2.8)$$

This equation shows that when there is no time delay between the arms of the interferometer, the mean intensity is 2 times larger than the measured intensity in one arm, whatever the coherence properties of the incoming field are. When the delay tends to infinity, the first-order correlation function vanishes and the mean intensity is equal to the sum of the intensities in arm 1 and arm 2. The coherence time T_2 is defined as the characteristic time of the decay of $G^{(1)}$. For a stationary process, it is important to recall that the first-order correlation function only depends on the time delay $\Delta\tau$. The dc-source is an example of stationary source in mesoscopic physics whereas the on-demand SES driven by a periodic voltage is not stationary. When we investigate the correlation functions of quantum fields, the brackets stand for the quantum statistical average which differs when considering bosons or fermions. For photons the average is made with respect to the vacuum described by a Fock state with 0 particles whereas for fermions, this average is made with respect to the state of the reservoir described by a Fermi distribution at a given energy.

The $G^{(1)}$ function decays in general as a function of the amplitude $A(t)$ and due to the loss of phase coherence. The decay of the amplitude is characterized by the lifetime T_1 (or relaxation time) defined as the characteristic time over which the correlation between the amplitudes decreases to 0. The relaxation is due to the finite width of the incoming pulse set by the source and by the inelastic processes that the pulse undergoes when interacting with its environment while it travels through the interferometer. The loss of phase coherence is characterized by the time T_φ or T_2^* which is the characteristic time over which the average relative phase $\langle e^{i(\phi_i(t)-\phi_j(t+\Delta\tau))}\rangle$ tends to 0. At time T_φ, the relative phase is not anymore determined and the two fields are completely uncorrelated [Walls 94, Yamamoto 99].

In an experiment, when the temporal shape of the pulse can be measured independently (this supposes to have detectors with a time resolution adapted to the source), the phase coherence time T_φ is extracted from the normalized first-order temporal correlation function $g_{12}^{(1)}(\Delta\tau)$:

$$g_{12}^{(1)}(t,\Delta\tau) = \frac{\langle E_1(t)E_2^*(t+\Delta\tau)\rangle}{\sqrt{\langle I_1(t)\rangle\,\langle I_2(t+\Delta\tau)\rangle}} \quad (2.9)$$

The function $g^{(1)}$ gives access to the phase coherence of the field. Its decay as a function of the imbalance of the interferometer does not depend anymore on the

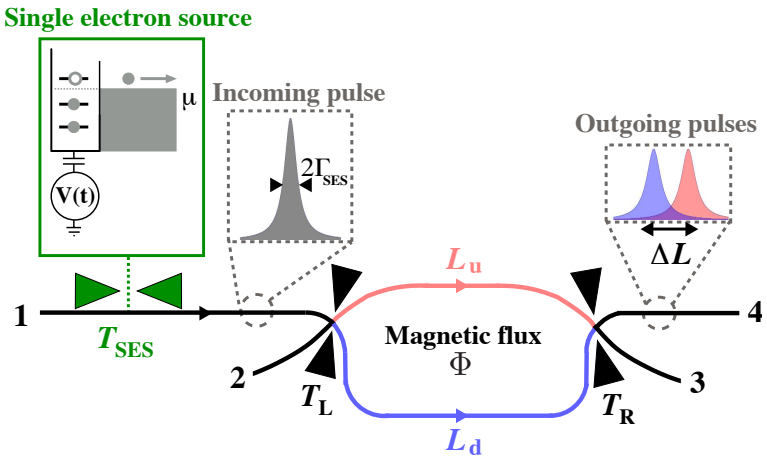

Figure 2.4: Single electron source (SES) coupled to a Mach-Zehnder interferometer (MZI) through a quantum point contact (QPC) with transmission probability T_{SES}. A periodic voltage $V(t) = V(t+\mathcal{T})$ drives the energy levels of the SES up and down the Fermi energy μ. On average over one time period $\mathcal{T}$, this leads to the injection into the input 1 of the MZI of an electron pulse of half duration Γ. The MZI is made of two QPCs characterized by their transmission probabilities T_{R} and T_{L}. The imbalance of the MZI is defined as $\Delta L = L_{\mathrm{u}} - L_{\mathrm{d}}$, with $L_{\mathrm{u(d)}}$ being the length of the upper (lower) arm of the MZI.

temporal shape of the incoming pulse. From previous works on nuclear magnetic resonance spins and on the optical Bloch equations, the three times are related via [Abragam 85, Grynberg] :

$$\frac{1}{T_2} = \frac{1}{2T_1} + \frac{1}{T_\varphi}\,. \tag{2.10}$$

When a field or a state is not subject to dephasing processes, T_φ tends to infinity and the coherence time T_2 is only set by the lifetime of the pulse T_1. In mesoscopic physics, inelastic scattering processes set T_1, whereas T_φ can originate both in inelastic scattering processes and in dephasing processes ruled for instance by a finite electronic temperature or by the weak interaction of the particle with its environment through charge fluctuations. Equation (2.10) is sometimes used in experiments to characterize the dephasing processes taking place. By measuring the lifetime of the pulse T_1 and by measuring the $G^{(1)}$ function which gives access to the coherence time T_2 in an interferometry experiment, T_φ can be determined. This is for instance the case in Circuit QED or with single-photon sources [Devoret 04, Santori 02].

In our work, we determine the coherence time or equivalently the coherence length of the single particles emitted by the on-demand single-electron source realized at the Laboratoire Pierre Aigrain. For this we propose an experiment where the single-particle states are injected into an electronic MZI as shown in Fig. 2.4. Due to

the AB effect, the output current exhibits oscillations as a function of the magnetic flux, which will decay as a function of the time delay between the two arms. The coherence time is then given by the characteristic time of this decay. We apply this protocol for the source in the adiabatic and in the non-adiabatic regime and with this we characterize the first-order coherence properties of the emitted single-particle quantum states.

2.2 System and model

In this section, we present the analytical expression of the first-order correlation function in terms of the scattering amplitude of the source S_{SES}. Within a Floquet scattering matrix approach, we derive the current at the output of the MZI in terms of S_{SES}. From the interference part, we define the first-order correlation function and from the intensities in the upper and lower arms, we provide an analytical expression of the current emitted by the source.

2.2.1 The mesoscopic capacitor as an on-demand SES

The source consists of a small cavity with a confined circular edge state, which has a discrete level spectrum characterized by the level spacing Δ, see Fig. 2.5. Screening due to a metallic top gate suppresses charging effects. By applying a time-dependent potential $V(t)$ homogeneously to the top gate, the energy levels are driven forth and back through the Fermi energy and the energy E of the emitted particles changes. Therefore the scattering matrix depends on two energies, the energy E of the incoming particle and the energy E_m of the outgoing particle, $E_m = E + m\hbar\Omega$, where Ω is the frequency of the applied potential $V(t)$ [Moskalets 08]. It is sometimes convenient to describe the scattering process with the energy E of the incoming particle and the time t at which the particle has left the cavity. The corresponding scattering matrix $S(t, E)$ is the Fourier transform of the Floquet scattering matrix $S(E_m, E)$:

$$S_{\mathrm{SES}}(E_m, E) = \int_0^{\mathcal{T}} \frac{dt}{\mathcal{T}} e^{im\Omega t} S_{\mathrm{SES}}(t, E)\,, \tag{2.11}$$

where $\mathcal{T}$ is the period of the applied potential, $\mathcal{T} = 2\pi/\Omega$. The scattering amplitude $S(t, E)$ of the source is given by a Fabry-Pérot like expression [Moskalets 08]:

$$S_{\mathrm{SES}}(t, E) = r_{\mathrm{SES}} + \frac{t_{\mathrm{SES}}^2}{r_{\mathrm{SES}}} \sum_{n=1}^{\infty} r_{\mathrm{SES}}^n \, e^{i\left(nk_E L - \Phi_n(t)\right)}\,. \tag{2.12}$$

The reflection (transmission) amplitude of the quantum point contact (QPC) coupling the states of the mesoscopic capacitor to the edge state of the MZI is labelled r_{SES} (t_{SES}). The accumulated phase during n revolutions in the cavity is composed of a dynamical phase which depends on the momentum k_E and on the circumference of the cavity L and of a phase due to the time-dependent potential $V(t)$:

$$\Phi_n(t) = \frac{e}{\hbar} \int_{t-n\tau}^{t} dt' V(t')\,. \tag{2.13}$$

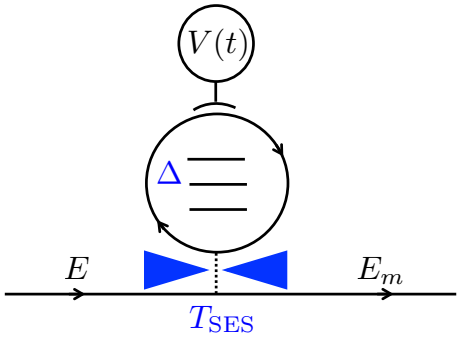

Figure 2.5: Mesoscopic capacitor with quantized energy levels characterized by the level separation energy Δ. The Floquet scattering amplitude depends on two energies E and E_m, respectively the energy of the incoming particle and the energy of the outgoing particle. Given the periodic potential $V(t)$ of frequency Ω, the particle absorbs or emits quanta of energy $\hbar\Omega$. The energy of the outgoing is $E_m = E + m\hbar\Omega$, $m \in \mathbb{N}$.

We assume that the time τ spent for one revolution in the cavity is independent of energy, it depends only on the size of the cavity L:

$$\tau = \sqrt{\frac{M}{2\mu}}\, L = \frac{L}{v_D}\,,$$

where μ is the Fermi energy, M is the mass of the electron and v_D is the drift velocity of the electrons. The dwell time of the particles $\tau_D = \tau/T_{\rm SES}$ and the temporal shape of the potential $V(t)$ define the working regimes of the SES. Here $T_{\rm SES} = |t_{\rm SES}|^2$ is the transmission probability of the QPC.

- If the potential varies smoothly in time compared to τ_D, the electron sees a *frozen* potential during the time it spends inside the cavity :

$$\Phi_n(t) = \frac{e}{\hbar}\int_{t-n\tau}^{t} dt'\, V(t') = \frac{e}{\hbar}\, n\tau\, V(t)\,. \tag{2.14}$$

  Such a smooth potential can be a sinusoidal potential $V(t) = V\cos(\Omega t)$ verifying $\Omega\tau_D \ll 1$. Even if the particles undergo many revolutions in the cavity corresponding to a time $n\tau$, this condition ensures that the potential does not vary over this time scale when $n \sim 1/T_{\rm SES}$. The scattering process is then described by the so-called *instantaneous* or *frozen* scattering matrix. This regime is the *adiabatic* regime [Moskalets 02, Moskalets 08, Ol'khovskaya 08].

- If the potential varies on a time faster than τ_D, the phase accumulated due to the potential varies over the time the particle spends in the cavity. $\Phi_n(t)$ is

given by Eq.(2.13) and the integral over time has to be done explicitly. This regime corresponds to the *non-adiabatic* regime and can be reached with a square potential for instance. It is important that this square potential also verifies the condition $\Omega\tau_D \ll 1$. This ensures that the particle has been emitted before the next excitation of the potential starts.

In this work we investigate the coherence properties of the single-particle states emitted by the on-demand source in these two regimes. We repeat that the methodology consists in coupling this source to an electronic MZI and to extract the coherence length from the decay of the $G^{(1)}$ function.

2.2.2 The Mach-Zehnder interferometer

The MZI consists of two arms of length L_u and L_d and two QPCs (left and right) at which the particles are scattered with transmission probabilities T_L and T_R respectively, see Fig. 2.4. Its scattering matrix reads:

$$
\begin{aligned}
S_\mathrm{MZI}(E) &= \begin{pmatrix} S_{\mathrm{MZI},41}(E) & S_{\mathrm{MZI},42}(E) \\ S_{\mathrm{MZI},31}(E) & S_{\mathrm{MZI},32}(E) \end{pmatrix} \\
&= \begin{pmatrix} -\sqrt{R_\mathrm{L}R_\mathrm{R}}\, e^{i\phi_\mathrm{u}(E)} + \sqrt{T_\mathrm{L}T_\mathrm{R}}\, e^{i\phi_\mathrm{d}(E)} & i\sqrt{T_\mathrm{L}R_\mathrm{R}}\, e^{i\phi_\mathrm{u}(E)} + i\sqrt{R_\mathrm{L}T_\mathrm{R}}\, e^{i\phi_\mathrm{d}(E)} \\ i\sqrt{T_\mathrm{L}R_\mathrm{R}}\, e^{i\phi_\mathrm{d}(E)} + i\sqrt{R_\mathrm{L}T_\mathrm{R}}\, e^{i\phi_\mathrm{u}(E)} & -\sqrt{R_\mathrm{L}R_\mathrm{R}}\, e^{i\phi_\mathrm{d}(E)} + \sqrt{T_\mathrm{L}T_\mathrm{R}}\, e^{i\phi_\mathrm{u}(E)} \end{pmatrix}.
\end{aligned}
$$

Compared to the SES, the scattering matrix of the MZI depends on a single energy E. Assuming that the left and right QPCs are described by energy-independent transmission and reflection probabilities, the dependence on energy only appears in the dynamical phase acquired by the electrons while traveling along the upper and lower arms, $\phi_\mathrm{u}(E)$ and $\phi_\mathrm{d}(E)$ respectively. The phase difference between the upper and lower arms reads:

$$
\begin{aligned}
\phi_\mathrm{u}(E) - \phi_\mathrm{d}(E) &= 2\pi\frac{\Phi}{\Phi_0} + k_\mu\big(L_\mathrm{u} - L_\mathrm{d}\big) + \big(E-\mu\big)\frac{\big(\tau_\mathrm{u} - \tau_\mathrm{d}\big)}{\hbar}\,, \\
&= 2\pi\phi + \big(E-\mu\big)\frac{\big(\tau_\mathrm{u} - \tau_\mathrm{d}\big)}{\hbar}\,. \qquad (2.15)
\end{aligned}
$$

where $\Phi_0 = h/e$ is the flux quantum and $\tau_\mathrm{u,d}$ are the traversal times for the upper and lower arms of the MZI, $\tau_\mathrm{u,d} = L_\mathrm{u,d}/v_D$. The Fermi energy is μ. The energy-independent part of the phase is given by:

$$
2\pi\phi = 2\pi\Phi/\Phi_0 + k_\mu\Delta L\,. \qquad (2.16)
$$

We can now derive the scattering matrix of the entire system, namely the source coupled to the MZI.

2.2.3 Scattering matrix of the SES coupled to the MZI

Given that the electrons propagate in chiral edge states, the transport is unidirectional. Moreover, assuming that we measure the current at the output 4 of the MZI and that the source is coupled to the input 1 with all the other contacts grounded, it is only the scattering amplitude $S_{\mathrm{MZI},41}$ that has to be taken into account. Therefore, the scattering amplitude of the entire setup is the product of the scattering amplitude $S_{\mathrm{MZI},41}$ of the MZI with the Floquet scattering amplitude S_{SES} of the source :

$$S_{41}(E_m, E) = S_{\mathrm{MZI},41}(E_m) S_{\mathrm{SES}}(E_m, E)\,. \tag{2.17}$$

The Floquet scattering matrix for the source coupled to the MZI depends on two energies, the energy E of the incoming particle and the energy E_m of the particle leaving the cavity and traveling through the MZI.

2.2.4 Current emitted by the source and first-order correlation function $G^{(1)}$

In a second quantized formulation, the current operator $\hat{I}_4$ in the output 4 of the MZI is given by [Büttiker 94]:

$$\hat{I}_4 = \frac{e}{h}\int_0^\infty dE \int_0^\infty dE' e^{i(E-E')t/\hbar}\left[\hat{b}_4^\dagger(E)\hat{b}_4(E') - \hat{a}_4^\dagger(E)\hat{a}_4(E')\right]\,. \tag{2.18}$$

The operators $\hat{a}_4(\hat{a}_4^\dagger)$ and $\hat{b}_4(\hat{b}_4^\dagger)$ are respectively the annihilation (creation) operators for the incoming and outgoing states whose quantum statistical average over the reservoir state is given by :

$$\langle \hat{a}_i^\dagger(E)\hat{a}_j(E')\rangle = \delta(E-E')\,\delta_{ij} f_i(E)\,.$$

The Fermi distribution $f_i(E)$ describes the reservoir i at energy E. The incoming and outgoing operators are related by the Floquet scattering amplitudes $S_{4\alpha}(E, E_m)$ where the index $\alpha = 1, \ldots, 4$ denotes the four contacts of the MZI:

$$\begin{aligned}
\hat{b}_4(E') &= \sum_{\alpha,n} S_{4\alpha}(E', E'_n)\hat{a}_\alpha(E'_n) \\
\hat{b}_4^\dagger(E) &= \sum_{\alpha,m} S_{4\alpha}^*(E, E_m)\hat{a}_\alpha^\dagger(E_m)\,.
\end{aligned}$$

The Floquet scattering amplitudes verify the unitarity property which ensures the conservation of the current :

$$\sum_n \sum_\alpha S_{\alpha\beta}^*(E_n, E_m) S_{\alpha\gamma}(E_n, E) = \delta_{m0}\delta_{\beta\gamma}\,. \tag{2.19}$$

In our setup, we assume no dc-bias and the chemical potentials of all the contacts are grounded to the Fermi energy μ so that :

$$f(E) \equiv f_1(E) = f_2(E) = f_3(E) = f_4(E)\,.$$

The SES being connected at the input 1 of the MZI, the current is determined by the scattering matrix element $S_{41}(E, E_m)$. From Eq.(2.18) and using the unitarity property of the scattering matrix (Eq.(2.19)), the current can be written as a Fourier series where $\big(I_{41}\big)_l$ are the Fourier coefficients :

$$\begin{aligned} I_4(t,\Phi) &\equiv \langle \hat{I}_4 \rangle = \sum_l e^{-il\Omega t}\big(I_{41}\big)_l \\ &= \sum_l e^{-il\Omega t}\frac{e}{h}\int_0^\infty dE \sum_m \left[f(E) - f(E_m)\right]\, S^*_{41}(E_m, E) S_{41}(E_{l+m}, E)\,, \end{aligned} \tag{2.20}$$

where $E_m = E + m\hbar\Omega$ and $E_{l+m} = E + (l+m)\hbar\Omega$. By inserting the expression of the scattering amplitude given by Eq.(2.17) and by replacing the Floquet scattering amplitudes by their Fourier transforms (Eq (2.11)), the average current reads :

$$\begin{aligned} I_4(t,\Phi) &= \frac{e}{h}\int_0^\infty dE \sum_m \left[f(E) - f(E_m)\right] \\ &\qquad \Big(R_{\rm L}R_{\rm R}\int \frac{dt'}{\mathcal{T}} e^{-im\Omega(t'-t)}\, S^*_{\rm SES}(t'-\tau_{\rm u}, E) S_{\rm SES}(t-\tau_{\rm u}, E) \\ &\qquad + T_{\rm L}T_{\rm R}\int \frac{dt'}{\mathcal{T}} e^{-im\Omega(t'-t)}\, S^*_{\rm SES}(t'-\tau_{\rm d}, E) S_{\rm SES}(t-\tau_{\rm d}, E)\Big) \\ &- \frac{e}{h}\sqrt{R_{\rm L}R_{\rm R}T_{\rm L}T_{\rm R}}\int_0^\infty dE \sum_m \left[f(E) - f(E_m)\right] \\ &\qquad \Big(e^{i2\pi\phi}e^{i(E-\mu)(\tau_{\rm u}-\tau_{\rm d})/\hbar}\int \frac{dt'}{\mathcal{T}} e^{-im\Omega(t'-t)}\, S^*_{\rm SES}(t'-\tau_{\rm d}, E) S_{\rm SES}(t-\tau_{\rm u}, E) \\ &\qquad + e^{-i2\pi\phi}e^{i(E-\mu)(\tau_{\rm d}-\tau_{\rm u})/\hbar}\int \frac{dt'}{\mathcal{T}} e^{-im\Omega(t'-t)}\, S^*_{\rm SES}(t'-\tau_{\rm u}, E) S_{\rm SES}(t-\tau_{\rm d}, E)\Big)\,. \end{aligned} \tag{2.21}$$

The dependence on the magnetic flux Φ is taken into account in the phase $2\pi\phi = 2\pi\Phi/\Phi_0 + k_\mu \Delta L$ defined by Eq.(2.16). The two first terms on the r.h.s stand for the separated contributions of the upper and lower arms to the output current which we call respectively $I_{\rm SES}(t-\tau_{\rm u})$ and $I_{\rm SES}(t-\tau_{\rm d})$. From the interference part of the current, we define the first-order correlation function $G^{(1)}$ in terms of the scattering

matrix of the source :

$$I_{\rm SES}(t-\tau_{\rm i}) = \frac{e}{h}\int_0^\infty dE \sum_m [f(E)-f(E_m)] \int \frac{dt'}{\mathcal{T}} e^{-im\Omega(t'-t)} S^*_{\rm SES}(t'-\tau_{\rm i},E) S_{\rm SES}(t-\tau_{\rm i},E)\,. \quad (2.22)$$

$$G^{(1)}_{\rm ij}(t,\tau_{\rm i},\tau_{\rm j}) = \frac{e}{h}\int_0^\infty dE \sum_m [f(E)-f(E_m)]\, e^{i(E-\mu)(\tau_{\rm j}-\tau_{\rm i})/\hbar} \int \frac{dt'}{\mathcal{T}} e^{-im\Omega(t'-t)}\, S^*_{\rm SES}(t'-\tau_{\rm i},E) S_{\rm SES}(t-\tau_{\rm j},E)\,. \quad (2.23)$$

The normalized first-order temporal correlation function $g^{(1)}$ is given by :

$$g^{(1)}(t,\Delta\tau) = \frac{G^{(1)}_{\rm ud}(t,\Delta\tau)}{\sqrt{I_{\rm SES}(t-\tau_{\rm u})}\sqrt{I_{\rm SES}(t-\tau_{\rm d})}}\,. \quad (2.24)$$

With Eqs. (2.22) and (2.23), we write the current at the output of the MZI as :

$$I_4(t,\Phi) = R_{\rm L}R_{\rm R}\, I_{\rm SES}(t-\tau_{\rm u}) + T_{\rm L}T_{\rm R}\, I_{\rm SES}(t-\tau_{\rm d}) - 2\sqrt{R_{\rm L}R_{\rm R}T_{\rm L}T_{\rm R}}\,{\rm Re}\Big\{e^{-i2\pi\phi}G^{(1)}_{\rm ud}(t,\Delta\tau)\Big\}\,. \quad (2.25)$$

Equations (2.22) - (2.25) are the central results of this section. They express the first-order correlation function in terms of the scattering matrix amplitude of the source. From the decay of $G^{(1)}$ as a function of the time delay $\Delta\tau = \tau_{\rm u} - \tau_{\rm d}$, we will determine the coherence time T_2 of the single-particle states emitted by the SES and by calculating the normalized first-order correlation function, we will show that within our model, the single-particle states are Fourier-transform limited, i.e, their phase coherence time T_φ tends to infinity.

When comparing the first-order correlation function introduced by Glauber for photons and the $G^{(1)}$ function defined by Eq. (2.23) for fermions, fundamental differences have to be pointed out. In particular, if we consider a fermionic field operator $\hat{\Psi}$, the analog of the intensity operator in quantum optics would be proportional to $\hat{\Psi}^\dagger\hat{\Psi}$. But the second quantized expression of the current is proportional to $\hat{\Psi}^\dagger\nabla\hat{\Psi} - (\nabla\hat{\Psi}^\dagger)\hat{\Psi}$. Moreover, for photons the quantum statistical average of the intensity operator is made with respect to the vacuum, namely a Fock state with 0 particles. In contrast, for fermions, the quantum statistical average is made with respect to the state of the reservoir characterized by the Fermi distribution taken at the energy of the reservoir.

In parallel to our work, C. Grenier *et al.* have also investigated the first-order correlation function for fermions [Grenier 11]. To take into account the differences between bosons and fermions mentioned above, they defined a fermionic field operator as a sum of one term describing the state of the Fermi sea and another term

corresponding to carriers on top of this Fermi sea. With such a definition, they were able to derive an expression of the first-order correlation function in terms of the fermionic operators for particles on top of the Fermi sea.

In our work, we consider a different approach, namely we define $G^{(1)}$ from an interferometry experiment. The interference term of the current which originates from the coherence properties of the single-particle state traveling through the interferometer is a natural measure of the first-order correlation function. Given that we calculate the current within a scattering-matrix approach, our definition of $G^{(1)}$ depends explicitly on the scattering matrix of the source. Importantly both approaches are equivalent. The main difference relies in the experimental determination of $G^{(1)}$. The proposal of C. Grenier *et al.* consists in an Hanbury-Brown and Twiss experiment, in which they measure the noise at the output. From this second-order measurement, they extract the information about the first-order coherence length. Our proposal is most probably more challenging with respect to the fabrication of the sample but the measurement of the current or of average first-order quantities is easier than noise measurements.

In the two next parts, we derive the analytical expressions of the scattering matrix for the mesoscopic capacitor in the adiabatic and in the non-adiabatic regime. This allows us to derive the explicit form of the first-order correlation functions in terms of the experimental parameters in these two regimes. From these expressions we are able to extract the coherence length of the single-particle states and to characterize the first-order coherence properties of these single-electron states.

2.3 The adiabatic regime

In this section, we take the source to be in the adiabatic regime, i.e when the potential varies much slower than the time spent by the particle inside the cavity, the dwell time. We first derive the scattering amplitude and the current emitted by this source in the adiabatic regime. Then, we derive an analytical expression of $G^{(1)}$ and $g^{(1)}$ as a function of time and of the time delay $\Delta\tau$ of the interferometer. From $G^{(1)}$ and $g^{(1)}$, we extract respectively the coherence time T_2 and the phase coherence time T_φ of the single-particle states emitted by the source in the adiabatic regime.

2.3.1 Description of the source

The frozen Floquet scattering amplitude

In the adiabatic regime, the phase acquired by the electron due to the periodic potential $V(t)$ is constant over the time that the particle spends inside the cavity. The phase $\Phi_n(t)$ in the Fabry-Pérot expression of the scattering amplitude, Eq. (2.12) becomes:

$$\Phi_n(t) = \frac{e}{\hbar}\int_{t-n\tau}^{t} dt'\, V(t') = \frac{e}{\hbar}\, n\tau V(t)\,, \tag{2.26}$$

and the scattering matrix amplitude can be simplified to get the *instantaneous* or *frozen* scattering matrix:

$$S_{\rm SES}(t,E) \;=\; r_{\rm SES} + \frac{t_{\rm SES}^2}{r_{\rm SES}}\sum_{n=1}^{\infty} r_{\rm SES}^n e^{in(k_E L - \tau eV(t)/\hbar)}\,. \tag{2.27}$$

Close to the Fermi energy μ, we can expand the momentum to the first-order in energy :

$$k_E \sim k_\mu + \frac{E-\mu}{\hbar v_D}\,,$$

with k_μ the momentum at the Fermi energy and v_D the drift velocity of the electrons. With $r_{\rm SES} = |r_{\rm SES}|e^{i\phi_r}$, ϕ_r being the phase of the reflection amplitude, we define the following phase of the instantaneous scattering amplitude:

$$\begin{aligned}\varphi_V(t,E) &= \phi_r + \big(k_\mu L - \frac{\tau\mu}{\hbar}\big) + \frac{\tau}{\hbar}\big(E - eV(t)\big)\\ &= \varphi(E) - \frac{eV(t)\tau}{\hbar}\,.\end{aligned} \tag{2.28}$$

We have split the phase into two parts: one part takes into account the full dependence on time and the other part $\varphi(E)$ depends only on energy:

$$\varphi(E) = \phi_r + k_\mu L + (E-\mu)\frac{\tau}{\hbar}\,. \tag{2.29}$$

The label V of the phase $\varphi_V(t,E)$ stands for the smooth potential $V(t)$. The scattering amplitude reads:

$$\begin{aligned} S_{\rm SES}(t,E) &= r_{\rm SES} + \frac{t_{\rm SES}^2}{r_{\rm SES}} \sum_{n=1}^{\infty} |r_{\rm SES}|^n \, e^{in\varphi_V(t,E)} \\ &= e^{i\phi_r} \frac{|r_{\rm SES}| - e^{i\varphi_V(t,E)}}{1 - |r_{\rm SES}| e^{i\varphi_V(t,E)}} , \end{aligned} \tag{2.30}$$

Experimentally it has been shown that the quantized emission of charges takes place in the Breit-Wigner regime characterized by $T_{\rm SES} \ll 1$, namely when the coupling between the states in the cavity and the edge state is weak. In this regime the particles exit the cavity when the energy levels of the cavity are in resonance with the Fermi energy of the edge state. This can happen thanks to the time-dependence of the applied potential $V(t)$. To find these resonance times which correspond to the times of emission of the single particles, we apply the resonance condition to the density of states. In terms of the scattering matrix amplitude and its energy derivative, the density of states reads [Büttiker 94]:

$$\begin{aligned} \nu_{\rm SES}(t,E) &= \frac{1}{2\pi i} S_{\rm SES}^*(E - eV(t)) \frac{\partial S_{\rm SES}(E - eV(t))}{\partial E} \\ &= \frac{1}{\Delta} \frac{T_{\rm SES}}{2 - T_{\rm SES} - 2\sqrt{1 - T_{\rm SES}} \cos(\varphi_V(t,E))} , \end{aligned}$$

with $\Delta = h/\tau$ the level spacing in the cavity. By setting the resonance condition $\varphi_V(t,E) = 2\pi k$, the emission times of the particles are defined as shown below.

We consider a sinusoidal potential with an arbitrary phase δ, $V(t) = V\cos(\Omega t + \delta)$. For the peak at $k = 0$ and expanding $\sqrt{1 - T_{\rm SES}} \sim 1 - T_{\rm SES}/2$, we find:

$$\begin{aligned} &\varphi_V(t,E) = \varphi(E) - \frac{2\pi e V(t)}{\Delta} \equiv 0 \\ &\Leftrightarrow \varphi(E) - \frac{2\pi e V}{\Delta} \cos\left(\Omega t + \delta\right) \equiv 0 \\ &\Leftrightarrow \Omega t^{\pm} = -\delta \pm \arccos\left(\frac{\varphi(E)\,\Delta}{2\pi e V}\right) . \end{aligned} \tag{2.31}$$

The times $t^{\mp}$ correspond respectively to the emission of an electron and to its absorption (or the emission of a hole). Setting $\delta = 0$, the phase close to the emission times is:

$$\varphi_V(t,E) = \pm(t - t^{\pm}) 2\pi\Omega \frac{eV}{\Delta} \sqrt{1 - \left(\frac{\varphi(E)\,\Delta}{2\pi e V}\right)^2} . \tag{2.32}$$

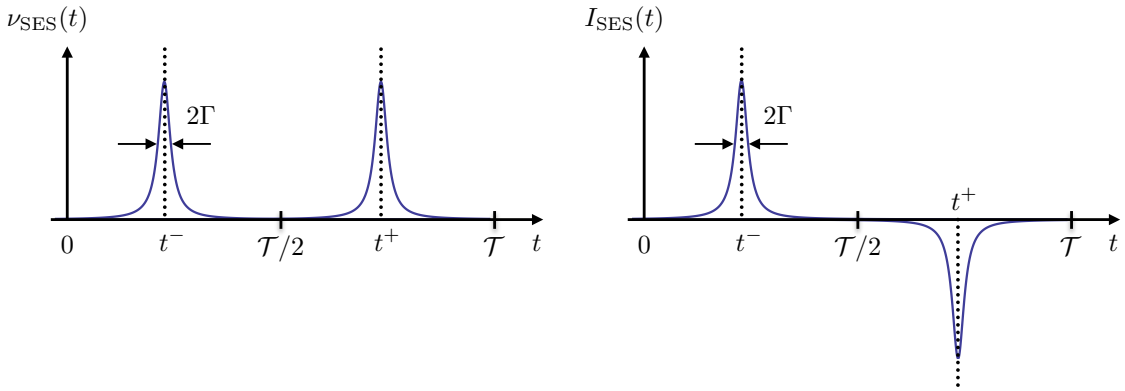

Figure 2.6: Density of states $\nu_{\rm SES}$ and current emitted by the source $I_{\rm SES}$ in the adiabatic regime evaluated at the Fermi energy μ (arbitrary units). Both quantities are calculated at the Fermi energy μ. Assuming the Breit-Wigner regime characterized by a weak coupling between the source and the edge state ($T_{\rm SES} \ll 1$), the resonance condition defines emission times t^- and t^+. The time t^- corresponds to the emission of an electron in the first half-period of the potential $[0, \mathcal{T}/2]$ and the time t^+ corresponds to the emission of a hole in the second half-period $[\mathcal{T}/2, \mathcal{T}]$. The density of states and the current consist in sharp Lorentzian peaks of half width Γ centered on these emission times.

The density of states can be written in the Breit-Wigner form :

$$\nu_{\rm SES}(t,E) \;=\; \frac{4}{\Delta\, T_{\rm SES}} \frac{\Gamma(E)^2}{\Gamma(E)^2 + (t-t^{\pm})^2}\,, \tag{2.33}$$

where the half width of the Lorentzian is given by $\Gamma(E)$:

$$\Gamma(E) \;=\; \frac{T_{\rm SES}\,\Delta}{eV} \frac{1}{4\pi\Omega} \frac{1}{\sqrt{1-\left(\frac{\varphi(E)\Delta}{2\pi eV}\right)^2}}\,. \tag{2.34}$$

"Half width" means the half width of the full width at half-maximum. By integrating the density-of-states over energy at a given time, we have checked that it verifies the normalization condition. At zero temperature, in the adiabatic regime, the particles are emitted close to the Fermi sea. Therefore $\varphi(E) \sim \varphi(\mu)$ and we have:

$$\Gamma(E) \sim \Gamma(\mu) \equiv \Gamma\,.$$

The density of states evaluated at the Fermi energy μ is shown in Fig. 2.6. By substituting the expression of the phase φ_V close to the emission times $t^{\mp}$ in Eq. (2.30), this yields the expression of the *frozen* scattering amplitude in terms of $t^{\mp}$ and of the half width Γ :

$$S_{\rm SES}(t,\mu) = e^{i\phi_r}\begin{cases} \frac{t-t^- +i\Gamma}{t-t^- -i\Gamma} & , \quad |t-t^-| \sim \Gamma \\ \frac{t-t^+ -i\Gamma}{t-t^+ +i\Gamma} & , \quad |t-t^+| \sim \Gamma \\ 1 & , \quad \text{elsewhere}\,. \end{cases} \tag{2.35}$$

This is the expression of the scattering amplitude of the source in the adiabatic regime. Close to the emission times $t^{\mp}$, an electron and a hole are emitted. It is important to recall that the source works in regimes where $|t^- - t^+| \gg \Gamma$ so that we assume that 2 single-particle states do not overlap at the output of the source. Below we calculate the current emitted by the source in the adiabatic regime.

Current emitted by the source

We recall the expression of the current emitted by the source at time t (Eq. (2.22)):

$$I_{\rm SES}(t) \;=\; \frac{e}{h}\sum_m \int_{\mu-m\hbar\Omega}^{\mu} dE \int \frac{dt'}{\mathcal{T}} e^{-im\Omega(t'-t)}\, S^*_{\rm SES}(t',\mu) S_{\rm SES}(t,\mu)\,. \tag{2.36}$$

By integrating by part, we obtain:

$$I_{\rm SES}(t) \;=\; \frac{-ie}{2\pi}\frac{S^*_{\rm SES}(t,\mu)}{\partial t} S_{\rm SES}(t,\mu)\;. \tag{2.37}$$

We recover the familiar expression of the current in terms of the scattering matrix and its time-derivative from quantum pumping where it provides the starting point for the evaluation of the pumped current [Brouwer 98, Avron 00, Polianski 01, Büttiker 94]. By substituting the frozen scattering amplitude by its explicit expression given by Eq.(2.35), we obtain the current emitted in the adiabatic regime:

$$I_{\rm SES}(t) \;=\; \frac{e}{\pi}\frac{1}{\Gamma}\left[\frac{1}{1+(t-t^-/\Gamma)^2} - \frac{1}{1+(t-t^+/\Gamma)^2}\right]\,. \tag{2.38}$$

It consists of two Lorentzian pulses characterized by their half width Γ defined previously (see Fig. 2.6). The half width sets the relaxation time T_1 of the single-particle states emitted by the cavity. The Lorentzian pulses are centered on the times of emission of an electron (t^-) and the time of emission of a hole (t^+). In the next part, we derive the first-order correlation function to extract the coherence time T_2.

2.3.2 First-order correlation function in the adiabatic regime

In the adiabatic regime, we have shown that the scattering amplitude is evaluated at the Fermi energy, $S_{\rm SES}(t,E) = S_{\rm SES}(t,\mu)$. As a consequence, at zero temperature, the integral over energy in the expression of the $G^{(1)}$ function can be evaluated easily given that the Fermi distributions are then given by the Heaviside-distribution :

$$\begin{aligned} G^{(1)}_{\rm ij}(t,\tau_{\rm i},\tau_{\rm j}) &= \frac{e}{h}\sum_m \int_{\mu-m\hbar\Omega}^{\mu} dE e^{i(E-\mu)(\tau_{\rm j}-\tau_{\rm i})/\hbar} \\ &\quad \int \frac{dt'}{\mathcal{T}} e^{-im\Omega(t'-t)}\, S^*_{\rm SES}(t'-\tau_{\rm i},\mu) S_{\rm SES}(t-\tau_{\rm j},\mu) \\ &= \frac{e}{h}\sum_m \frac{1-e^{-im\Omega(\tau_{\rm j}-\tau_{\rm i})}}{i(\tau_{\rm j}-\tau_{\rm i})/\hbar} \int \frac{dt'}{\mathcal{T}} e^{-im\Omega(t'-t)}\, S^*_{\rm SES}(t'-\tau_{\rm i},\mu) S_{\rm SES}(t-\tau_{\rm j},\mu)\,. \end{aligned}$$

By using the identity relation:

$$\sum_{m=-\infty}^{\infty} e^{-im\Omega t} = \frac{2\pi}{\Omega}\delta(t)\,, \tag{2.39}$$

we obtain a simple expression for the $G^{(1)}$ function in the adiabatic regime in terms of the scattering amplitude of the source :

$$G^{(1)}_{\rm ud}(t,\Delta\tau) = \frac{ie}{2\pi\Delta\tau}\Big[S^*_{\rm SES}(t,\mu)S_{\rm SES}(t+\Delta\tau,\mu)-1\Big]\,. \tag{2.40}$$

The time delay is defined as $\Delta\tau = \tau_{\rm u} - \tau_{\rm d}$. In our time-dependent problem, $G^{(1)}$ depends on time t and on the time difference $\Delta\tau$. When $\Delta\tau$ tends to zero, the single-particle first-order correlation function converges to the current emitted by the source, $I_{\rm SES}$, whereas when $\Delta\tau$ increases, it decreases to zero. In this limit the current pulses traveling through different arms have a vanishing overlap at the output as shown in Fig. 2.4. Let us note that $G^{(1)}(t,\Delta\tau)$ vanishes independently of $\Delta\tau$ at all times t far away from the emission time of an electron t^- (or from its absorption time t^+, emission time of a hole). In other words the coherence $G^{(1)}$ vanishes far away from the peaks of the current pulses $|I_{\rm SES}(t^\pm)| = I_{\rm max}$.

In the following, we introduce the dimensionless coherence function $\mathcal{C}_{\rm SES}$ to simplify the notation :

$$\mathcal{C}_{\rm SES}(t,\Delta\tau) \equiv \frac{G^{(1)}_{\rm ud}(t,\Delta\tau)}{I_{\rm max}}\,. \tag{2.41}$$

The normalization factor $I_{\rm max}$ corresponds to the current emitted by the source at the time of emission of an electron or a hole (it ensures that the coherence function is equal to 1 at zero imbalance) :

$$I_{\rm max} = |I_{\rm SES}(t^\pm)| = \frac{e}{\pi\Gamma}\,.$$

Let us emphasize that, as $\mathcal{C}_{\rm SES}$ is obtained by dividing $G^{(1)}$ by a constant factor, it provides exactly the same information as $G^{(1)}$. The coherence function $\mathcal{C}_{\rm SES}$ is therefore fundamentally different from the $g^{(1)}$ function, where the normalization is time-dependent (see below).

Given that the source emits one electron and one hole per period of the potential, the coherence function has two contributions. In this work, we are interested in the coherence properties of single-particle states, either the single-electron state or the single-hole state. The expression of the coherence function for the single-electron state $\mathcal{C}^{(e)}_{\rm SES}$ is obtained by inserting the expression of the frozen scattering amplitude $S_{\rm SES}$ at times close to t^-, the time of emission of an electron :

$$\mathcal{C}^{(e)}_{\rm SES}(t,\Delta\tau) \;=\; \frac{1}{(1-it/\Gamma)(1+i(t+\Delta\tau)/\Gamma)}\,. \tag{2.42}$$

The coherence function for the hole $\mathcal{C}^{(h)}_{\rm SES}$ is the complex conjugate of $\mathcal{C}^{(e)}_{\rm SES}$. Let us remark that, depending on time t, the coherence function behaves differently with $\Delta\tau$. For such nontrivial time-dependent coherence functions, the coherence time is defined from the time-average coherence function. This is consistent with experiments where traditionally average quantities have been measured, either in quantum optics or mesoscopic physics. Indeed, even with a huge technical development of experimental facilities in both fields, it remains challenging to measure the intensity or the current resolved in time. Let us notice that when the coherence function is an exponential, its characteristic time T_2 is the same at all times so that it does not make any difference to look at the coherence function or at the time-average coherence function.

Given that the on-demand SES is driven by a potential whose period (and half-period) is much longer than any other time scales, we integrate the coherence function $\mathcal{C}^{(e)}_{\rm SES}$ ($G^{(1)}$ divided by $I_{\rm SES}$) over half a period during which one electron is emitted. The decay of this function is quantified by looking at the modulus of this expression:

$$\frac{1}{\pi\Gamma}\left|\int_0^{\mathcal{T}/2} dt\,\mathcal{C}^{(e)}_{\rm SES}(t,\Delta\tau)\right| = \left|\frac{1}{1+i\Delta\tau/(2\Gamma)}\right| = \frac{1}{\sqrt{1+\left(\Delta\tau/2\Gamma\right)^2}}\,. \tag{2.43}$$

This expression reflects the shape of the wave-packet emitted by the source in the adiabatic regime and shows that the pulse duration $\Gamma = T_1$ sets the coherence time :

$$T_2 = 2\,\Gamma\,. \tag{2.44}$$

The Floquet scattering matrix approach used to derive the current at the output of the MZI enables us to derive in a consistent way the relaxation time $T_1 = \Gamma$ and the coherence time $T_2 = 2\,T_1$ of the source in the adiabatic regime. We find that the single-particle states are Fourier-transform limited meaning that there is no

loss of phase coherence. We can check this by considering the normalized first-order correlation function $g^{(1)}$. The calculation is straightforward and we find :

$$\left|g^{(1)}(t,\Delta\tau)\right| = \left|\frac{G^{(1)}(t,\Delta\tau)}{\sqrt{I(t)\,I(t+\Delta\tau)}}\right| = 1\,. \tag{2.45}$$

This verifies that the phase coherence time is infinite, $T_\varphi = \infty$ and that the coherence time is only set by the relaxation time, i.e by the finite temporal linewidth of the pulse. The single-particle coherence length Λ for electrons emitted by the SES is therefore :

$$\Lambda = 2\,v_{\rm D}\,\Gamma\,. \tag{2.46}$$

Here $v_{\rm D}$ is the drift velocity of the electrons along the edge of the sample. This velocity ranges from a lower value of 10^4 m/s [Van der Vaart 94] up to higher values of the order of 10^5m/s [McClure 09]. Considering the lower limit of this range, we find $\Lambda \sim 2.10^{-6}$m which is of the order of the typical size of a MZI and sufficiently small compared to the actual dephasing length in an MZI which is of the order of $10\,\mu$m [Roulleau 08, Bieri 09, Hashisaka 10]. Therefore, considering the SES as an emitter of single electrons and the electronic MZI as an interferometer, it is possible to detect the effect of the single-particle coherence length.

Experimental considerations

Experimentally it is important to emphasize that in our setup, we need to change the asymmetry of the interferometer to extract the coherence length. To ensure that the decrease of the AB oscillations is due to the finite coherence length and not due to a change in the dephasing length, the total size of the MZI has to remain constant, $L_{\rm u} + L_{\rm d} = cst$. Indeed it has been measured that the dephasing length scales with the circumference of the MZI [Roulleau 08].

In a quantum transport experiment, the integral of the coherence function (Eq. (2.43)) corresponds to nothing else but to the interference part of the mean charge measured over half a period of the potential. Indeed, the time-dependent current $I_4(t,\Phi)$ at the output of the MZI can be written in terms of the coherence function :

$$\begin{aligned} I_4(t,\Phi) &= R_{\rm L}R_{\rm R}\,I_{\rm SES}(t-\tau_{\rm u}) + T_{\rm L}T_{\rm R}\,I_{\rm SES}(t-\tau_{\rm d}) \\ &\quad -2\sqrt{R_{\rm R}R_{\rm L}T_{\rm R}T_{\rm L}}I_{\rm max}\,{\rm Re}\big\{\,e^{-i2\pi\phi}\mathcal{C}_{\rm SES}(t,\Delta\tau)\big\}\,, \end{aligned}$$

with $I_{\rm SES}(t-\tau_{\rm u,d})$ given by Eq. (2.22). We recall that the interference part depends explicitly on the magnetic flux Φ and on the imbalance of the MZI through the phase $2\pi\phi = 2\pi\Phi/\Phi_0 + k_\mu\Delta L$, where $\Delta L = L_{\rm u} - L_{\rm d}$ is the length imbalance between the upper and lower arms of the MZI.

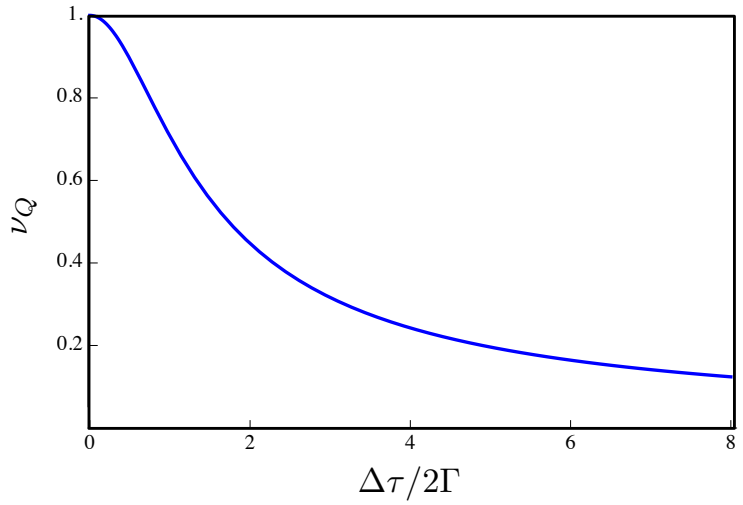

Figure 2.7: Charge visibility ν_Q as a function of the imbalance $\Delta\tau$. This visibility reflects the shape of the incoming single-particle state. The decay as a function of the delay is characterized by the coherence time $T_2 = 2\Gamma$.

The charge Q is given by the integral over half a period of the current I_4 (the charge over a full period is zero because of the emission of an electron and a hole):

$$Q(\Delta\tau) \;=\; \int_0^{\mathcal{T}/2} \frac{dt}{\mathcal{T}}\, I_4(t,\Phi)\,.$$

This quantity exhibits AB oscillations whose decay is characterized by a visibility ν_Q defined as the ratio of the amplitudes of the AB oscillations at finite imbalance to their maximum amplitude at $\Delta\tau = 0$:

$$\nu_Q = \frac{1}{\sqrt{1+\left(\Delta\tau/2\Gamma\right)^2}}\,. \tag{2.47}$$

This expression is exactly the same as Eq. (2.43) and it is shown in Fig. 2.7. Evaluating the half width Γ to be of the order 1 micron (see above), the visibility of the charge decays over a distance of several microns. Importantly, with the actual design of the samples of the electronic MZI, the maximal delay they can implement without damaging the sample is of the order of 1 micron [Roche]. Therefore, it is convenient for experimentalists to measure a quantity that decays faster with the delay $\Delta\tau$ than the charge. Such a quantity is for instance the mean squared current as shown below.

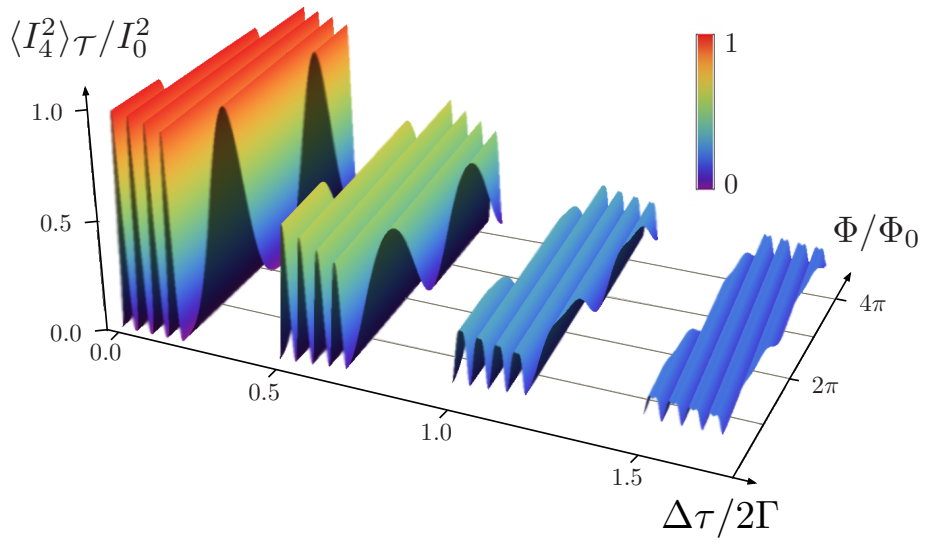

Figure 2.8: Mean squared current in units of $I_0^2 = e^2\Omega/(2\pi^2\Gamma)$ as a function of the magnetic flux Φ and the imbalance $\Delta\tau$. Here we have assumed symmetric QPCs, $T_\mathrm{R} = T_\mathrm{L} = 0.5$. For clarity we show only 4 cuts of the function at $\Delta\tau/(2\Gamma) = 0.0$, 0.5, 1.0 and 1.5, allowing to see the projection for different constant values of $\Delta\tau/(2\Gamma)$.

Alternative to the measurement of the charge

The mean squared current is defined as :

$$\langle I_4^2\rangle_\mathcal{T} = \int_0^\mathcal{T} \frac{dt}{\mathcal{T}} \left(I_4(t,\Phi)\right)^2 , \tag{2.48}$$

where $\langle\ldots\rangle_\mathcal{T}$ is the average over a period of time $\mathcal{T}$. Analytically, as this period is much bigger than any other time scales in the problem, the integral ranges over the real axis. Taking into account the expressions of the current derived previously, we get :

$$\langle I_4^2\rangle_\mathcal{T} = \frac{e^2\Omega}{2\pi^2\Gamma}\Big(A - B\cos(2\pi\phi) + C\cos(4\pi\phi)\Big) ,$$

with

$$A = R_\mathrm{R}^2R_\mathrm{L}^2 + T_\mathrm{R}^2T_\mathrm{L}^2 + 4R_\mathrm{R}R_\mathrm{L}T_\mathrm{R}T_\mathrm{L}\frac{1}{1+(\Delta\tau/2\Gamma)^2} , \tag{2.49a}$$

$$B = 4\sqrt{R_\mathrm{R}R_\mathrm{L}T_\mathrm{R}T_\mathrm{L}}\big(R_\mathrm{R}R_\mathrm{L} + T_\mathrm{R}T_\mathrm{L}\big)\frac{1}{\big(1+(\Delta\tau/2\Gamma)^2\big)^2} , \tag{2.49b}$$

$$C = 2R_\mathrm{R}R_\mathrm{L}T_\mathrm{R}T_\mathrm{L}\frac{1-3(\Delta\tau/2\Gamma)^2}{\big(1+(\Delta\tau/2\Gamma)^2\big)^3} . \tag{2.49c}$$

Here we recall that $2\pi\phi = 2\pi\Phi/\Phi_0 + k_\mu\Delta L$. The time-average quantity $\langle I_4^2\rangle_\mathcal{T}$

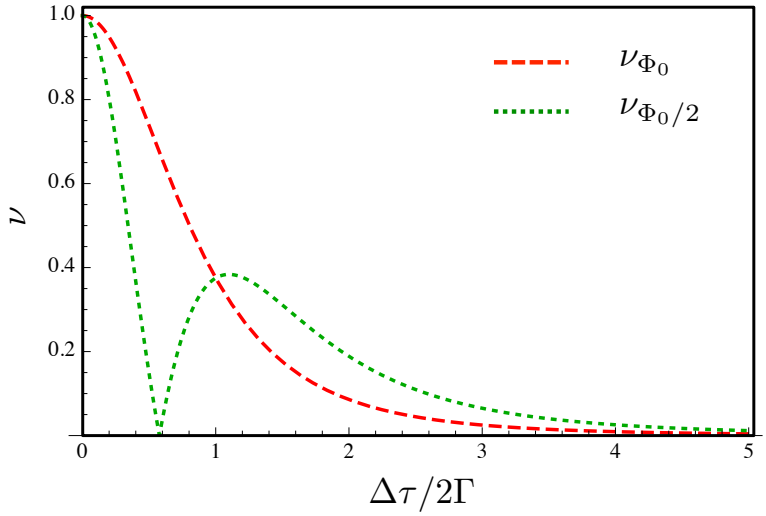

Figure 2.9: Visibilities of the first harmonic ν_{Φ_0} (red dashed curve), and of the second harmonic, $\nu_{\Phi_0/2}$ (green dotted curve) of the mean squared current as a function of the imbalance $\Delta\tau$ in units of the single-particle coherence length $\Lambda = 2\Gamma$. Compared to the charge visibility, they decay faster. Given the actual samples of the MZI in which the maximal implementable delay is of the order of Γ, the mean squared current is the relevant average quantity to be measured experimentally to extract the coherence length.

exhibits AB oscillations as a function of the magnetic flux with two periods, Φ_0 (first harmonic) and $\Phi_0/2$ (second harmonic), as shown in Fig. 2.8. At large imbalance, the function tends to a constant value $(R_{\rm R}R_{\rm L})^2 + (T_{\rm R}T_{\rm L})^2$ corresponding to the classical contribution of the mean squared current. When $\Delta\tau \sim 2\Gamma$, the second harmonic starts contributing. To characterize the decay of the oscillations for the first and second harmonics, we define a visibility for each harmonic, ν_{Φ_0} and $\nu_{\Phi_0/2}$ in a similar way as for the visibility of the oscillations in the interference part of the charge. They are given by the ratio of the amplitude of the oscillations of the first or second harmonics at finite imbalance and their maximal amplitude at $\Delta\tau = 0$:

$$\nu_{\Phi_0} = \left|\frac{B(\Delta\tau)}{B(\Delta\tau=0)}\right| = \frac{1}{(1+(\Delta\tau/2\Gamma)^2)^2}\,, \tag{2.50a}$$

$$\nu_{\Phi_0/2} = \left|\frac{C(\Delta\tau)}{C(\Delta\tau=0)}\right| = \frac{|1-3(\Delta\tau/2\Gamma)^2|}{(1+(\Delta\tau/2\Gamma)^2)^3}\,, \tag{2.50b}$$

where the coefficients B and C are defined in Eqs. (2.49b-2.49c). These visibilities are much more sensitive functions of the MZI's imbalance $\Delta\tau$ than the charge visibility. This could facilitate the measurement of the coherence length $\Lambda = 2v_D\Gamma$. The strong decay of the visibilities of the AB oscillations of the mean squared current can be explained by the electron-hole asymmetry inherent to any mesoscopic circuit with energy-dependent transmission. Consequently electron and hole contributions partially cancel each other in the interference part, leading to the predicted strong decay. We would like to emphasize that the modulus of the time-average coherence

function, the charge and the mean squared current all provide the same information on the coherence time of the emitted single-particle states. These quantities differ only in their experimental measurement (time-resolved or average measurements).

2.3.3 Validity of the approach for different kind of sources

Interestingly, Eq. (2.40) which expresses $G^{(1)}$ in terms of the scattering matrix of the source in the adiabatic regime is also valid for a dc-source or the Lorentzian source presented in the introduction. For convenience, we recall this expression :

$$G^{(1)}_{\rm ud}(t,\Delta\tau) = \frac{ie}{2\pi\Delta\tau}\Big[S^*_{\rm SES}(t,\mu)S_{\rm SES}(t+\Delta\tau,\mu) - 1\Big]\,. \tag{2.51}$$

The dc-source

For a metallic contact at a dc-voltage $V(t) = V$, the scattering amplitude corresponds to a plane wave at energy eV, $S_{\rm dc}(t,\mu) = e^{-ieVt/\hbar}$. The average current emitted by such a source does not depend on time, $I_{\rm dc} = e^2V/h$. This implies that the relaxation time T_1 of the emitted electrons tends to infinity. To the contrary, the coherence function reads:

$$\mathcal{C}_{\rm dc}(\Delta\tau) = e^{i\pi eV\Delta\tau/h}\,\frac{\sin\left(\pi eV\Delta\tau/h\right)}{\pi eV\Delta\tau/h}\,. \tag{2.52}$$

This first-order coherence length does not depend on time as expected for a stationary source. Remarkably it reflects the structure of a wave-packet incident in a single quantum channel subject to a dc-bias. The decay of the coherence function with the time delay originates from the destructive interferences from electrons arriving at different energies. This induces an energy averaging characterized by the time h/eV, where eV is the energy window in which the electrons are emitted. In the situation where neither electron-electron interaction are considered, nor temperature effects nor interaction with an environment, a dc-source is therefore characterized by a coherence time T_2 which is entirely set by h/eV, the relaxation time T_1 tends to infinity :

$$T_2 = \frac{h}{eV}\,.$$

If carriers are injected through a tunnel contact with transmission probability T, the mean time between carriers transmitted through the MZI, $h/(eVT)$, increases. However, as long as the energy dependence of the transmission T can be neglected, the coherence function is independent of T: it is given by Eq. (2.52) as for the case of a perfect quantum channel.

To emphasize the importance of the characterization of the particle states by their coherence length, let us evaluate it for instance for the dc-source. Considering an applied voltage of $1\,\mu$V and a drift velocity of 10^4 m/s in ballistic samples [Van der Vaart 94, Roulleau 08, McClure 09], the coherence length corresponding to the time h/eV can be estimated to be of the order of $40\,\mu$m. Given that mesoscopic interferometers are typically about $10\,\mu$m or less [Ji 03, Roulleau 07], this length is

sufficiently large to not constitute the limiting length scale for the observation of single-particle quantum interferences. In contrast, dephasing processes have been widely investigated and the corresponding dephasing length has been measured in several samples [Roulleau 08, Bieri 09, Hashisaka 10]: it is of the order of $10\,\mu$m in an electronic MZI and depends on the electronic temperature of the sample, on the interactions with the Fermi sea and/or on the interactions with a coupled environment.

The Lorentzian source

Equation (2.40) is also valid for the Lorentzian source. We recall that this source consists in applying a periodic bias $V(t) = V(t+\mathcal{T})$, where $V(t)$ is a Lorentzian voltage pulse carrying one electron in one period $\mathcal{T}$ [Keeling 06] :

$$V(t) = \frac{h}{e\pi}\frac{1}{\Gamma_L}\frac{1}{1+(t/\Gamma_L)^2}\,.$$

Here the Lorentzian is characterized by its half width Γ_L. The label L stands for "Lorentzian". Such a potential applied to the Fermi sea leads to the emission of pulses with an integer number of charges without any spurious electron-hole pairs [Ivanov 93, Levitov 96, Keeling 06]. This potential verifies the area quantization condition :

$$\frac{h}{e}\int dt' V(t') = 1\,.$$

Compared to the SES based on the mesoscopic capacitor, the current emitted by this source has a dc- and an ac-component. The dc-part of the potential V_0 corresponds to the 0-th Fourier component of $V(t)$:

$$V_0 = \int_0^{\mathcal{T}} \frac{dt'}{\mathcal{T}} V(t) = \frac{\hbar\Omega}{e}\,.$$

This on-demand single-particle source is described by the instantaneous scattering amplitude S_L:

$$S_L(t,\mu) = \exp\Big(\frac{-ie}{\hbar}\int_0^t dt' V(t')\Big) = e^{i\Omega t}\frac{t-t^- + i\Gamma_L}{t-t^- - i\Gamma_L}\,,$$

Defining $\widetilde{S}_L(t) \equiv e^{-ieV_0 t/\hbar} S_L(t)$, the current emitted by this Lorentzian source is given by:

$$\begin{aligned} I_L(t) &= \frac{-ie}{2\pi}\,\widetilde{S}_L(t)\,\frac{\partial \widetilde{S}_L^*(t)}{\partial t} \\ &= \frac{e}{\pi}\frac{1}{\Gamma_L}\frac{1}{1+(t/\Gamma_L)^2}\,, \end{aligned} \tag{2.53}$$

This current corresponds to the emission of one electron per period of the potential and the half width Γ_L corresponds to the relaxation time T_1 of the single-particle state emitted by this Lorentzian source. Using Eq. (2.40), the coherence function at time $t = t^-$ is given by :

$$\mathcal{C}_{\mathrm{L}}(t^-, \Delta\tau) = \frac{-i\Gamma_L}{2\Delta\tau}\left(e^{-i\Omega\Delta\tau}\,\frac{1 - i\Delta\tau/\Gamma}{1 + i\Delta\tau/\Gamma} - 1\right) . \tag{2.54}$$

The phase factor $e^{-i\Omega\Delta\tau}$ comes from the dc-part of the current. If this part would vanish, we would recover the expression of the coherence function for the mesoscopic capacitor in the adiabatic regime. As for the source in the adiabatic regime, the coherence time is obtained by considering the decay of the modulus of the time-average coherence function. The coherence length of the single electrons emitted by the Lorentzian source is set by the half width of the Lorentzian pulses, $T_2 = 2\,\Gamma_L$.

2.3.4 Summary for the adiabatic regime

The adiabatic regime for the source is reached when the periodic potential which drives the cavity varies slowly compared to the time spent by one particle in this cavity. The current emitted by the source in this regime consists in two Lorentzians per period of the driving potential characterized by their half width Γ. The current pulses are centered on the times of emission of an electron and a hole. Given that the scattering matrix is evaluated at the Fermi energy in the adiabatic regime (the particles are emitted close to the Fermi sea), the first-order correlation $G^{(1)}$ function takes a simple form:

$$G^{(1)}_{\mathrm{ud}}(t,\Delta\tau) = \frac{ie}{2\pi\Delta\tau}\Big[S^{*}_{\mathrm{SES}}(t,\mu)S_{\mathrm{SES}}(t+\Delta\tau,\mu)-1\Big]\,.$$

By inserting the expression of the scattering matrix in this expression and by considering only the contribution of the electron because we are interested in single-particle interferences, we obtained the coherence function:

$$G^{(1)}_{\mathrm{ud}}(t,\Delta\tau) \;=\; \frac{e\Gamma}{\pi}\frac{1}{(t+i\Gamma)(t+\Delta\tau-i\Gamma)}\,.$$

This function depends in a non-trivial way on the time delay $\Delta\tau$ of the interferometer. Therefore the coherence time T_2 is extracted from the time-average expression of $G^{(1)}$ or equivalently from the mean charge or from the mean squared current. For the charge, the decay of the amplitude of the AB oscillations in the interference part of the charge as a function of the time delay $\Delta\tau$ is characterized by the visibility ν_Q :

$$\nu_Q = \frac{1}{\sqrt{1+\left(\Delta\tau/2\Gamma\right)^2}}\,.$$

This function reflects the single-particle state emitted by the source in the adiabatic regime and decays with the characteristic time $T_2 = 2\Gamma$. The coherence time is only set by the relaxation time of the source. With the explicit calculation of the normalized first-order correlation function $g^{(1)}$ whose modulus is equal to unity, $|g^{(1)}| = 1$, we have shown that the pulses emitted by the source in the adiabatic regime are Fourier-transform limited, i.e their coherence time is only set by their temporal shape characterized by the relaxation time $T_1 = \Gamma$. These analytical results motivate further investigation of the source in this regime, in particular the investigation of the second-order correlation function.

2.4 The non-adiabatic regime

The emission of single-particle states at controlled times by the on-demand SES is achieved in two regimes, the adiabatic regime and the non-adiabatic one. In the previous part, we have investigated the first-order coherence properties of states emitted in the adiabatic regime and show that their coherence time is set by their relaxation time, i.e the emitted single-particle states are Fourier-transform limited. To complete the characterization of the on-demand SES as single-particle emitter, we present in this part the results we obtained for the first-order correlation function as well as for the coherence time for single-particle states emitted in the non-adiabatic regime.

This regime is reached when the potential has an abrupt change compared to the time spent by the particle in the cavity, the dwell time. We recall that the cavity is characterized by the energy level spacing Δ and that the states of the cavity are coupled to an outer edge state through a QPC with a transmission probability $T_{\rm SES}$. The dwell time is defined as $\tau_D = h/(\Delta T_{\rm SES})$. A driving potential which varies much faster than the dwell time is for example a periodic square potential $U(t) = U(t+\mathcal{T})$, see Fig. 2.10 :

$$U(t) = \begin{cases} U_0\,, & -\mathcal{T}/2 < t < -\mathcal{T}/4\,, \\ U_1\,, & -\mathcal{T}/4 < t < \mathcal{T}/4\,, \\ U_0\,, & +\mathcal{T}/4 < t < \mathcal{T}/2\,. \end{cases} \tag{2.55}$$

The first step of the potential at $-\mathcal{T}/4 \equiv t^-$ is at the origin of the emission of an electron whereas the second step at $\mathcal{T}/4 \equiv t^+$ provokes the emission of a hole. In this work, we focus on single-particle interferences so that we assume that the times of emission of an electron and a hole are well separated, i.e $|t^- - t^+| \gg \tau_D$.

In contrast to the adiabatic regime, the analytical derivation of the scattering amplitude as well as the expression of the current emitted by the source in this regime is a new result. Given the technicality of the calculations, we refer the reader to the Appendix 4.3 for more details (Ref. [Haack 12]). Here, we only present the main assumptions made to derive the expression of the Floquet scattering amplitude in the non-adiabatic regime.

We have to start again from the Fabry-Pérot expression given by Eq.(2.12) with now a phase $\Phi_n(t)$ which varies over the time the particle spends inside the mesoscopic capacitor. For simplicity, we consider here the time interval $[-\mathcal{T}/2, 0]$ during which an electron is emitted. The abrupt change of the potential occurs at $t^- = -\mathcal{T}/4$:

$$S^{(e)}_{\rm na}(t,E) \;=\; r_{\rm SES} + \frac{t^2_{\rm SES}}{r_{\rm SES}} \sum_{n=1}^{\infty} r^n_{\rm SES}\, e^{i\left(nk_E L - \Phi_n(t)\right)}\,, \tag{2.56}$$

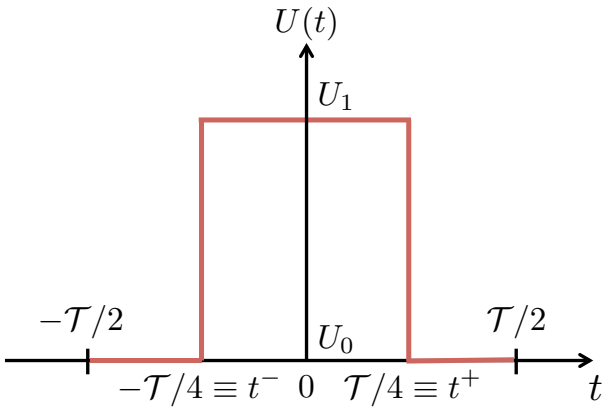

Figure 2.10: Periodic square potential to operate the source in the non-adiabatic regime, shown in the time interval $[-\mathcal{T}/2, \mathcal{T}/2]$. The abrupt changes between the lower value U_0 and the higher value U_1 at times $t^{\mp}$ lead to the emission of an electron and of a hole. One condition to operate the source in the optimal regime consists in setting the difference $U_1 - U_0$ equal to the energy level spacing in the cavity Δ.

with

$$\begin{aligned} \Phi_n(t) &= \frac{e}{\hbar}\int_{t-n\tau}^{t} dt'\, U(t') \\ &= \frac{e}{\hbar}\begin{cases} n\tau U_0 & -\mathcal{T}/2 < t < t^- \\ n\tau U_0 + \delta U t & t^- < t < t^- + n\tau \\ n\tau U_1 & t^- + n\tau < t < 0\,. \end{cases} \end{aligned} \tag{2.57}$$

The potential difference is $\delta U = U_1 - U_0$ and we recall that the sum over n is the sum over the number of tours of the cavity that the particle makes before being transmitted to the edge state. Important simplifications concerning the derivation of the scattering amplitude can be made when assuming that the source is operated in the *optimal* regime :

1) The potential difference δU corresponds exactly to one level spacing $\Delta = h/\tau$ of the mesoscopic capacitor. This assumption is in agreement with the experimental regime in which the emission of quantized charges is observed.

2) At $t = 0$, the Fermi energy μ lies exactly in the middle of two levels of the cavity.

These two conditions ensure that only one electron and one hole are emitted in each half-period of the potential $U(t)$. Similarly to the adiabatic regime, the Floquet

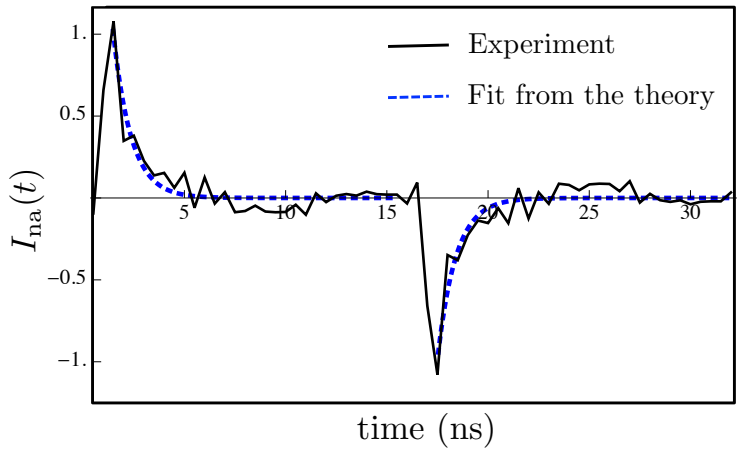

Figure 2.11: Current emitted by the on-demand SES in the non-adiabatic regime. The experimental data are shown in black (courtesy of G. Fève). The fit (dotted blue curve) is found from the analytical expression of the current derived with a scattering matrix approach (see Eq. (2.59)). The characteristic time of the exponential (or relaxation time T_1) corresponds to the dwell time of the particle inside the cavity, $\tau_D = h/(\Delta T_{\rm SES})$. Its numerical value is deduced from the fit, $\tau_D = T_1 = 0.9$ ns.

scattering matrix $S_{\rm na}(E_m, E)$ consists of two parts describing the emission of an electron and the emission of a hole :

$$S_{\rm na}(E_m,E) = \begin{cases} S_{\rm na}^{(e)}(E_m,E) & , \quad |t-t^-| \sim \tau_D \\ S_{\rm na}^{(h)}(E_m,E) & , \quad |t-t^+| \sim \tau_D \\ \sim \delta_{m,0} & , \quad \text{elsewhere}\,. \end{cases} \tag{2.58}$$

The label "na" stands for non-adiabatic whereas (e,h) denote respectively the electron and hole part of the Floquet scattering amplitude. The exact expressions of $S_{\rm na}^{(e,h)}$ can be found in the Appendix 4.3.

At zero temperature, the current $I_{\rm na}$ emitted by the source in the non-adiabatic regime can be calculated analytically. We have shown that only one level of the cavity contributes to the current and the current reads :

$$I_{\rm na}(t) = \frac{e}{\tau_D} e^{-(t-t^-)/\tau_D}\Theta(t-t^-) - \frac{e}{\tau_D} e^{-(t-t^+)/\tau_D}\Theta(t-t^+)\,. \tag{2.59}$$

Here Θ is the Heaviside function. Again, the details of the calculations are provided in Appendix 4.3. With this calculation, we have derived consistently the current emitted by the source in this regime. It fits remarkably well with the experimental measurement as shown in Fig. 2.11. In previous works on the on-demand SES [Fève 06, Mahé 10, Parmentier 12], the fit of the experimental data has been made

by modeling the mesoscopic capacitor as a non-linear RC-circuit, where the non-linearity was taken into account in the expression of the capacitance and of the resistance which both depended on the high-frequency of the driving potential $U(t)$. This model is based on the first theoretical descriptions of the mesoscopic capacitor, where a low-frequency drive was assumed [Büttiker 93a, Büttiker 93b, Prêtre 96]. With our work, we provide a consistent derivation of the current emitted in the non-adiabatic regime at zero temperature from the Floquet scattering amplitude of the source.

In the next section, we investigate the first-order correlation function to characterize the first-order coherence properties of the single-particle states emitted in this non-adiabatic regime.

2.4.1 First-order correlation function

We recall the definition of the first-order correlation function $G^{(1)}(t, \Delta\tau)$ in terms of the scattering amplitude of the source given by Eq.(2.23). The scattering amplitude is now the one in the non-adiabatic regime, $S_{\rm na}$:

$$\begin{aligned} G^{(1)}_{\rm ud}(t,\Delta\tau) &= \frac{e}{h}\int_0^\infty dE \sum_m \left[f(E)-f(E_m)\right] e^{-i(E-\mu)\Delta\tau/\hbar} \\ &\quad \int \frac{dt'}{\mathcal{T}} e^{-im\Omega(t'-t)}\, S^*_{\rm na}(t',E) S_{\rm na}(t+\Delta\tau,E)\,. \end{aligned}$$

In the non-adiabatic regime, the particles are emitted further from the Fermi sea than in the adiabatic regime [Bocquillon 12]. As a consequence, the scattering matrix $S_{\rm na}$ depends on energy (it can not be evaluated at the Fermi energy) and the expression of the first-order correlation function can not be simplified more without doing explicitly the different integrals. Due to the emission of one electron and one hole on average during one period, the first-order correlation function is composed of two terms. As in the adiabatic regime, we are interested in the single-particle coherence properties so that we provide here only the explicit expression of the single-electron coherence function in the non-adiabatic regime:

$$\mathcal{C}^{(e)}_{\rm na}(t,\Delta\tau) = e^{-(t-t^-)/\tau_D} e^{-\Delta\tau/2\tau_D} e^{i\pi\Delta\tau/\tau}\,\Theta(t-t^-)\,. \tag{2.60}$$

Here Θ is the Heaviside function and we assume that $\Delta\tau > 0$. The coherence function depends explicitly on the parameters of the experimental setup, namely the asymmetry of the MZI and the dwell time of the cavity τ_D which is the relaxation time T_1 of the emitted single-particle state. As a function of the delay $\Delta\tau$, it decays with the characteristic time $2\tau_D$:

$$\left|\mathcal{C}^{(e)}_{\rm na}(t,\Delta\tau)\right| \propto e^{-\Delta\tau/2\tau_D}\,. \tag{2.61}$$

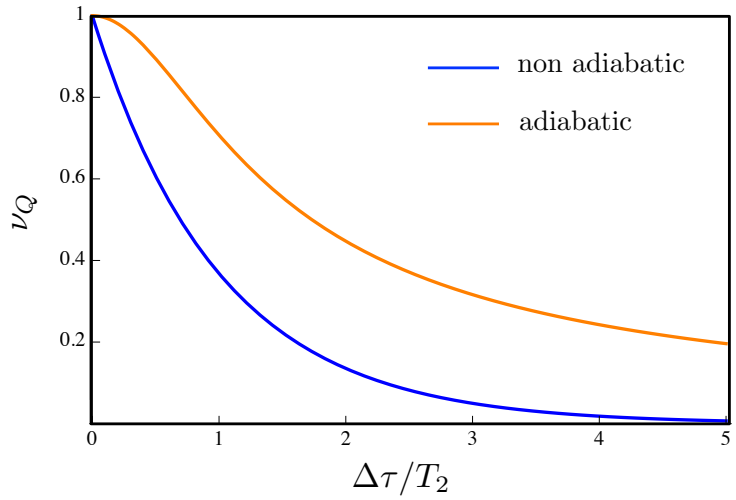

Figure 2.12: Comparison of the visibilities of the AB oscillations in the charge as a function of the imbalance $\Delta\tau$ for the source in the non-adiabatic regime (blue curve) and in the adiabatic regime (orange curve).

Compared to the adiabatic regime, the characteristic time of the decay $2\tau_D$ is the same at all times t. Therefore, considering the decay of $\mathcal{C}^{(e)}_{\rm na}(t,\Delta\tau)$ or of the time-integrated coherence function gives access to the T_2 coherence time :

$$T_2 = 2\,\tau_D = 2\,T_1\,.$$

This relation implies that there are no dephasing processes which reduce the coherence time in our model. The coherence length in the non-adiabatic regime is given by:

$$\Lambda_{\rm na} = 2v_D\tau_D\,, \tag{2.62}$$

where we recall that $\tau_D = h/(T_{\rm SES}\Delta)$ is the characteristic time of the emitted quantized exponential current pulse and v_D is the drift velocity of the electrons through the MZI. This expression is similar to the one derived in the adiabatic regime.

2.4.2 The coherence length

An advantage of our setup as explained above is that it allows to extract the coherence length from time-average measurements. The charge, defined as the integral of the current $I_{4,\rm na}(t)$ over half a period, is given by:

$$Q_{\rm na}(\Delta\tau) = e\big(R_{\rm L}R_{\rm R} + T_{\rm L}T_{\rm R} - 2\sqrt{R_{\rm L}R_{\rm R}T_{\rm L}T_{\rm R}}e^{-\Delta\tau/2\tau_D}\cos\left(2\pi\phi - \pi\Delta\tau/\tau\right)\big). \tag{2.63}$$

We only take into account the contribution of the electron. The charge exhibits one harmonic with frequency Φ_0 (we repeat that $2\pi\phi = 2\pi\Phi/\Phi_0 + k_\mu\Delta L$). Interestingly, the AB oscillations are shifted by a term depending on the delay $\Delta\tau$ and on the

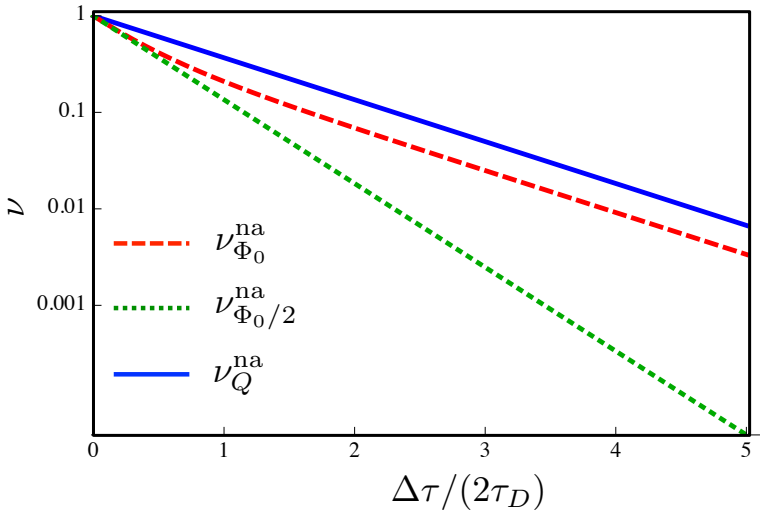

Figure 2.13: Envelopes of the visibilities in the non-adiabatic regime in a semi-log scale. The visibilities of the first harmonic $\nu^{\rm na}_{\Phi_0}$ (dashed red line), and of the second harmonic, $\nu^{\rm na}_{\Phi_0/2}$ (green dotted line) decay faster than the charge visibility $\nu^{\rm na}_{Q}$ (blue line) as a function of the time delay.

energy of the level contributing to the transport $\Delta/2$, where $\Delta = h/\tau$ is the energy level separation in the cavity. To compare the adiabatic and non-adiabatic regimes, we calculate the visibility $\nu^{\rm na}_{Q}$ of the AB oscillations in the charge using the same definition, namely the ratio of the amplitude of the AB oscillations in the interference part of the charge at a finite time delay with their maximal amplitude at $\Delta\tau = 0$:

$$\nu^{\rm na}_{Q} = e^{-\Delta\tau/2\tau_D} \,. \tag{2.64}$$

The visibility of the AB oscillations in the charge decays with the coherence time $T_2 = 2\tau_D$ as shown in Fig. 2.12. From an experimental point of view, the visibility in the non-adiabatic regime decays over several microns. As in the adiabatic regime, it could be convenient to look at a quantity whose visibility decays faster in order to avoid damaging the sample with high side gate voltages. We therefore investigate the mean squared current, as we have done in the adiabatic regime.

The mean squared current has a similar form compared to the adiabatic regime:

$$\left\langle I^2_{4,\rm na}\right\rangle_{\mathcal{T}} = \frac{e^2}{2\tau_D\mathcal{T}}\Big(A_{\rm na} - B_{\rm na}\cos(2\pi\phi) + C_{\rm na}\cos(4\pi\phi)\Big)\,, \tag{2.65}$$

with

$$\begin{aligned}
A_{\rm na} &= R^2_{\rm R}R^2_{\rm L} + T^2_{\rm R}T^2_{\rm L} + 4R_{\rm R}R_{\rm L}T_{\rm R}T_{\rm L}\, e^{-\Delta\tau/\tau_D} \\
B_{\rm na} &= 4\sqrt{R_{\rm R}R_{\rm L}T_{\rm R}T_{\rm L}}e^{-\Delta\tau/2\tau_D}\left(R_{\rm R}R_{\rm L} + T_{\rm R}T_{\rm L}\, e^{-\Delta\tau/\tau_D}\right)\cos(\pi\Delta\tau/\tau) \\
C_{\rm na} &= 2R_{\rm R}R_{\rm L}T_{\rm R}T_{\rm L}e^{-\Delta\tau/\tau_D}\cos(2\pi\Delta\tau/\tau)
\end{aligned}$$

The oscillating term in $B_{\rm na}$ and $C_{\rm na}$ depends on the asymmetry $\Delta\tau$ of the MZI and on the energy level separation in the cavity $\tau = h/\Delta$. Considering symmetric QPCs, $T_{\rm L} = T_{\rm R} = 1/2$, the visibilities of the first and second harmonics of the mean squared current are :

$$\nu^{\rm na}_{\Phi_0} = \left|\frac{B_{\rm na}(\Delta\tau)}{B_{\rm na}(0)}\right| = e^{-\Delta\tau/2\tau_D}(1+e^{-\Delta\tau/\tau_D})|\cos(\pi\Delta\tau/\tau)|\,, \tag{2.66a}$$

$$\nu^{\rm na}_{\Phi_0/2} = \left|\frac{C_{\rm na}(\Delta\tau)}{C_{\rm na}(0)}\right| = e^{-\Delta\tau/\tau_D}|\cos(2\pi\Delta\tau/\tau)|\,. \tag{2.66b}$$

The visibilities of the harmonics of the mean squared current decay faster than the visibility of the charge as shown in Fig. 2.13. Again, this can be explained by the electron-hole asymmetry visible in the energy-dependent transmission amplitude of the MZI. It leads to a partial cancellation of the signal, making the visibilities of the harmonics of the mean squared current decaying faster than the visibility of the interference part of the charge. In particular, the visibility of the second harmonics is more sensitive to the time delay $\Delta\tau$ and could make easier the experimental determination of the coherence time $T_2 = 2\tau_D$ as explained in the adiabatic regime.

2.5 Conclusion

The realization of novel single electron sources demands a characterization of their coherence properties. In this chapter, by coupling such a source to a MZI, we have investigated the first-order correlation function $G^{(1)}$ which characterizes the first-order coherence properties of the single-particle states emitted by the source. Instead of expressing $G^{(1)}$ in terms of field operators as it is the case in quantum optics, we have derived an expression in terms of the scattering matrix of the source.

In the adiabatic regime characterized by a periodic potential which varies slowly compared to the dwell time of the particle inside the cavity, the expression of the scattering amplitude for the source was known from previous works, it is the frozen scattering matrix. The current emitted by the source consists in two Lorentzian pulses characterized by their half width Γ. From the analytical expression of the first-order correlation function, we have shown that this width determines the coherence length of the single-particle states, $\Lambda = 2v_D\Gamma$, where v_D is the drift velocity of the electrons.

In the non-adiabatic regime characterized by a potential which varies much faster than the dwell time, we have derived an analytical expression for the scattering amplitude, which was not known before. This expression is one of the main results of this chapter. From it, we calculated the current emitted by the source in this regime. It consists of two exponentials curves characterized by the dwell time τ_D and it agrees well with the experimental measurements. From the decay of the first-order correlation function, we extracted the coherence length of the single-particle states emitted in the non-adiabatic regime. This length is proportional to the dwell time, $\Lambda_{\mathrm{na}} = 2v_D\tau_D$. This expression is the analog to the one in the adiabatic regime.

In both regimes, the coherence time of the single-particle states is twice their relaxation time. Within our model which does not include dephasing or relaxation processes present in the MZI, the source emits Fourier-transform limited pulses whose coherence time is only set by their relaxation time. Such single-electron states are therefore promising for the future of electron quantum optics, i.e electron optics at the single charge level. This work constitutes a first step towards the reconstruction of the single-particle state, which is an essential concept for electronics and for applications for quantum information processing.

From an experimental point of view, the coherence length of the single-particle states can be determined from time-average measurements such as the mean charge or the mean squared current. Thus a current measurement that is slow compared to the evolution of the single-electron pulses opens a path to experimentally extract information on the quantum nature of the emitted states. This constitutes a strong advantage of our work compared to other proposals based on noise measurements. One of the perspectives to this work is the possibility to include relaxation

and dephasing processes in our model to be in a closer agreement with a possible experimental realization of our proposal.

Chapter 3

Electron waiting times in mesoscopic conductors

Contents

3.1 Introduction

This chapter presents the results we obtained on the distributions of waiting times in mesoscopic conductors. The distribution of waiting times between elementary physical events is an important tool to characterize and investigate temporal correlations and transport statistics of stochastic processes [Van Kampen 07]. Waiting time distributions play a significant role in various branches of science, for instance in quantum optics [Tannoudji 86, Zoller 87, Carmichael 89] and in single-molecule chemistry [English 06]. Previous works on waiting times in mesoscopic physics have been done within the formalism of Markovian rate equations [Schriefl 05, Koch 05, Brandes 08, Welack 08, Welack 09, Albert 11]. This formalism allows to take into account the coherent effects of the mesoscopic scatterer and therefore to extract information about the short-time physics taking place in these transport experiments. To give an example, my collaborators Mathias Albert, Christian Flindt and Markus Büttiker investigated the waiting times of the ac-driven single-electron source presented in the previous chapter [Fève 07]. The waiting times between the emission of two electrons allowed them to better characterize the single-particle emission process [Albert 11]. However this Markovian rate equations describe only single-particle processes. The project presented in this chapter started with the following question: Can we develop a full quantum description for the distribution of waiting times? As the single-electron source is a rather complex system, we decided to consider first one of the simplest systems in mesoscopic physics, namely a biased quantum point contact (QPC).

The chapter is organized as follows. We first give a brief introduction to Full Counting Statistics (FCS) and on waiting times distributions (WTDs) to emphasize the importance of these statistical tools to investigate the transport properties of a mesoscopic conductor. Sections 2 and 3 present our main results, which are the quantum derivation of the WTDs that can be applied to any biased mesoscopic conductor and the illustration of that formalism for a biased QPC. The quantum formula of the WTDs can be expressed as a determinant formula, similar to the one derived in FCS for the generating function by Levitov and Lesovik [Levitov 93, Levitov 96]. Importantly, we did not assume any Markovian properties when deriving this result, making it valid for numerous mesoscopic transport problems.

3.1.1 Full Counting statistics

The investigation of the fluctuations in a transport experiment through a mesoscopic conductor is at the heart of mesoscopic physics. By looking at the transport statistics, important informations are gained on short- and long-time correlations. Repeating an experiment many times gives access to the measurement of the average conductance proportional to the mean number $\langle n \rangle$ of transferred charges in a time interval t or gives access for instance to the shot noise proportional to the variance

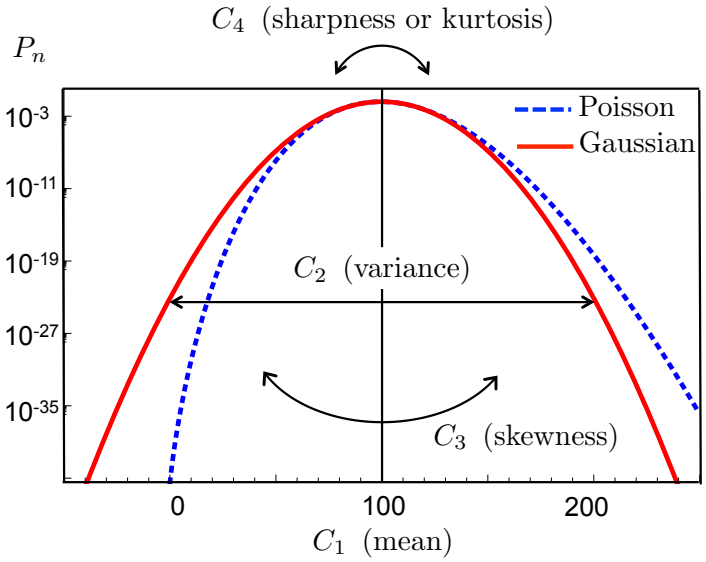

Figure 3.1: The Poisson and the normal distributions are plotted as a function of the number of events n in a semi-log scale. The Poisson and normal distribution are plotted with the same mean $C_1 = 100$. Due to the central limit theorem, for large n, the distributions differ only far away in the tales. The second cumulant C_2 characterizes the variance of the width of the distribution, whereas the skewness C_3 characterizes the asymmetry of the distribution with respect to the mean. The normal distribution is characterized by $C_3 = 0$ whereas the Poisson distribution has a non-zero skweness. The 4-th cumulant (the kurtosis) characterizes the sharpness of the distribution.

$\langle \big(n - \langle n \rangle\big)^2 \rangle$. The measurement of these averaged quantities has been crucial in mesoscopic physics. Striking examples are the quantization of the conductance through a QPC or the importance of the charge quantization in the observation of shot noise. However, to get a more complete characterization of the stochastic transport process through a mesoscopic conductor, the determination of the full probability distribution $P_n(t)$ is necessary, where $P_n(t)$ is the probability to have n transferred charges in a long time interval t. The distribution is characterized by its successive cumulants C_k, see Fig. 3.1 for their interpretation:

$$
\begin{aligned}
C_1 &= \langle\langle n \rangle\rangle = \langle n \rangle = \textstyle\sum_n n\, P_n(t) && : \text{mean} \\
C_2 &= \langle\langle n^2 \rangle\rangle = \langle (n - \langle n \rangle)^2 \rangle && : \text{variance} \\
C_3 &= \langle\langle n^3 \rangle\rangle = \langle (n - \langle n \rangle)^3 \rangle && : \text{skewness} \\
C_4 &= \langle\langle n^4 \rangle\rangle = \langle (n - \langle n \rangle)^4 \rangle - 3\langle (n - \langle n \rangle)^2 \rangle^2 && : \text{sharpness (kurtosis)}
\end{aligned}
$$

Single brackets denote averaging with respect to the probability distribution $P_n(t)$. The first cumulant is identical to the average of the distribution whereas the second cumulant (the variance) and the third cumulant (the skewness) are identical to the central moments. Higher cumulants differ in general from the central moments as the fourth cumulant expression (sharpness) shows. The cumulants can be calculated

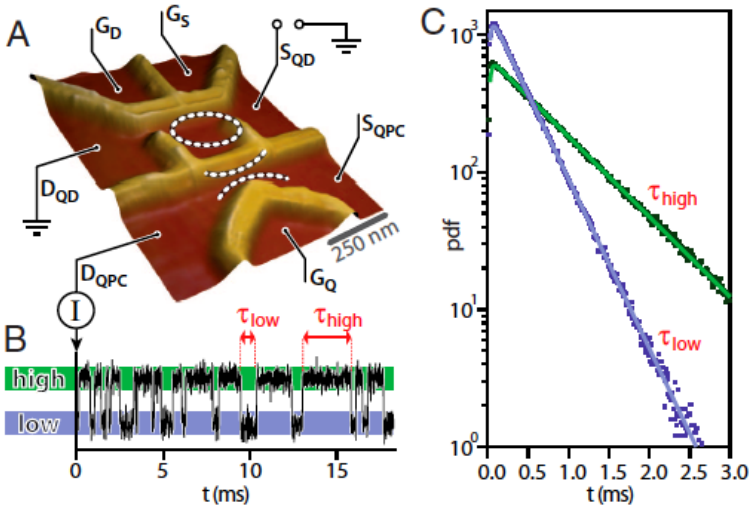

Figure 3.2: Experiment in Full Counting Statistics (FCS). Inset A: The number of tunneling events through a QD (dashed white circle) is counted by measuring the current in a nearby QPC (white dashed lines). The tunneling rates of the QD are controlled with the side voltage gates G_S and G_D, where the letters S and D indicate the source and the drain. An additional gate voltage is applied to the QPC, G_Q, to control its transmission probability. Inset B shows the trace of the current measured through the QPC, from its source to its drain. The jumps in the current trace indicate that one electron jumped in the QD from the source (current goes down) or that one electron left the QD for the drain (current goes up). Inset C: From the trace of the current, they can reconstruct the probability distribution function of the number of transferred charges and deduce from it the tunneling rates of the QD, $\tau_{\rm low}^{-1}$ and $\tau_{\rm high}^{-1}$. Figure taken from Ref. [Flindt 09].

from the successive derivatives of the cumulant generating function (CGF), $S(\chi,t)$:

$$e^{S(\chi,t)} = \sum_n P_n(t)\, e^{i\chi n}\,, \tag{3.1}$$

$$C_k = \frac{\partial^k S(\chi,t)}{\partial (i\chi)^k}\Big|_{\chi=0}\,, \tag{3.2}$$

where χ is the counting field. Full Counting Statistics (FCS) aims at reconstructing the CGF and at extracting the maximal amount of information about the transport process from this probability distribution [Levitov 93, Levitov 96, Nazarov 03]. It is experimentally very challenging to reconstruct the CGF but there are now a few experimental groups able to do it [Gustavsson 06, Gabelli 09, Flindt 09]. In one setup, they count the number of tunneling processes through a quantum dot (QD) by measuring the trace of the current in a nearby QPC as shown in Fig. 3.2 . By operating the QD in the strong Coulomb blockade regime, they can reach a regime where only few electrons tunnel through the QD in a time interval of 1 second. The counting of events is therefore possible and they can deduce from it the CGF.

To illustrate the above definitions let us consider two well-known distributions, the Poisson and the binomial distributions. The Poisson process corresponds to a binomial distribution with a small probability of success Γ compared to 1. It describes rare and uncorrelated events. Its probability distribution $P_n(t)$ and its CGF are:

$$\begin{aligned} P_n(t) &= \frac{(\Gamma t)^n}{n!} e^{-\Gamma t}\,, \\ S(\chi,t) &= \ln\Big(\sum_n P_n(t)\, e^{i\chi n}\Big) = \Gamma t\big(e^{i\chi}-1\big)\,. \end{aligned}$$

From the probability distribution, one can see that Γt corresponds to the mean number of transferred charges in a time t. The cumulants are directly calculated from Eq.(3.2):

$$C_1 = C_2 = C_3 = C_4 = \ldots = \Gamma t\,.$$

All cumulants are identical and they grow linearly in time, $\langle\langle n^k \rangle\rangle(t) = \Gamma t$. For comparison a deterministic process has zero variance and zero skewness. By normalizing the cumulants with respect to the first cumulant, we find $\langle\langle n^k \rangle\rangle / \langle\langle n \rangle\rangle = 1$. This property is often taken to be the hallmark of a Poissonian process.

A binomial process with success probability $\Gamma \in [0,1]$ is described by the following probability distribution:

$$P_n(t) = \left(\begin{array}{c} N \\ n \end{array} \right) \Gamma^n \,(1-\Gamma)^{N-n}\,,$$

where N is the total number of attempts. The corresponding CGF and the three first cumulants are:

$$\begin{aligned} &S(\chi,t) = t\,\ln\left[1+\Gamma(e^{i\chi}-1)\right]\,, \\ &C_1 = \Gamma t \\ &C_2 = \Gamma t(1-\Gamma) \\ &C_3 = \Gamma t(1-\Gamma)(1-2\Gamma)\,. \end{aligned}$$

We recognize the cumulants characteristic of a transport process through a QPC with a transmission probability T [Levitov 93, Levitov 96]. At zero temperature, when the QPC is connected through a single quantum channel to the reservoirs with a dc-bias eV, the average current $\langle I \rangle$ and the zero-frequency noise $S(\omega = 0)$ are given by [Khlus 87, Lesovik 89, Büttiker 90]:

$$\langle I \rangle = \frac{e^2 V}{h} T\,, \tag{3.3}$$

$$S(\omega = 0) = \frac{e^3 V}{h} T(1-T)\,. \tag{3.4}$$

At zero temperature and finite bias, the fluctuations originate from the stochastic nature of the transport through the QPC: the particle can either be reflected or transmitted. For a perfect quantum channel characterized by a transmission $T = 1$ (no scatterer), the low-frequency transport is noiseless, in other words, the transport is deterministic and regular at long times [Büttiker 90, Blanter 00]. At long times there are no fluctuations in the transport statistical properties of a perfect quantum channel.

What is important to emphasize for the work on waiting times which will be presented below, is that the cumulants in FCS characterize the fluctuations of the transferred charges in a *long* time interval compared to the time scales of the problem. FCS looks at the fluctuations of the integrated current over a long period of time and investigates therefore correlations that arise at times much longer than the characteristic time scale at which the particles are emitted by the source. For instance in the experiment presented above [Flindt 09], the QD is operated in the strong Coulomb blockade regime. Only single-particle events take place. When electrons tunnel to the drain, they no longer contain information about the characteristic time rate h/eV at which they have been emitted by a dc-source with bias eV.

A question that arises at this point is to know if the time scale characterizing the source, h/eV for a dc-source, is accessible by looking at the distribution of events after a scatterer. This requires us to look at the distribution of events at very short time scales, or equivalently at high-frequencies. For instance, if the bias voltage V is of the order of few μV, experiments will have to go up to frequencies of the order of GHz to probe the source time scale. Even if there have been important technical progresses in high-frequency measurements [Zakka-Bajjani 10], as seen also for instance with the single-electron source [Gabelli 06, Fève 07, Mahé 10], this remains experimentally very challenging. Looking at finite-frequency fluctuations is therefore not sufficient for this purpose and important information may be lost if one investigates only the probability distribution of the number of transferred charges. To look at the physics of short-time scales, another statistical distribution is more convenient: the distribution of waiting times.

3.1.2 Waiting time distributions

Considering a statistical process, we can define a measurement process whose outcome can be represented as a sequence of random pulses as a function of a given parameter. This pulses define the events of the distribution. For instance, we can look at the energy spectrum of heavy atoms or at en electronic current represented as a random sequence of peaks as a function of time. To characterize such a distribution of events, one can look at the interval between two events. In spectral statistics this would correspond to the level spacing between two energy levels [Metha 04, Haake 10] whereas for a current, it would correspond to the time interval between two consec-

utive events. This time interval is the waiting time.

The distribution of waiting times has attracted lots of interest in various fields like single-molecule chemistry [English 06, Gopich 06] or quantum optics [Tannoudji 86, Zoller 87, Carmichael 89, Vyas 99]. In quantum optics the waiting time is defined as the time between two consecutive photodetection events. Of particular interest is the discussion of the antibunching of photons in WTDs compared to the definition of antibunching in terms of the normalized second order correlation function g^2 between two events occurring at times t and t' [Carmichael 89, Vyas 99]. As the photon flux is stationary, this correlation function only depends on the time difference $\tau = t' - t$:

$$g^2(\tau) = \frac{\langle : \hat{I}(t+\tau)\hat{I}(t) : \rangle}{\langle \hat{I} \rangle^2}\,, \tag{3.5}$$

where $\hat{I}(t)$ is the intensity operator at time t. The intensity $\langle \hat{I} \rangle$ is the number of photons detected per unit time and $\langle : \cdots : \rangle$ denotes the average with the normal ordering defining the detection process: as soon as one photon is detected, it is destroyed. For statistically independent events $g^2(\tau) = 1$ whereas for perfect antibunched photons, $g^2(0) = 0$ [Glauber 63b, Walls 94, Mandel 99]. By definition the g^2 function investigates correlations between events separated by an arbitrary time τ, that can be much longer than the average time between two successive photodetections. From a statistical point of view, the g^2 function is a non-exclusive probability: the detection of photons during the time interval τ between the two points at which the correlation function is calculated, does not enter the probability. In contrast, the distribution of waiting times, $\mathcal{W}(\tau)$, is an exclusive probability: it investigates the correlations between two *successive* detections of photons and the definition ensures that no photons have been emitted in the time interval $\tau = t' - t$. It probes short-time correlations, correlations between successive events. There is one case for which exclusive and non-exclusive probabilities are the same: when the time interval τ is very short compared to the average time between two events, the two probabilities coincide as the probability to detect a photon during τ is vanishingly small. The g^2 function and the distribution $\mathcal{W}$ are related by:

$$\mathcal{W}(\tau) = \langle \hat{I} \rangle\, g^2(\tau)\,, \quad \tau \ll \langle \hat{I} \rangle^{-1}\,, \tag{3.6}$$

where $\langle \hat{I} \rangle$ corresponds to the mean photodetection rate.

For time intervals longer than $\langle \hat{I} \rangle^{-1}$, there is in general no simple relation between g^2 and the WTD. This is also the case when considering mesoscopic conductors without specifying any particular properties as presented in the next two sections.

However, quantum optics constitutes an exception as the photodetection process is often Markovian. To be more precise, let us first recall the definition of a Markovian process. We consider a distribution of n events which are defined as the state X of a

given system at the times $t_1, \ldots, t_{n-1}, t_n$. This statistical process is Markovian if the state at time t_n, $X(t_n)$, only depends on the prior event, namely the state $X(t_{n-1})$ at time t_{n-1}. In that case the conditional probability to detect the state $X(t_n)$ can be written as :

$$P\big(X(t_n)|X(t_{n-1}), X(t_{n-2}), \ldots, X(t_1)\big) = P\big(X(t_n)|X(t_{n-1})\big)\,. \tag{3.7}$$

This simplification of the conditional probability defines a Markovian process. In quantum optics, the photoelectron counting statistics is often Markovian. For instance, when considering a two-level system such as an atom with a ground and an excited state, the atom will always return to its ground state as soon as it has emitted one photon which will be detected. As a consequence the atom always evolves from the ground state and the detection process only depends on the prior event, it knows nothing about the whole history of the atom [Carmichael 89]. For a Markovian system, the WTD is similar to a random walk, in which each step is independent of the previous one and only depends on the last position. It is only in that specific situation that a relation between the g^2 function and the WTD can be derived at any time. In the Laplace space, it reads:

$$\widetilde{\mathcal{W}}(s) = \frac{\langle\hat{I}\rangle\tilde{g}^2(s)}{1+\langle\hat{I}\rangle\tilde{g}^2(s)}\,, \tag{3.8}$$

where $\tilde{\mathcal{W}}(s)$ and $\tilde{g}^2(s)$ are the Laplace transforms of $\mathcal{W}(\tau)$ and $g^2(\tau)$ with respect to τ. For more details, we refer the reader to the publications by Carmichael, Singh, Vyas and Rice [Carmichael 89, Vyas 99].

We would like to emphasize again that it is only under a Markovian assumption, which is justified in the case of a photodetection process, that the two-point correlation function g^2 can be expressed in terms of the distribution $\mathcal{W}$ at any time. In contrast, for systems with a more complex dynamics that does not depend only on the prior time, the WTD and the g^2 function provide different informations on the statistical distribution. In mesoscopic physics, investigations of WTDs have until now mostly dealt with either classical systems or Markovian quantum systems as it is presented below.

3.1.3 Waiting time distributions in mesoscopic physics

In mesoscopic physics, WTDs have been used to investigate charge transport statistics through coherent scatterers such as a double quantum dot [Brandes 08], molecules [Koch 05] or the single-electron source presented in the previous chapter [Fève 07, Albert 11]. In these works, a weak coupling between the reservoirs and the scatterer has been assumed. Formally such a system is well-described by Markovian rate equations: single-particle tunneling processes through the mesoscopic conductor take place and are described with an incoming rate Γ_L from the left reservoir to the

scatterer and an outgoing rate Γ_R from the scatterer to the right reservoir. Under the assumption of a weak coupling making the system Markovian, FCS is fully encoded in WTDs and a relation between the distribution $\mathcal{W}$ and the noise spectrum $S(\omega)$ was derived [Brandes 08, Albert 11]. The symmetrized noise spectrum $S(\omega)$ is defined as:

$$S(\omega) = \frac{1}{2}\int_{-\infty}^{\infty} dt\, e^{-i\omega t}\, \langle \hat{I}(t)\hat{I}(0) + \hat{I}(0)\hat{I}(t)\rangle\,, \tag{3.9}$$

where $\hat{I}(t)$ is the current operator [Blanter 00]. The noise spectrum is a non-exclusive probability which investigates the correlations between two events at times t and $t = 0$. In that sense, it plays a similar role as the second-order correlation function for photons g^2. For a Markovian mesoscopic conductor, a similar relation to Eq.(3.8) was derived [Brandes 08, Albert 11] between the Laplace transform of the WTD $\tilde{\mathcal{W}}(s = i\omega)$ and the noise spectrum $S(\omega)$:

$$S(\omega) \propto \frac{\tilde{\mathcal{W}}(i\omega)}{1 - \tilde{\mathcal{W}}(i\omega)}\,. \tag{3.10}$$

However in general, the transport process through mesoscopic conductors does not satisfy Markovian properties. It is for the simplest reason that electrons are fermions. The fermionic statistics generates short- and long-time correlations between consecutive electrons: due to the Pauli repulsion, two electrons with the same energy can not be transmitted at the same time through a scatterer. As a consequence the dynamics is then similar to a random walk *with* memory effects. When using Markovian rate equations, the fermionic statistics is also taken into account, but only in the description of the reservoirs. The tunneling processes are single-particle tunnelings well separated in time due to the weak coupling assumption. Within such a description, the Pauli principle does not induce short-time correlations, except the fact that two electrons with the same energy can not be emitted at the same time. When assuming Markovian property, the noise spectrum and the WTD provide similar information about the distribution of transferred charges as in the case of quantum optics mentioned above.

A derivation of the WTDs considering a many-electron incoming state has so far been missing in mesoscopic physics. The goal of the work done with Mathias Albert, Christian Flindt and Markus Büttiker was to fill this gap with a *quantum derivation* of the WTD for mesoscopic conductors. This is the subject of the next two sections.

3.2 Quantum derivation of waiting time distributions (WTDs)

In the following two sections we present our quantum derivation for the WTDs for mesoscopic conductors and its illustration to a biased quantum point contact(QPC). As a central result we formulate a determinant formula for the WTD in terms of the transmission amplitudes in the scattering matrix $\mathcal{S}$ of the coherent scatterer. Importantly this formula has been derived without making any Markovian assumption. This is presented in the first part of this section. In the second part, we illustrate the formalism by considering a QPC as scatterer and show that WTDs effectively probe the coherent nature of the scatterer but also the quantum nature of the incoming many-body state. These results have been the subject of a publication [Albert 12].

3.2.1 WTD in terms of the idle time probability

As seen in the previous section, there is no simple expression of the WTD in terms of the noise spectrum when a mesoscopic conductor whose dynamics is not Markovian is considered. The WTD has to be defined with an auxiliary probability which we called in our work the idle time probabilty $\Pi(\tau)$. Given a random time t_0, the idle time probability $\Pi(\tau)$ is the probability that *no* electrons are detected in the time interval $[t_0, t_0 + \tau]$ with $\tau \geq 0$, see Fig. 3.3. By definition $\Pi(0) = 1$, the probability to detect two electrons in the same quantum channel at the same time is 0. At long times, $\Pi(\tau)$ decays to zero. For stationary processes, $\Pi(\tau)$ does not depend on t_0. The expression of $\mathcal{W}(\tau)$ in terms of $\Pi(\tau)$ reads:

$$\mathcal{W}(\tau) = \langle\tau\rangle \frac{d^2}{d\tau^2}\Pi(\tau). \tag{3.11}$$

Here $\langle\tau\rangle$ is the mean waiting time. Considering the definition of $\Pi(\tau)$, it ensures the proper normalization $\int_0^\infty d\tau \mathcal{W}(\tau) = 1$. This important relation can be justified considering again Fig. 3.3.

The idea is first to pick a random time t_0 and to assume that the *last* prior detection of an electron occurred at the earlier time $t_e \leq t_0$. Instead of computing the idle time probability, we can first compute its complementary probability, the probability to detect something in the time interval $[t_0, t_0 + \tau]$. As we have assumed that the last detection has occurred at the time t_e, the probability to detect something in the interval $[t_0, t_0 + \tau]$ is identical to the probability to detect something in the interval $[t_e, t_0 + \tau]$. This probability is given by the integral:

$$\int_{t_e}^{t_0+\tau} dt' \, \mathcal{W}(t' - t_e)\,. \tag{3.12}$$

The idle time probability is the complementary probability of the previous expression. As it should not depend on the last detection time t_e, we integrate over all the

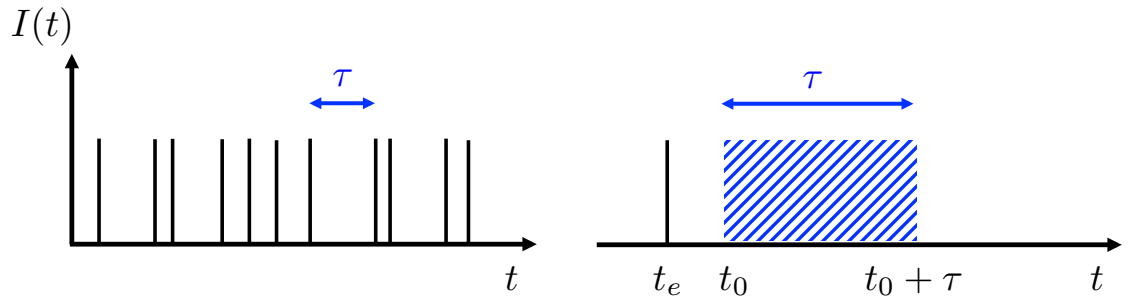

Figure 3.3: Left: A distribution of events, for instance a current $I(t)$ which consists of a sequence of pulses. The waiting time τ is the time delay between two *consecutive* events. Right: The idle time probability is the probability to detect no particles in a time interval τ, namely between t_0 and $t_0 + \tau$, where t_0 is arbitrarily chosen. To express the idle time probability in terms of the waiting time distribution, we assume that the last detection occured at the time t_e.

possible times for the last electron to be detected, i.e. $-\infty \leq t_e \leq t_0$. Considering that detection events are uniformly distributed in time with weight $1/\langle\tau\rangle$, we obtain for the idle time probability:

$$\Pi(\tau) = \frac{1}{\langle\tau\rangle}\int_{-\infty}^{t_0} dt_e \Big(1 - \int_{t_e}^{t_0+\tau} dt\, \mathcal{W}(t-t_e)\Big)\,. \tag{3.13}$$

With two changes of integration variables, one finally gets:

$$\Pi(\tau) = \int_{\tau}^{\infty} du \int_{u}^{\infty} dv \mathcal{W}(v)/\langle\tau\rangle\,, \tag{3.14}$$

which explicitly shows that the idle time probability is independent of t_0 and immediately leads us to Eq. (3.11). Importantly, in deriving Eq. (3.11) we have made no Markov assumption.

3.2.2 The idle time probability

The next task is to evaluate the idle time probability for a generic mesoscopic conductor described by the scattering matrix $\mathcal{S}$. To this end we make use of the first-quantized many-body formalism developed by Hassler *et al.* [Hassler 08, Lesovik 11], which allows us to define orthogonalized wave-packets. Our methodology applies to arbitrary geometries of the electronic leads and the scatterer, but to keep the discussion simple we consider a one-dimensional problem with a single in-coming and out-going quantum channel connected to the scatterer (see Fig. 3.4).

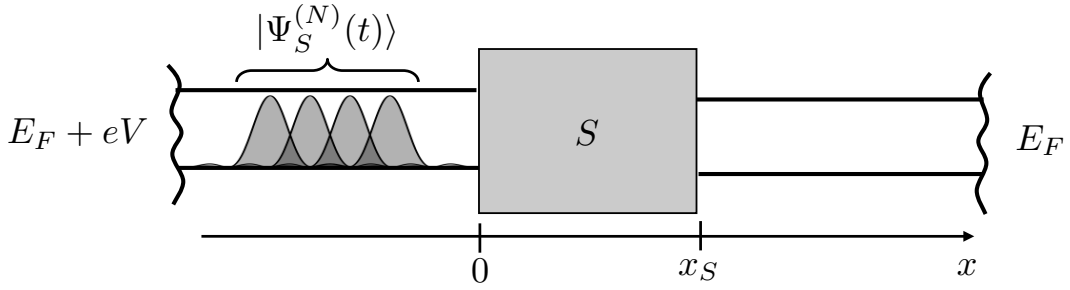

Figure 3.4: A scattering region described by the scattering matrix S is connected to two contacts via a single quantum channel. Scattering states are defined outside of the scattering region $[0, x_s]$. A bias voltage eV is applied to the contacts so that a regular train of N wave-packets is emitted in the energy window eV above the Fermi sea characterized by its energy E_F. We describe this many-body state within a first-quantized formulation by a Slater-determinant state $|\Psi_S^{(N)}(t)\rangle$ which takes into account the Fermionic statistics of the incoming electrons.

The electrons are non-interacting and spinless and the temperature is zero. An applied voltage bias V brings the system out of equilibrium such that in-coming electrons on the left side of the scatterer occupy states in the energy window $I_V = [E_F, E_F + eV]$ above the Fermi level E_F. The scattering states take the form

$$\varphi_k(x) = e^{ikx} + r_k e^{-ikx}\,, \quad x < 0\,, \tag{3.15a}$$
$$\varphi_k(x) = t_k e^{ikx}\,, \quad x > x_s > 0\,, \tag{3.15b}$$

where r_k and t_k are the reflection and transmission amplitudes in $\mathcal{S}$ and k is the momentum. We need not specify the scattering states in the scattering region $[0, x_s]$, see Fig. 3.4. We work close to the Fermi level where the dispersion relation is linear in k, $E_k = \hbar v_F k$, and all wave components propagate with the Fermi velocity v_F.

Next, we split the energy window I_V into N intervals of size eV/N, where N is the number of incoming particles. We first consider a finite N. To simulate a stationary process, we will then consider the limit $N \to \infty$. The energy splitting defines intervals in the momentum space of width κ:

$$\kappa = \frac{eV}{N\hbar v_F}\,. \tag{3.16}$$

To the m'th energy interval, we associate the corresponding time-dependent wave-packet:

$$\phi_m(x,t) = \langle x|\phi_m(t)\rangle = \int_{-\infty}^{\infty} \frac{dk}{2\pi} e^{-iv_F kt}\varphi_k(x) f_m(k)\,. \tag{3.17}$$

The phase factor $e^{-iv_F kt}$ gives the time evolution, with v_F being the Fermi velocity of the electrons. For a biased source the amplitude $f_m(k)$ of the m-th's wave-packet

in the momentum space is given by:

$$f_m(k) = \begin{cases} \sqrt{2\pi/\kappa} & \text{if} \quad k_F + \kappa(m-1) \leq k \leq k_F + \kappa m \\ \\ 0 & \text{otherwise} \end{cases}$$

The width of the momentum interval is $\kappa = eV/(N\hbar v_F)$. In a first-quantization formulation, the m-th wave-packet is therefore given by:

$$\phi_m(x,t) = \int_{I_m} \frac{dk}{2\pi} e^{-iv_F kt} \varphi_k(x) \sqrt{\frac{2\pi}{\kappa}} \,. \tag{3.18}$$

The integration interval $I_m = [k_F + \kappa(m-1), k_F + \kappa m]$ is of width κ and $\varphi_k(x)$ is the scattering state in the region $x > x_s$. This defines orthonormalized wave-packets:

$$\begin{aligned} \langle \phi_m | \phi_n \rangle &= \int_{-\infty}^{\infty} dx \int_{I_m} \frac{dk'}{2\pi} \int_{I_n} \frac{dk}{2\pi} \, e^{i(k-k')x} \frac{2\pi}{\kappa} \\ &\simeq \frac{\kappa}{2\pi} \int_{-\infty}^{\infty} dx \, e^{i\kappa x(n-m)} \\ &= \delta(n-m) \,, \end{aligned} \tag{3.19}$$

For simplicity, here we have considered $\kappa \to 0$. If the number of particles N tends to infinity, the wave-packet is completely localized in the momentum space and completely delocalized in the position space as it should be for a scattering state.

To build the many-body incoming state, we assume that all the m-th momentum intervals are filled, $m = 1, \ldots, N$ with particles so that the N-particle incoming state can be written as a Slater determinant $|\Psi_S^{(N)}(t)\rangle$ of the states $|\phi_m(t)\rangle$:

$$|\Psi_S^{(N)}(t)\rangle = \frac{1}{\sqrt{N!}} \det\left(|\phi_m(t)\rangle\right), \quad m = 1, \ldots, N \,. \tag{3.20}$$

Measurement process

At this point of the derivation of the idle time probability, we have to define the measurement process for the electrons in the region after the scatterer at $x > x_s$. In this work, we have considered explicitly a projective measurement. Starting from the single-particle projector in the position space $\mathcal{Q} = \int_{-\infty}^{\infty} dx \, |x\rangle\langle x|$, we have defined the single-particle counting projective operator $\mathcal{Q}_\tau$ at the right of the scatterer at $x_0 > x_s$ as:

$$\mathcal{Q}_\tau = \int_{x_0}^{x_0 + v_F\tau} dx |x\rangle\langle x| \,. \tag{3.21}$$

Given the single-particle state $\phi(x,t) = \langle x|\phi(t)\rangle$, the expectation value of $\mathcal{Q}_\tau$ with respect to $\phi(x,t)$ gives the probability to detect this single particle in the space interval $[x_0, x_0 + v_F\tau]$. This single-particle projective operator over a finite space interval

is not a projector anymore but describes a projective measurement of the quantum state over a finite space interval.

The idle time probability gives the probability to detect no particles in a *time* interval. Let us recall that in this work, we assume a sufficiently small bias eV of the source so that the dispersion relation is linear, $E_F = \hbar v_F k_F$. As a consequence, this system is invariant under Galilean transformations. The idle time probability in a finite time interval $[t_0, t_0 + \tau]$ is equivalent to the idle time probability in the corresponding finite space interval $[x_0, x_0 + v_F\tau]$. We can therefore make use of the single-particle projective operator $\mathcal{Q}_\tau$ to define the idle time probability. Considering the single-particle state $\phi(x,t)$,

$$\langle\phi(x,t)|1-\mathcal{Q}_\tau|\phi(x,t)\rangle \tag{3.22}$$

is the probability to not detect this single particle in the time interval τ or equivalently in the space interval $v_F\tau$. The generalization to a N-particle incoming state is direct as the electrons are non-interacting. The N-particle projective operator is the N-tensor product of the single-particle projective operator $\mathcal{Q}_\tau$ and its expectation value has to be made with respect to the Slater determinant. The idle time probability reads:

$$\Pi(\tau) = \langle\Psi_S^{(N)}(t)|\bigotimes_{i=1}^{N}(1-\mathcal{Q}_\tau)|\Psi_S^{(N)}(t)\rangle \tag{3.23}$$

The idle time probability $\Pi(\tau)$ can itself be cast in a determinant formula. Indeed the expectation value of a tensor product of single-particle operators with respect to a determinant can be written as the expectation value of the single-particle operator with respect to the single-particle states:

$$\begin{aligned}\langle\Psi_S^{(N)}|\bigotimes_{i=1}^{N}(1-\mathcal{Q}_\tau)|\Psi_S^{(N)}\rangle &= \frac{1}{N!}\sum_{\pi,\pi'\in S_N}\mathrm{sgn}(\pi\circ\pi')\prod_{m=1}^{N}\langle\phi_{\pi(m)}|1-\mathcal{Q}_\tau|\phi_{\pi'(m)}\rangle \\ &= \frac{1}{N!}\sum_{\pi,\pi''\in S_N}\mathrm{sgn}(\pi'')\prod_{m=1}^{N}\langle\phi_m|1-\mathcal{Q}_\tau|\phi_{\pi''(m)}\rangle \\ &\equiv \det(\mathbb{1}-\mathbf{Q}_\tau)\,. \end{aligned} \tag{3.24}$$

Here π and π' denote elements of the permutation group S_N. This mathematical property is at the origin of most of the determinant formulae in FCS. The single-particle matrix elements are:

$$[\mathbf{Q}_\tau]_{mn} \equiv \langle\phi_m(\tau)|\mathcal{Q}_\tau|\phi_n(\tau)\rangle = \int_{I_m}\int_{I_n} dk'\,dk\,t_{k'}^*\,t_k\frac{K_\tau(k-k')}{2\pi\kappa}\,, \tag{3.25}$$

where the kernel $K_\tau(q)$ takes into account the time evolution of the wave-packet:

$$\begin{aligned} K_\tau(q) &= \int_{x_0}^{x_0+v_F\tau} dx\, e^{iq(x-v_F\tau)} \\ &= 2e^{-iq(x_0-v_F\tau/2)}\frac{\sin(qv_F\tau/2)}{q}\,. \end{aligned} \tag{3.26}$$

Finally, to obtain a stationary process we take the limit $N \to \infty$ for which $\kappa \to 0$. In this limit we consider that the transmission amplitude t_k is constant over κm so that $t_k = t_{\kappa m}$. We then have:

$$[\mathbf{Q}_\tau]_{m,n} = t_{\kappa n}t^*_{\kappa m}e^{i(n-m)\kappa(x_0-v_F\tau/2)}\frac{\sin(\kappa v_F\tau(n-m)/2)}{\pi(n-m)} \quad \text{for } m,n = 1,\ldots,N\,. \tag{3.27}$$

With the definition of the single-particle matrix elements $[\mathbf{Q}_\tau]_{m,n}$, the idle time probability can be written as a determinant formula in a compact way:

$$\Pi(\tau) = \det(\mathbb{1} - \mathbf{Q}_\tau)\,. \tag{3.28}$$

Equations (3.11) and (3.28) are the central results of this section as they allow us to calculate the WTD for an arbitrary voltage-biased scatterer. It is important to emphasize that they were derived without invoking Markovian properties. The first-quantized approach followed here allows to consider a many-body incoming state taking into account the fermionic statistics of the electrons through the incoming Slater determinant state $|\Psi_S^{(N)}\rangle$. We recall that this is different to the Markovian rate equations formalism developed until now [Schriefl 05, Koch 05, Brandes 08, Welack 08, Welack 09], where only single-particle tunneling processes from the left reservoir can be described. The coherence of the scatterer is fully encoded in the scattering matrix S. The determinant formula for $\Pi(\tau)$, Eq.(3.28), enables the probe of the scatterer, but also of the incoming many-body state and this, at short time scales. It is also important to mention that we considered here incoming fermions described by the Slater determinant but this approach is generalizable to incoming bosonic, classical particles or entangles states, as long as there are no interactions.

In the following we illustrate the formalism by considering a quantum point contact as scatterer. This will clearly show that the WTD gives access to the fluctuations due to the scatterer but also to the fluctuations due to fermionic statistics in the case of a fully open QPC, a perfect quantum channel.

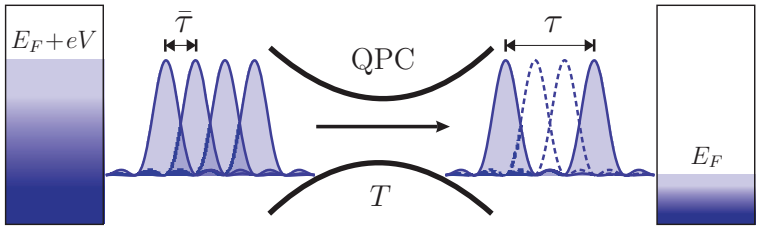

Figure 3.5: Quantum point contact (QPC) connected to voltage-biased contacts. The QPC transmission is denoted as T, the Fermi energy is E_F, and V is the voltage applied to the source electrode. The average time separation of the in-coming electrons is $\bar{\tau} = h/eV$. The distribution of waiting times τ between transmitted electrons is determined by the many-body state of the in-coming electrons as well as the QPC which may cause electrons to reflect back. Reflected (missing) electrons are indicated by dashed lines. After Ref. [Albert 12].

3.3 WTDs for a biased quantum point contact

3.3.1 Results

We illustrate our method by calculating the WTD for a QPC with energy independent transmission $|t(k)|^2 = T$ as shown in Fig. 3.5. Wave-packets are emitted by the biased source with an average waiting time $\bar{\tau} = h/eV$. We calculated the WTDs after the scatterer for different values of the transmission probability T using Eqs. (3.11-3.28). It is not possible to calculate the above determinant analytically so results are numerical. To simulate a stationary process of incoming particles, a sufficiently large number N of incoming particles has to be chosen. We have checked that$N = 50$ is sufficient to ensure stable results for the calculations. This value of N may change if the amplitude transmission depends on the momentum k: a bigger value might be necessary to ensure the convergence of the numerical calculations.

Figure 3.6 displays the WTDs calculated for different transmission probabilities T. For a fully open QPC, $T = 1$, the WTD reflects only the fermionic statistics and correlations in the many-body state. In particular, $\mathcal{W}(0) = 0$, since two electrons cannot occupy the same state due to the Pauli principle. This suppression is similar to the Fermi-hole in the density-density correlation function of a free electron gas [Landau 59, Büttiker 92]. The fermionic correlations also force the WTD to decay strongly beyond a few mean waiting times, where it essentially vanishes. The mean waiting time is :

$$\langle \tau \rangle = \frac{1}{\mathrm{Tr}(\dot{\mathbf{Q}}_{\tau=0})}\,, \tag{3.29}$$

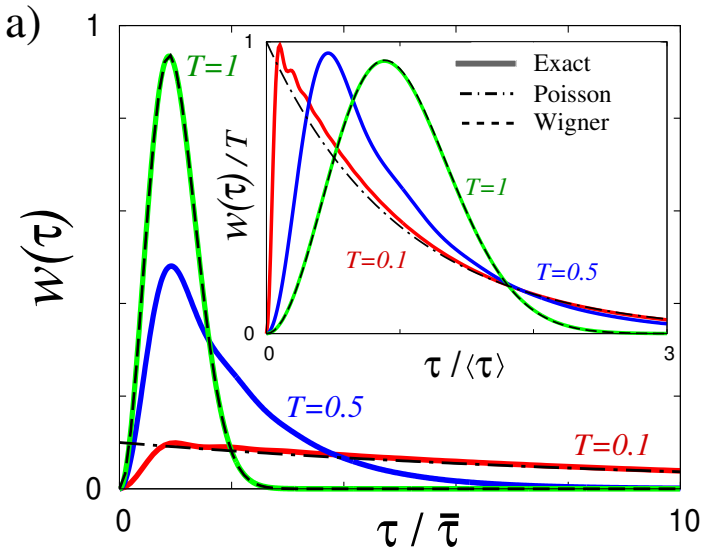

Figure 3.6: Numerical calculations for the electron waiting time distributions (WTDs) for different transmission probabilities T of the quantum point contact(QPC). The waiting time τ is given in units of $\bar{\tau} = h/eV$ or $\langle\tau\rangle = \bar{\tau}/T$ for the inset. For a fully open QPC, $T = 1$ (green curve), the WTD is well approximated by a Wigner–Dyson distribution, Eq. (3.31) (dashed black curve). Close to pinch-off, $T \simeq 0$ (red curve), the WTD approaches Poisson statistics given by the exponential distribution $\mathcal{W}(\tau) \simeq e^{-\tau/\langle\tau\rangle}/\langle\tau\rangle$ (dotted-dashed curve). Inset: The WTDs are renormalized by the transmission probability T of the QPC to clearly show the crossover from the Poissonian distribution (in red) to the Wigner-Dyson distribution (in green) when the QPC is gradually opened. After Ref. [Albert 12].

with $\dot{\mathbf{Q}}_\tau \equiv \partial_\tau \mathbf{Q}_\tau$. It easily follows that:

$$\mathrm{Tr}(\dot{\mathbf{Q}}_{\tau=0}) = \mathrm{Tr}(\dot{\mathbf{Q}}_\tau) = \frac{eV}{Nh}\sum_{m=1}^{N}|t_{\kappa m}|^2 = \frac{\langle I\rangle}{e} \tag{3.30}$$

is the average (particle) current. For the QPC, we find $\langle\tau\rangle = \bar{\tau}/T$ with $\bar{\tau} = h/eV$. This is in line with the common wave-packet picture that electrons emitted from a constant-voltage source into a quantum channel on average are separated by the fundamental time scale h/eV [Landauer 87, Martin 92]. However, the electrons are not equally spaced in time due to their inherent wave nature which introduces fluctuations in the waiting time. Interestingly, for $T = 1$ the WTD is well approximated by the Wigner–Dyson surmise of the Gaussian Unitary Ensemble (GUE) in random matrix theory [Metha 04, Haake 10]. We find :

$$\mathcal{W}_{\mathrm{WD}}(\tau) = \frac{32\tau^2}{\pi^2\bar{\tau}^3}e^{-4\tau^2/\pi\bar{\tau}^2}, \quad \bar{\tau} = \frac{h}{eV}. \tag{3.31}$$

This can be understood using analogies with level spacing statistics and random matrix theory as we discuss below.

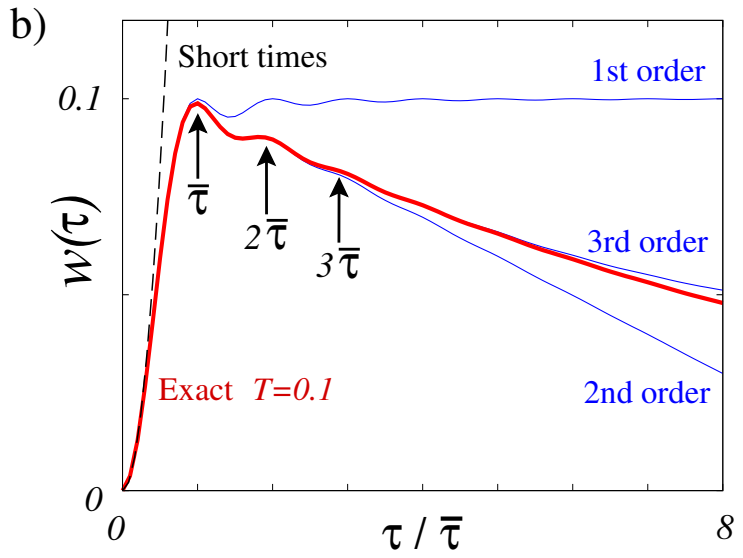

Figure 3.7: Numerical calculations for the WTD in the low-transmission regime, $T \simeq 0.1$ (red curve) in units of $\bar{\tau} = h/eV$. The WTD exhibits oscillations peaked on h/eV, $2h/eV$ and $3h/eV$ showed by arrows. These oscillations are a consequence of the Pauli principle between consecutive wave-packets. The short-time behavior given by Eq. (3.32) is indicated with a dashed line. Thin lines show expansions of the WTD to first, second, and third order in T. After Ref. [Albert 12].

As the transmission T is reduced below unity, the WTD widens as electrons may now reflect back on the QPC, allowing for longer waiting times between transmitted charges, Fig. 3.6. Close to pinch-off, $T \simeq 0$, the mean waiting time becomes much longer than $\bar{\tau}$ and the WTD approaches an exponential distribution corresponding to Poisson statistics involving rare and uncorrelated tunneling events. In this regime, the WTD is mainly determined by the scatterer, although the complete suppression at $\tau = 0$ persists. In fact, for arbitrary transmission, we can expand the WTD to lowest order in τ as:

$$\mathcal{W}(\tau) \simeq \frac{\pi^2}{3}\frac{T}{\bar{\tau}}\left(\frac{\tau}{\bar{\tau}}\right)^2, \quad \tau \ll \bar{\tau}. \tag{3.32}$$

The Pauli exclusion principle manifests itself in a τ^2-dependence of the WTD for short waiting times and a complete suppression at $\tau = 0$. Equation (3.32) is indicated in Fig. 3.7 and is in good agreement with the WTD for arbitrary transmissions T as we have checked.

The WTD exhibits a cross-over from Wigner–Dyson statistics to Poisson statistics with decreasing transmission. The intermediate regime displays small oscillations with period $\bar{\tau}$ due to the quasi-regular train of incoming electrons superimposed on an exponential decay, Fig. 3.7. Physically, the wave packets have a large overlap leading to small-amplitude oscillations. This situation resembles the density-density

correlations of a liquid whose particles have a large degree of freedom and where the structure of the many-body state decays fast with the inter-particle distance. In contrast, for a solid-like system, whose constituents are placed in a nearly perfect "crystal", long-range correlations lead to well-isolated periodic peaks in the WTD. This behavior occurs in periodically driven classical systems [Albert 11] and is also expected for nearly non-overlapping quantum states produced by coherent single-electron sources (SES) [Fève 07, Moskalets 08, Keeling 08].

To further understand the low transmission regime of the QPC, we expand the idle time probability in T. To this end we rewrite it as:

$$\Pi(\tau) = \det(1 - \mathbf{Q}_\tau) = \exp\left[\mathrm{Tr}(\log\{1 - \mathbf{Q}_\tau\})\right]. \tag{3.33}$$

Since $\mathbf{Q}_\tau$ is proportional to T, we can expand the idle time probability:

$$\Pi(\tau) = 1 - \mathrm{Tr}(\mathbf{Q}_\tau) + \frac{[\mathrm{Tr}(\mathbf{Q}_\tau)^2 - \mathrm{Tr}(\mathbf{Q}_\tau^2)]}{2} + \mathcal{O}(T^3) \tag{3.34}$$

The second derivative with respect to time is readily performed, allowing us to express the WTD as a series in T. Figure 3.7 illustrates how the series improves as more terms are included. In particular, to fully account for the long-time behavior of the WTD high-order terms must be included. To lowest order in T we find:

$$\mathcal{W}(\tau) = \frac{\langle I \rangle g^{(2)}(\tau)}{e} + \mathcal{O}(T^2), \tag{3.35}$$

where $g^{(2)}(\tau) = 1 - \sin^2(\pi\tau/\bar{\tau})/(\pi\tau/\bar{\tau})^2$ is the two-point correlation function which is independent of T [Metha 04, Haake 10]. This is consistent with Markovian properties and renewal theory [Carmichael 89, Brandes 08]. Indeed a distribution of discrete events is a renewal process if all the intervals defined by two consecutive events are independent from each other and equally distributed [Cox 62]. At low transmission probabilities, events are well-separated in time and short-time correlations vanish. As a consequence the WTD corresponds to a Poissonian process which verifies the renewal properties and the first-quantized formulation is in agreement with the Markovian rate equation formalism. It is then possible to express the WTD in terms of the two-point correlation function as presented in the introduction of this chapter. High-order terms in the transmission, however, cannot be obtained from renewal theory. The break-down of renewal theory becomes evident by considering the cumulants of the WTD, which is the topic of the next paragraph.

3.3.2 Moments and cumulants: breakdown of renewal theory

The first three cumulants of the WTD are the mean, the variance and the skewness:

$$\langle\langle \tau \rangle\rangle = \langle \tau \rangle \tag{3.36}$$

$$\langle\langle \tau^2 \rangle\rangle = \langle (\tau - \langle \tau \rangle)^2 \rangle \tag{3.37}$$

$$\langle\langle \tau^3 \rangle\rangle = \langle (\tau - \langle \tau \rangle)^3 \rangle. \tag{3.38}$$

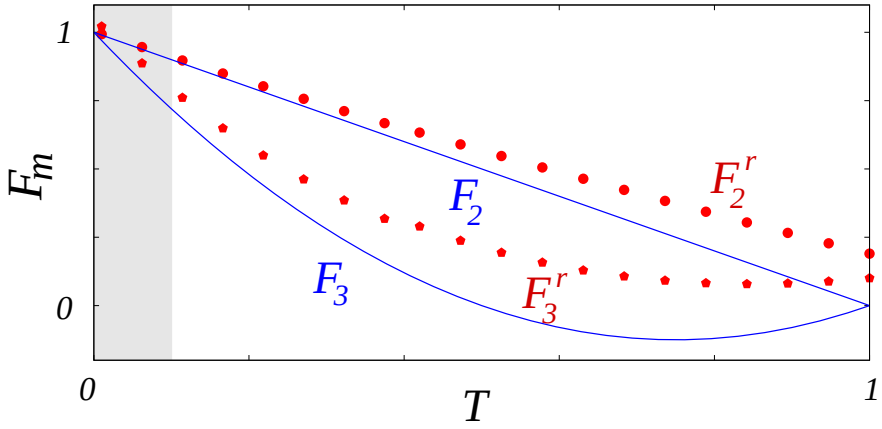

Figure 3.8: Fano factors as functions of QPC transmission T. The exact results $F_2 = 1-T$ and $F_3 = (1-T)(1-2T)$ are shown together with predictions based on renewal theory $F_2^r = \langle\langle\tau^2\rangle\rangle/\langle\langle\tau\rangle\rangle^2$ and $F_3^r = 3\langle\langle\tau^2\rangle\rangle^2/\langle\langle\tau\rangle\rangle^4 - \langle\langle\tau^3\rangle\rangle/\langle\langle\tau\rangle\rangle^3$, where $\langle\langle\tau^m\rangle\rangle$ are the cumulants of the waiting time τ. Renewal theory only holds in the low-transmission regime (shaded area), where $F_m \simeq F_m^r$. After Ref. [Albert 12].

We recall that the cumulants of the FCS are similarly denoted as $\langle\langle n^k\rangle\rangle$, $k = 1, 2, 3, \ldots$, where n is the number of transferred charges. The corresponding Fano factors are:

$$F_k \equiv \frac{\langle\langle n^k\rangle\rangle}{\langle\langle n\rangle\rangle}\,, \tag{3.39}$$

which for a QPC are well-known and read [Levitov 93, Levitov 96, Nazarov 03]:

$$F_2 = 1-T\,, \tag{3.40}$$
$$F_3 = (1-T)(1-2T)\,. \tag{3.41}$$

Importantly, for systems where renewal theory applies, the FCS can be directly related to the WTD and the Fano factors in terms of the waiting time τ [Albert 11, Budini 11] read:

$$F_2^r = \frac{\langle\langle\tau^2\rangle\rangle}{\langle\langle\tau\rangle\rangle^2} \tag{3.42}$$
$$F_3^r = \frac{3\langle\langle\tau^2\rangle\rangle^2}{\langle\langle\tau\rangle\rangle^4} - \frac{\langle\langle\tau^3\rangle\rangle}{\langle\langle\tau\rangle\rangle^3} \tag{3.43}$$

For a fully open QPC, the second Fano factor is zero, corresponding to regular transport without zero-frequency fluctuations. However, the width (or variance) of the WTD is finite. In Fig. 3.8 we examine the validity of renewal theory as a function of the QPC transmission. Only close to pinch-off ($T \simeq 0$), where the transport is Poissonian, we find $F_m \sim F_m^r$ in agreement with renewal theory. When the transmission

increases, the second and third cumulants differ from the corresponding Fano factors. Due to the fermionic statistics of the in-coming electrons, the waiting times are not independent from each other anymore and the renewal property of the WTD breaks down. We expect that renewal theory for mesoscopic conductors is only valid in the low-transmission regime where tunneling events are rare and nearly uncorrelated.

3.3.3 Analogy with Random Matrix Theory

There are several analogies between WTDs and level spacing distributions in spectral statistics [Metha 04, Haake 10]. The latter are useful to discriminate complex systems according to their symmetry class or underlying classical dynamics and they may carry signatures of quantum chaos according to the Bohigas–Giannoni–Schmit conjecture [Bohigas 84]. Let us first recall some basic concepts of random matrix theory (RMT).

A short introduction to Random Matrix Theory (RMT)

This small introduction is mainly based on the first chapter of the review of C. W. J. Beenakker on "Random-matrix theory of quantum transport" [Beenakker 97], on the thesis of P. W. Brouwer [Brouwer 97] and on lecture notes given by V. E. Kravtsov in Trieste in 2009 [Kravtsov 09].

Random matrix theory investigates the statistical properties of large matrices with random values. Physical properties of the system are encoded through the symmetry of the matrix. Invariant random matrix ensembles are characterized by a probability distribution function which is invariant under the rotation of the entry $N \times N$ matrix $\mathcal{H}$, $\mathcal{H} \to \mathcal{T}\mathcal{H}\mathcal{T}^{-1}$:

$$P(\mathcal{H}) \propto \exp\big(-\operatorname{Tr} V(\mathcal{H})\big)\,, \tag{3.44}$$

where V is an arbitrary function of $\mathcal{H}$ and analytic for $\mathcal{H} = 0$. The invariance property is ensured by the trace. One ensemble is of particular importance, namely the Gaussian random matrix ensemble of Wigner and Dyson with the following properties:

$$\text{i) } \mathcal{H} \text{ is an Hermitian matrix } , \mathcal{H} = \mathcal{H}^\dagger \tag{3.45}$$

$$\text{ii) } V(\mathcal{H}) = \mathcal{H}^2\,. \tag{3.46}$$

To relate $\mathcal{H}$ to the Hamiltonian of a physical system, the limit $N \to \infty$ has to be taken. To investigate the distribution of the eigenvalues $\{E_n\}$ and eigenvectors of $\mathcal{H}$, we have to multiply the probability distribution function $P(\mathcal{H})$ by the Jacobian J which relates an infinitesimal volume element $d\mu(\mathcal{H})$ of the space of the Hermitian matrices $\mathcal{H}$ to the infinitesimal volume element dE_n of the space of the eigenvalues and eigenvectors. It is only for invariant random matrix ensembles that the Jacobian

is independent of the ensemble of eigenvectors; it depends only on the ensemble of eigenvalues $\{E_n\}$:

$$J = |\Delta|^\beta = \prod_{n<m} |E_n - E_m|^\beta \,, \tag{3.47}$$

where Δ is called the Vandermond determinant. The index β stands for the symmetry of the matrix $\mathcal{T}$ which leaves $P(\mathcal{H})$ invariant under $\mathcal{H} \to \mathcal{T}\mathcal{H}\mathcal{T}^{-1}$: $\mathcal{T}$ can be orthogonal ($\beta = 1$), unitary ($\beta = 2$) or symplectic ($\beta = 4$). Each group implies some symmetry for the physical system under consideration: $\beta = 2$ characterizes a system in which time reversal symmetry (TRS) is broken, $\beta = 1, 4$ conserves the TRS but $\beta = 4$ stays for a system with broken spin-rotation symmetry whereas $\beta = 1$ conserves the spin. The probability distribution function then reads:

$$\begin{aligned} P(\{E_n\}) &= \prod_{n<m} |E_n - E_m|^\beta \exp\big(-\operatorname{Tr} V(\mathcal{H})\big) \\ &= \prod_{n<m} |E_n - E_m|^\beta \prod_i e^{-\beta V(E_i)} \,. \end{aligned} \tag{3.48}$$

To interpret it in RMT, it has been shown to be very useful to compare Eq.(3.48) with the Gibbs distribution in statistical mechanics:

$$P(\{E_n\}) = \exp\left[-\beta\left(\sum_{n<m} u(E_n, E_m) + \sum_n V(E_n)\right)\right] \,, \tag{3.49}$$

$$\tag{3.50}$$

$$u(E_n, E_m) = -\ln|E_n - E_m| \,. \tag{3.51}$$

Here the index β plays the inverse role of temperature. The potential V is a parabolic potential (as $V(\mathcal{H}) = \mathcal{H}^2$) and u is a logarithmic repulsive potential. If one considers N *classical* particles in $1D$ with energies $E_1, \ldots, E_N$ in such potentials, this system is a Coulomb gas due to the logarithmic Coulomb repulsion. The Jacobian in Eq.(3.47) expresses the *level repulsion* in RMT: energy levels can not be degenerate.

Analogy with the perfect quantum channel

For a fully open QPC the analogy is due to the equivalence between the ground state of one-dimensional fermions and the joint probability distribution of eigenvalues of random matrices [Lenard 64, Calogero 69, Sutherland 70, Metha 04, Haake 10]. This can be seen by looking at the Jacobian which is expressed in terms of the Vandermond determinant, Eq.(3.47). By definition of the Vandermond determinant, we have the following properties: it changes sign under the permutation of two energies E_n and E_m and

$$\sum_{n=1}^{N} \frac{\partial^2 \Delta}{\partial E_n^2} = 0 \,. \tag{3.52}$$

These two properties enable us to interpret the Vandermond determinant as the wave-function $\Psi(\{E_n\})$ of the ground state of N free fermions in $1D$ with only a kinetic Hamiltonian. For the Gaussian unitary ensemble (GUE, $\beta = 2$), the Jacobian $J = |\Delta|^2$ corresponds to the density probability of the $1D$ free fermions. Electrons on top of the Fermi sea in a perfect quantum channel are described in a similar way than free fermions in $1D$.

The fact that the analogy is for *free* fermions in $1D$ can also be seen from the Calogero-Sutherland Hamiltonian which maps the canonical ensemble of random matrices labeled by their symmetry parameter β onto a model of interacting one-dimensional fermions with coupling constant proportional to $\beta - 2$ [Calogero 69, Sutherland 70]:

$$\mathcal{H}_{\text{Cal}} = -\frac{1}{2}\sum_{n=1}^{N}\frac{\partial^2}{\partial E_n^2} + \frac{\beta}{2}\left(\frac{\beta}{2} - 1\right)\sum_{n>m}^{N}\frac{1}{(E_n - E_m)^2}\,. \tag{3.53}$$

For $\beta = 2$, the system is non-interacting, there is only a kinetic term. The entire repulsion is due to the fermionic statistics. When starting this project, we did not expect such an analogy between transport properties through one of the simplest mesoscopic conductor, a biased QPC, and the Wigner-Dyson surmise in RMT. One related question is whether we would be able to simulate the distributions for the other symmetry groups, $\beta = 1$ and $\beta = 4$, which describe $1D$ fermions with interactions.

3.4 Conclusion

In this chapter, we have presented a quantum theory of electron waiting time distributions (WTDs) in mesoscopic conductors expressed by a determinant formula. This was derived without any Markovian assumption and is valid for any biased mesoscopic scatterer. To illustrate the formalism, we have considered a QPC. Interestingly, it exhibits a cross-over from Wigner–Dyson statistics for a fully open QPC to Poisson statistics close to pinch-off. These two extreme regimes probe respectively the fluctuations due to the source (the fermionic statistics) and the fluctuations due to the scatterer (shot noise). In contrast to previous works on WTDs in quantum transport, we explicitly demonstrated the break-down of renewal theory for mesoscopic conductors: in general FCS is not fully encoded in the WTD. Both statistical tools provide different, yet complementary informations about the system. In particular, WTDs investigate short-time physics and allows for instance the probe of correlations at times of the order of h/eV, the characteristic time of a dc-source. Remarkably, the crossover from a Poissonian distribution to the Wigner–Dyson surmise leads us to discuss analogies between WTDs and level spacing distributions in spectral statistics. WTDs for a perfect quantum channel (fully open QPC) corresponds to the level spacing statistics of the GUE in RMT. A mapping can be done between this ensemble and the ground state of free fermions in $1D$.

The results for the QPC look very promising for the WTD to be an efficient statistical tool to investigate fluctuations and coherence effects of mesoscopic conductors. As we did not make restrictive assumptions for the derivation of the determinant formula which allows the calculation of the WTD, this work motivates further investigation of the validity of this formalism applied to different scatterers and to different kind of many- or single-particle states.

Perspectives

The main goal of this thesis was to address the coherence of single and many-particle states in mesoscopic systems, emitted either by dc-sources or by the recent on-demand single-electron source realized at the Laboratoire Pierre Aigrain. Both sources emit coherent electrons. The on-demand single-electron source provides a control on their time of emission, heralding an emerging field in low-temperature electron physics which is promising for manipulating quantum information on a single charge level.

In Chapter 1 we have made use of the coherence properties of electrons emitted by dc-sources to create entanglement between two charge qubits. In Chapter 2 we have investigated the first-order coherence properties of single-particle states emitted by the on-demand single-electron source. For the latter, we have proposed a general framework by deriving analytically the expression of the current at the output of an interferometry experiment. We have been able to distinguish the coherence time T_2, the relaxation time T_1 and the dephasing time T_φ by considering the single-particle state sent onto the Mach-Zehnder interferometer as a time-dependent orbital qubit. We have treated the non-interacting case which will serve as an important reference for future treatments which include dephasing and relaxation processes. This would lead to a theory which is closer to experimental reality.

To complete the characterization of the coherence properties of many-particle states, it is essential to also consider the second-order coherence properties. Starting from the results of Chapter 2, the second-order correlation function $g^{(2)}$ could be derived within the same framework as the first-order correlation functions. In particular, the determination of second-order coherence properties provides complementary informations to the waiting times distribution. In Chapter 3, we have addressed the quantum-mechanical derivation of the waiting times distribution for stationary sources. It would be of interest to find it for dynamical quantum problems like quantum pumps.

Chapter 4

Appendices

4.1 The scattering-matrix approach

The scattering matrix relates asymptotically free incoming states on a scattering region to the free outgoing states. In quantum transport, it has been proven to be a very efficient tool to describe phase-coherent systems. One of the most famous results is the expression of the conductance as the sum over the transmission probabilities of the quantum channels of a quasi-one-dimensional mesoscopic conductor :

$$G = \frac{2e^2}{h} \sum_{n,m} T_{nm} \,, \tag{4.1}$$

where $G_0 = 2e^2/h$ is the conductance quantum and T_{nm} are the transmission probabilities to go from channel m to the channel n. For details about the results presented below, we refer the reader to the articles by M. Büttiker [Büttiker 92] and G.B Lesovik and I.A. Sadovskyy [Lesovik 11].

A quasi-one-dimensional mesoscopic conductor is generally modeled as a three-dimensional waveguide with high potentials in the transverse direction $(\hat{y}, \hat{z})$ so that the motion only takes place in the $\hat{x}$-direction as shown in Fig. 4.1. Assuming asymptotic translation invariance along the $\hat{x}$-axis, the plane waves that propagate in such a conductor are obtained by solving the Scrödinger equation for the wave-function ψ of a single-electron :

$$\left[-\frac{h^2}{2m} \Delta + V(y,z) \right] \psi(x,y,z) = E\psi(x,y,z) \,, \tag{4.2}$$

with the ansatz $\psi(x,y,z) = \chi(y,z)e^{ikx}$. After separating the variables, the quantized energies E_n of the transverse modes $\chi_n(y,z)$ are solutions of :

$$\left[-\frac{h^2}{2m} (\partial_y^2 + \partial_z^2) + V(y,z) \right] \chi_n(y,z) = E_n \chi_n(y,z) \,.$$

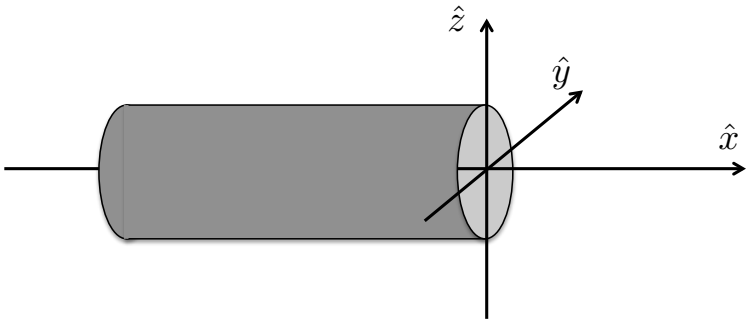

Figure 4.1: Schematic view of a quasi-one-dimensional conductor modeled as a wave-guide. A potential in the directions $\hat{y}$ and $\hat{z}$ defines quantized modes in these transverse directions which can propagate along the $\hat{x}$-direction.

The transverse modes $\chi_n(y,z)$ form a complete and orthonormal set :

$$\sum_n \chi_n(y,z)\chi_n^*(y',z') = \delta(y-y')\delta(z-z')\,,$$
$$\int dy\,dz\,\chi_n(y,z)\chi_m^*(y,z) = \delta_{mn}\,.$$

The solution of the Schrödinger equation (4.2) reads :

$$\psi(x,y,z) = \sum_n c_n \chi_n(y,z) e^{ik_n x}\,, \tag{4.3}$$

with k_n being the wave-vector of the n-th quantum channel, $k_n = \sqrt{2m(E-E_n)}/\hbar$. Here m is the mass of the electron and c_n are constants. To formulate a scattering problem, we assume an additional scattering potential. The incident wave function has the asymptotic form derived above, it corresponds to $\psi(x,y,z)$ in Eq. (4.3). The wave functions to the left and to the right of the scattering region are given by :

$$\begin{aligned}
\psi_{Ln}(x,y,z) &= \textstyle\sum_m \chi_m(y,z)\left(\delta_{mn}\,e^{ik_m x} + \sqrt{\frac{v_{Ln}}{v_{Lm}}}\,S_{LL,mn}\,e^{-ik_m x}\right)\,,\\
\psi_{Rn}(x,y,z) &= \textstyle\sum_m \chi_m(y,z)\sqrt{\frac{v_{Ln}}{v_{Rm}}}\,S_{RL,mn}\,e^{ik_m x}\,.
\end{aligned} \tag{4.4}$$

These are the scattering states of the system. The indices L, R stand for the left and right leads respectively whereas the indices m, n label the modes in each lead. The scattering matrix element $S_{LR,mn}$ corresponds to the amplitude of probability to go from the channel n in lead R to the channel m in lead L. The transmission and reflection amplitudes which relate the incoming to the outgoing wave-functions form the scattering matrix S of the system :

$$S = \begin{pmatrix} S_{LL} & S_{LR} \\ S_{RL} & S_{RR} \end{pmatrix}\,. \tag{4.5}$$

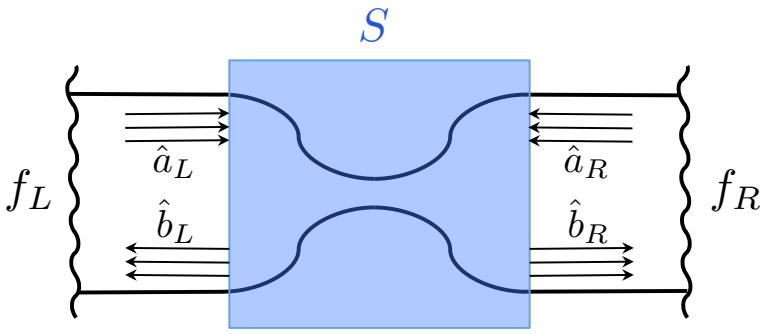

Figure 4.2: The transport properties of a conductor connected to two reservoirs characterized by their Fermi energies f_L and f_R are described by the scattering matrix S. The indices L, R label the left and right reservoirs or leads. The scattering matrix relates the incoming amplitudes to the outgoing amplitudes. The corresponding field operators are expressed in terms of the incoming annihilation operators $\hat{a}_{L,R}$ and of the outgoing annihilation operators $\hat{b}_{L,R}$. The three arrows stand for the finite number of channels in the left and right leads.

The block $S_{\alpha\beta}$ has the dimension $N_\alpha \times N_\beta$ with $\alpha, \beta = L, R$ and $N_{L,R}$ is the number of channels in the left and right leads respectively. If there is only one channel in each lead, each block of the scattering matrix consists in only one amplitude of probability. The conservation of the current implies that the scattering matrix is unitary :

$$SS^\dagger = S^\dagger S = \mathbb{1}\,. \tag{4.6}$$

If the system is time reversal symmetric, the scattering matrix is orthogonal. In general, the scattering matrix depends on energy. One well-known example is the scattering matrix of a double tunnel barrier. The corresponding transmission probability is maximum at the resonant energy even if the transmission probabilities of each of the barriers taken separately are not maximum.

To express the current in the contact α in terms of the scattering matrix elements, we fist introduce the creation and annihilation operators for incoming particles, $\hat{b}^\dagger(E)$ and $\hat{b}(E)$, and outgoing particles $\hat{a}^\dagger(E)$ and $\hat{a}(E)$ at energy E in terminal α, see Fig. 4.2. These operators are related by the scattering-matrix elements:

$$\hat{b}_{\alpha n} = \sum_{\beta,m} S_{\alpha\beta,nm}\, \hat{a}_{\beta m}\,. \tag{4.7}$$

The operator $\hat{b}_{\alpha n}$ annihilates a particle in the incoming channel n in lead α whereas the operator $\hat{a}_{\beta m}$ annihilates a particle in the outgoing channel m of the lead β. The total current $\hat{I}_\alpha$ entering the reservoir α in terms of the second quantization expression of the current density operator $\hat{j}_\alpha(\vec{r}, t)$ is given by :

$$\hat{I}_\alpha(t) = \iint_{\mathcal{A}} dy\, dz\, \hat{j}_\alpha(\vec{r}, t) = \frac{\hbar}{2mi} \iint_{\mathcal{A}} dy\, dz \left[\hat{\Psi}^\dagger_\alpha \nabla \hat{\Psi}_\alpha - (\nabla \hat{\Psi}^\dagger_\alpha)\hat{\Psi}_\alpha\right]. \tag{4.8}$$

The integral is over an arbitrary cross section of the reservoir. In the scattering-matrix approach, it is assumed that, deep in the reservoirs, the current operator does not depend on the position of the cross section along the $\hat{x}$-axis. This explains why the only argument in the current is the time. The Fermi field operator $\hat{\Psi}_\alpha$ is a superposition of the incoming and outgoing states in reservoir α:

$$\begin{aligned}\hat{\Psi}_\alpha(\vec{r},t) &= \sum_n \int \frac{dE_{\alpha n}}{\sqrt{h v_{\alpha n}}} e^{ik_{\alpha n}x}\, e^{-i\omega_{\alpha n}t} \chi_{\alpha n}(y,z) \times \hat{a}_{\alpha n} \\ &\quad + \sum_n \int \frac{dE_{\alpha n}}{\sqrt{h v_{\alpha n}}} e^{-ik_{\alpha n}x}\, e^{i\omega_{\alpha n}t} \chi_{\alpha n}(y,z) \times \hat{b}_{\alpha n}\,. \end{aligned} \tag{4.9}$$

Inserting this expression in Eq. (4.8) and within certain limits, some algebra gives :

$$\hat{I}_\alpha(t) = \frac{e}{h} \sum_n \iint dE\, dE'\, e^{i(E-E')t/\hbar} \left[\hat{a}^\dagger_{\alpha n}(E)\hat{a}_{\alpha n}(E') - \hat{b}^\dagger_{\alpha n}(E)\hat{b}_{\alpha n}(E')\right]. \tag{4.10}$$

This expression is exact in the zero-frequency limit and is a good approximation for for a large range of small frequencies. For a detailed discussion of the validity of this expression, we refer to the Ref. [Büttiker 92] where the derivation can be found in its entirety. Equation (4.10) will be used all along this thesis to calculate the average current at the output of the MZI.

Now, making use of Eq. (4.7), the current operator in reservoir α can be written in terms of the scattering matrix amplitudes and the operators $\hat{a}$ only :

$$\hat{I}_\alpha(t) = \frac{e}{h} \iint dE\, dE' \sum_{\beta\gamma,mn} \hat{a}^\dagger_{\beta m}(E) \Big(\mathbf{A}_{\beta\gamma}(\alpha,E,E')\Big)_{mn} \hat{a}_{\gamma n}(E')\,. \tag{4.11}$$

where the matrix $\mathbf{A}$ is the *current* matrix :

$$\mathbf{A}_{\beta\gamma}(\alpha,E,E') = \mathbb{1}_\alpha \delta_{\alpha\beta}\,\delta_{\alpha\gamma} - S^\dagger_{\alpha\beta}(E)\, S_{\alpha\gamma}(E')\,. \tag{4.12}$$

The average current can be easily calculated, since the quantum statistical average of combinations of $\hat{a}^\dagger\hat{a}$ are proportional to by Fermi functions f :

$$\langle \hat{a}^\dagger_\alpha(E)\hat{a}_\beta(E')\rangle = \delta_{\alpha\beta}\,\delta(E-E')\,f_\alpha(E)\,.$$

The reservoir α is characterized by its Fermi distribution $f_\alpha(E)$. To linear response, the average current is expressed in terms of a conductance matrix $G_{\alpha\beta}$:

$$\begin{aligned}\langle \hat{I}_\alpha\rangle &= \sum_\beta G_{\alpha\beta}\, V_\beta \quad \text{with} \\ G_{\alpha\beta} &= \frac{e^2}{h} \int dE \left(-\frac{\partial f(E)}{\partial E}\right) \Big(\delta_{\alpha\beta} - S^\dagger_{\alpha\beta}(E)\, S_{\alpha\beta}(E)\Big)\,. \end{aligned} \tag{4.13}$$

Here V_β is the voltage applied to the contact β and $f(E)$ is the equilibrium Fermi distribution at energy E. At zero temperature, this reduces to Eq. (4.1).

4.2 Self-consistent determination of the fluctuating potential U

In this appendix, we present the self-consistent derivation of the potential in the upper and lower arms due to the presence of the charge qubits. For more details, we refer the reader to the following references: [Büttiker 93a, Martin 00, Pilgram 02, Pilgram 04]. As shown in this work, one condition to operate the MZI as parity meter is to assume that the acquired phase $\Delta\chi$ by the electrons is the same on the upper and lower arms. As a consequence the potentials in the upper and lower arm have to be also the same, $U_1 = U_2 = U$. In this section, we derive this potential U considering only the upper arm (the derivation for the lower arm is similar). Given that the two arms of the MZI are not subject to the Coulomb interaction, we consider the setup shown in Fig. 4.3 which depicts the coupling between one charge qubit and one arm of the MZI in the region Ω. Assuming that the potential is constant in the region Ω of the coupling, the fluctuating phase acquired by the electrons in the arm is given by:

$$\frac{e}{\hbar}\int_0^\tau dt'\, U(t') = \frac{e}{\hbar}\, U\, \tau\,, \tag{4.14}$$

where τ is the traversal time of the electrons to travel over the region of interaction Ω. The corresponding scattering matrix is given by:

$$S_u = \begin{pmatrix} i\sqrt{T_{\rm R}R_{\rm L}}e^{i\phi_u}e^{ieUt/\hbar} & \sqrt{T_{\rm R}T_{\rm L}}e^{i\phi_u}e^{ieUt/\hbar} \\ -\sqrt{R_{\rm L}R_{\rm R}}e^{i\phi_u}e^{ieUt/\hbar} & i\sqrt{R_{\rm R}T_{\rm L}}e^{i\phi_u}e^{ieUt/\hbar} \end{pmatrix}$$

The phase ϕ_u is the sum of a dynamical phase $k_\mu L$ and a phase acquired due to the magnetic field.

From the interaction term of the Coulomb Hamiltonian (Eq. (1.9)), the coupling capacitance is C_i. The charge $\hat{Q}$ in the region Ω can be expressed in two ways: first with the help of the potential operator in this region, $\hat{Q} = C_i\,\hat{U}$ and second as the sum of the bare charge in this region $e\hat{\mathcal{N}}$ and the induced charges generated by the fluctuating potential in this same region, $-e^2N\hat{U}$:

$$\hat{Q} = C_i\hat{U} = e\hat{\mathcal{N}} - e^2N\hat{U} \tag{4.15}$$

From these equations, we can express the potential operator $\hat{U}$ self-consistently:

$$\hat{U} = \frac{e\hat{\mathcal{N}}}{C_i + e^2N} = \frac{e\hat{\mathcal{N}}}{e^2N}\frac{C_\mu}{C_i}\,. \tag{4.16}$$

Here C_μ is the electrochemical capacitance defined as the sum in series of the geometrical capacitances and the quantum capacitance $C_q = e^2N$. The density-of-states in the arm is N. These capacitances have been defined in the main text in Eqs.(1.18).

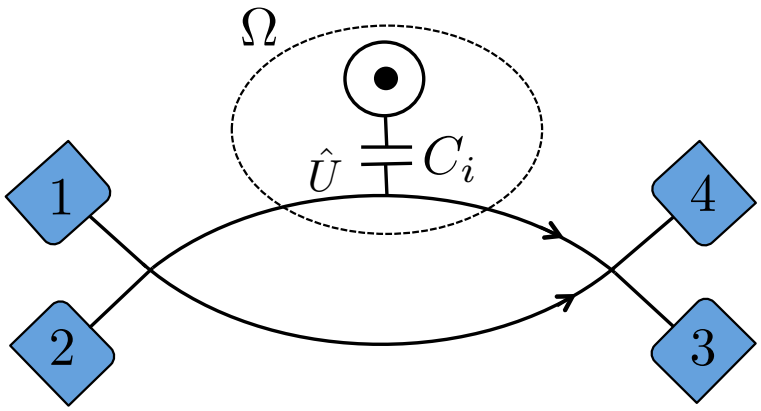

Figure 4.3: Self-consistent determination of the fluctuating potential $\hat{U}$ in the upper arm of the MZI. A charge is coupled to this upper arm by a capacitance C_i. The potential is determined by considering the charge in the upper arm in the region Ω. This charge is the sum of the bare charge and the charges induced by the fluctuating potential $\hat{U}$ in the arm.

The bare charge and the induced charge are calculated from the Wigner-Smith time-delay matrix (or density-of-states matrix) $\mathcal{N}_{\alpha\beta}$ [Martin 00]:

$$\mathcal{N}_{\alpha\beta}(E) = \frac{-1}{2\pi i} \sum_{\nu} S^{\dagger}_{\nu\alpha}(E,U) \frac{\partial S_{\nu\beta}(E,U)}{e\partial U} \,. \tag{4.17}$$

The indices $\alpha, \beta = 1, 2$ label the leads that connect the region Ω to the reservoirs. The diagonal elements of this matrix are widely used to describe quantum pumping [Brouwer 98]. The charge operator $e\hat{\mathcal{N}}$ in the region Ω is defined as:

$$e\hat{\mathcal{N}} = e \sum_{\alpha,\beta} \int dE \, a^{\dagger}_{\alpha}(E) \, \mathcal{N}_{\alpha\beta}(E) \, a_{\beta}(E) \,. \tag{4.18}$$

In the above equation $a^{\dagger}_{\alpha}(E)$ creates an incoming electron in lead α. The density of states N is given as the sum of the elements of the *local* Wigner-Smith time-delay matrix:

$$N = \sum_{\gamma} \mathcal{N}_{\gamma\gamma}(E) \,. \tag{4.19}$$

With the scattering matrix of the upper arm, we have that:

$$S^{\dagger}_{u} S_{u} = \begin{pmatrix} R_{\mathrm{L}} & -i\sqrt{R_{\mathrm{L}} T_{\mathrm{L}}} \\ i\sqrt{R_{\mathrm{L}} T_{\mathrm{L}}} & T_{\mathrm{L}} \end{pmatrix} .$$

With these different definitions and expressions, the potential operator $\hat{U}$ in the region Ω is calculated. We recover the expression of the additional phase $\Delta\chi$ acquired by the electrons due to the presence of the DQDs, Eq. (1.17):

$$\Delta\chi = \frac{e}{\hbar} U\tau = 2\pi \frac{C_{\mu}}{C_i} \,. \tag{4.20}$$

4.3 Description of the source in the non-adiabatic regime

In this appendix, we provide the details on the derivations of the scattering matrix amplitude and of the current emitted by the source in the non-adiabatic regime.

4.3.1 The scattering amplitude

In the non-adiabatic regime, the emissions of a single electron and a single hole per period are triggered by an applied periodic potential. Compared to the adiabatic case, the non-adiabatic regime is reached when the potential has an abrupt change compared to the time spent by the particle in the cavity. This is for instance the case with a periodic square potential $U(t) = U(t+\mathcal{T})$ as shown in Fig. 4.4 :

$$U(t) = \begin{cases} U_0\,, & -\mathcal{T}/2 < t < -\mathcal{T}/4\,, \\ U_1\,, & -\mathcal{T}/4 < t < \mathcal{T}/4\,, \\ U_0\,, & +\mathcal{T}/4 < t < \mathcal{T}/2\,. \end{cases} \tag{4.21}$$

The first step of the potential at $-\mathcal{T}/4 \equiv t^-$ is at the origin of the emission of an electron whereas the second step at $\mathcal{T}/4 \equiv t^+$ provokes the emission of a hole. In this work, we focus on single-particle interferences so that we assume that the times of emission of an electron and a hole are well separated, i.e $|t^- - t^+| \gg \tau_D$.

To derive the scattering amplitude in the time interval $[-\mathcal{T}/2, 0]$, we have to start again from the Fabry-Pérot expression given by Eq.(2.12) with now a phase $\Phi_n(t)$ which varies over the time the particle spends inside the mesoscopic capacitor :

$$S^{(e)}_{\rm na}(t,E) \;=\; r_{\rm SES} + \frac{t^2_{\rm SES}}{r_{\rm SES}} \sum_{n=1}^{\infty} r^n_{\rm SES}\, e^{i\left(nk_E L - \Phi_n(t)\right)}\,, \tag{4.22}$$

with

$$\begin{aligned} \Phi_n(t) \;&=\; \frac{e}{\hbar}\int_{t-n\tau}^{t} dt'\, U(t') \\ &=\; \frac{e}{\hbar}\begin{cases} n\tau U_0 & -\mathcal{T}/2 < t < t^- \\ n\tau U_0 + \delta U t & t^- < t < t^- + n\tau \\ n\tau U_1 & t^- + n\tau < t < 0\,. \end{cases} \end{aligned} \tag{4.23}$$

The potential difference is $\delta U = U_1 - U_0$.

Defining $N = [t/\tau]$ as the integer part of t/τ, the sum over n in the Fabry-Pérot expression is splitted into 3 parts corresponding to the 3 expressions of the phase

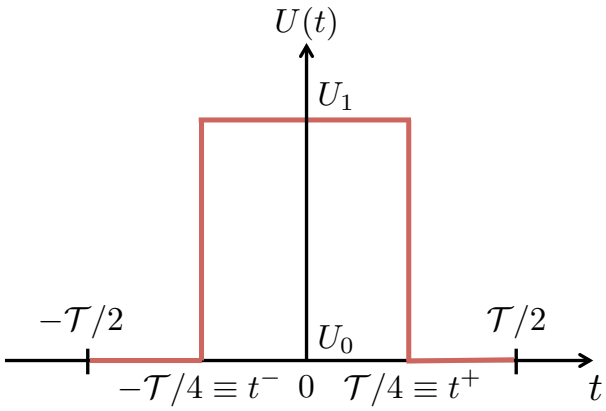

Figure 4.4: Periodic square potential to operate the source in the non-adiabatic regime, shown in the time interval $[-\mathcal{T}/2, \mathcal{T}/2]$. The abrupt changes between the lower value U_0 and the higher value U_1 at the times $t^{\pm}$ lead to the emission of an electron and of a hole. One condition to operate the source in the optimal regime consists in setting the difference $U_1 - U_0$ equal to the energy level spacing in the cavity Δ.

$\Phi_n(t)$:

- If $t < t^-$, the potential is constant and is given by its value U_0. The scattering matrix amplitude will be given by the frozen scattering matrix amplitude (Eq.(2.30)) with $V = U_0$:

$$S(U_0[t], E) = e^{i\phi_r} \frac{|r_{\rm SES}| - e^{i\varphi_{U_0}(t,E)}}{1 - |r_{\rm SES}| e^{i\varphi_{U_0}(t,E)}} \,. \tag{4.24}$$

- If $t^- < t < 0$, and $n > N$, the scattering amplitude depends on the potential step δU.

- If $t^- < t < 0$, and $n < N$, the potential recovers a constant value, namely U_1.

The scattering matrix in the non adiabatic regime $S_{\rm na}(t, E)$ can therefore be written as the sum of a frozen scattering amplitude for $t < t^-$ before the step in the potential and a more complicated term depending on N for $t > t^-$:

$$S^{(e)}_{\rm na}(t, E) = S(U_0[t - t^-], E)\, \Theta(-(t - t^-)) + \delta S(t - t^-, E)\, \Theta(t - t^-) \,, \tag{4.25}$$

with

$$S(U_0[t], E) = e^{i\phi_r} \frac{|r_{\rm SES}| - e^{i\varphi_{U_0}(t,E)}}{1 - |r_{\rm SES}| e^{i\varphi_{U_0}(t,E)}} \,, \tag{4.26a}$$

$$\delta S(t, E) = e^{i\phi_r} T_{\rm SES} R_{\rm SES}^{N/2} \left(\frac{e^{i(N+1)\varphi_{U_1}(t,E)}}{1 - \sqrt{R_{\rm SES}} e^{i\varphi_{U_1}(t,E)}} - \frac{e^{i(N+1)\varphi_{U_0}(t,E)} e^{-i2\pi e\delta U t/h}}{1 - \sqrt{R_{\rm SES}} e^{i\varphi_{U_0}(t,E)}} \right) . \tag{4.26b}$$

The optimal regime

Important simplifications can be made when assuming that the source is operated in the *optimal* regime which consists in the two following assumptions:

1) The potential difference δU corresponds exactly to one level spacing $\Delta = h/\tau$ of the mesoscopic capacitor. This corresponds to the experimental regime in which the emission of quantized charges is observed. It ensures that only one charge is emitted in each half-period of the potential $U(t)$:

$$e\delta U = \pm\Delta\,. \tag{4.27}$$

The sign + corresponds to the emission of an electron whereas the sign − corresponds to the emission of a hole.

2) At $t = 0$, the Fermi energy μ lies exactly in the middle of two levels of the cavity. As a consequence U_0 and U_1 play the same role, $U_1 = -U_0 \equiv U$ and the phase φ_U does not depend on time anymore, as shown below. This condition requires that $\varphi_U(\mu) \equiv \pi$:

$$\varphi_U(\mu) = \phi_r + k_\mu L - \frac{eU\tau}{\hbar} \equiv \pi\,, \tag{4.28}$$

where we recall that ϕ_r is the phase of the reflection amplitude, $r_{\rm SES} = |r_{\rm SES}|e^{i\phi_r}$. With these two assumptions, the expression of the phase $\varphi_U(E)$ is greatly simplified :

$$\begin{aligned}\varphi_U(E) &= \phi_r + k_\mu L + (E-\mu)\frac{\tau}{\hbar} - \frac{eU\tau}{\hbar} \\ &= \pi + 2\pi\frac{E-\mu}{\Delta}\,,\end{aligned} \tag{4.29}$$

Then the resonance condition reads:

$$\begin{aligned}&\varphi(E) = 2\pi k\,, k = 0,1,2,\ldots \\ \Leftrightarrow\quad &E_k - \mu = \Delta(k - \frac{1}{2})\,, k = 0,1,2,\ldots\end{aligned} \tag{4.30}$$

These assumptions simplify the analytical calculations but are fully justified by the experiment which works in this optimal regime. The scattering matrix corresponding to the emission of an electron reads:

$$S^{(e)}_{\rm na}(t,E) = S(E) + \delta S(t - t^-, E)\,\Theta(t - t^-)\,, \tag{4.31}$$

with

$$S(E) = e^{i\phi_r} \frac{|r_{\rm SES}| - e^{i\varphi(E)}}{1 - |r_{\rm SES}| e^{i\varphi(E)}} \,, \tag{4.32a}$$

$$\delta S(t - t^-, E) = e^{i\phi_r} T_{\rm SES} R_{\rm SES}^{N/2} \frac{e^{i(N+1)\varphi(E)}}{1 - \sqrt{R_{\rm SES}} e^{i\varphi(E)}} \left(1 - e^{-i2\pi(t-t^-)/\tau}\right) \,, \tag{4.32b}$$

where we have redefined $N = [(t - t^-)/\tau]$. The scattering amplitude satisfies the conservation of the current :

$$\int_0^{\mathcal{T}} \frac{dt}{\mathcal{T}} S_{\rm na}^{(e)}(t, E) S_{\rm na}^{(e)*}(t, E) = 1 \,. \tag{4.33}$$

For the time interval $[0, \mathcal{T}/2]$ corresponding to the emission of a hole, the derivation of the scattering amplitude $S_{\rm na}^{(h)}(t, E)$ is similar, with $e\delta U = -\Delta$ and $N = [(t - t^+)/\tau]$:

$$S_{\rm na}^{(h)}(t, E) = S(E) + \delta S(t - t^+, E)\, \Theta(t - t^+) \,, \tag{4.34}$$

with

$$S(E) = e^{i\phi_r} \frac{|r_{\rm SES}| - e^{i\varphi(E)}}{1 - |r_{\rm SES}| e^{i\varphi(E)}} \,, \tag{4.35a}$$

$$\delta S(t - t^+, E) = e^{i\phi_r} T_{\rm SES} R_{\rm SES}^{N/2} \frac{e^{i(N+1)\varphi(E)}}{1 - \sqrt{R_{\rm SES}} e^{i\varphi(E)}} \left(1 - e^{i2\pi(t-t^+)/\tau}\right) \,. \tag{4.35b}$$

Floquet scattering amplitudes

The Floquet scattering amplitude $S_{\rm na}(E_m, E)$ is the Fourier transform of the scattering amplitude $S_{\rm na}(t, E)$:

$$S_{\rm na}(E_m, E) = \int_0^{\mathcal{T}} \frac{dt}{\mathcal{T}} e^{im\Omega t} S_{\rm na}(t, E) \,,$$

We recall that $E_m = E + m\hbar\Omega$ and we obtain for the electron and for the hole contribution :

$$S_{\rm na}^{(e)}(E_m, E) = \frac{1}{m(m\Omega\tau - 2\pi)} \frac{i e^{im\Omega t^-} e^{i\theta_r} T e^{i\phi}}{1 - \sqrt{R} e^{i\phi}} \frac{e^{im\Omega\tau} - 1}{1 - \sqrt{R} e^{i(\phi + m\Omega\tau)}} \,, \tag{4.36a}$$

$$S_{\rm na}^{(h)}(E_m, E) = \frac{1}{m(m\Omega\tau + 2\pi)} \frac{-i e^{im\Omega t^+} e^{i\theta_r} T e^{i\phi}}{1 - \sqrt{R} e^{i\phi}} \frac{e^{im\Omega\tau} - 1}{1 - \sqrt{R} e^{i(\phi + m\Omega\tau)}} \,. \tag{4.36b}$$

The Floquet scattering amplitude in the non-adiabatic regime is therefore :

$$S_{\rm na}(E_m, E) = S^{(e)}_{\rm na}(E_m, E) + S^{(h)}_{\rm na}(E_m, E)\,, \tag{4.37}$$

we derive the current emitted by the source in this non-adiabatic regime as well as the current at the output of the MZI from which we extract the first-order correlation function and the coherence length.

4.3.2 Current emitted by the source

The current $I_{\rm na}$ emitted by the source at time $t-\tau_{\rm i}$ in the non-adiabatic regime in terms of the Floquet scattering amplitude of the source $S_{\rm na}$ is given by Eq. (2.22) which we repeat here :

$$I_{\rm na}(t-\tau_{\rm i}) \;=\; \sum_l e^{-il\Omega(t-\tau_{\rm i})}\frac{e}{h}\int_0^\infty dE \sum_m \left[f(E)-f(E_m)\right]\; S^*_{\rm na}(E_m,E)S_{\rm na}(E_{l+m},E)\,.$$

Here $E_m = E + m\hbar\Omega$ and $E_{l+m} = E + (m+l)\hbar\Omega$ and $S_{\rm na}(E_m, E)$ is given by Eq. (4.37).

The product of the scattering amplitudes $S^*_{\rm na}(E_m,E)S_{\rm na}(E_{l+m},E)$

Importantly we repeat that the emissions of an electron and a hole are separated by a long time compared to the dwell time τ_D of the single particles in the cavity :

$$|t^- - t^+| \gg \tau_D\,.$$

The product of the Floquet scattering amplitudes $S^*_{\rm na}(E_m,E)S_{\rm na}(E_{l+m},E)$ consists therefore in two terms, one contribution from the electron and one contribution from the hole; the cross product vanishes. To simplify the presentation, we outline below the derivation for the current produced by the emission of electrons, i.e we consider only $S^{(e)}_{\rm na}$. The time period $\mathcal{T}$ is assumed to be much longer than any other time scale, in particular $\mathcal{T} \gg \tau$, so that we can go to the continuous limit for the sums over m and l :

$$\begin{aligned} l\Omega \;&\equiv\; \omega' \quad \text{so that} \quad \sum_l \to \int \frac{d\omega'}{\Omega}\,, \\ m\Omega \;&\equiv\; \omega \quad \text{so that} \quad \sum_m \to \int \frac{d\omega}{\Omega}\,. \end{aligned}$$

We get :

$$\begin{aligned} I^{(e)}_{\rm na}(t) \;=\; & \frac{e}{h}\int dE \int \frac{d\omega}{\Omega}\left[f(E)-f(E+\hbar\omega)\right] \\ & \int \frac{d\omega'}{\Omega} e^{-i\omega' t} S^{(e)*}_{\rm na}(E+\hbar\omega,E) S^{(e)}_{\rm na}(E+\hbar(\omega+\omega'),E)\,. \end{aligned} \tag{4.38}$$

Defining $\varepsilon \equiv E - \mu$, we can express the product of the two scattering matrices as:

$$\frac{1}{\Omega^2}\, S^{(e)*}_{\rm na}(E+\hbar\omega, E) S^{(e)}_{\rm na}(E+\hbar(\omega+\omega'), E) = T^2_{\rm SES} j(\varepsilon,\omega,\omega')\zeta^{(e)}(\omega,\omega')\,, \quad (4.39)$$

with $T_{\rm SES}$ the transmission probability of the QPC coupling the source to the edge state and

$$\begin{aligned} j(\varepsilon,\omega,\omega') &= \frac{1}{|1-\sqrt{R_{\rm SES}}e^{i\varphi(\varepsilon)}|^2}\frac{1}{\Big(1-\sqrt{R_{\rm SES}}e^{-i(\varphi(\varepsilon)+\omega\tau)}\Big)\Big(1-\sqrt{R_{\rm SES}}e^{i(\varphi(\varepsilon)+(\omega+\omega')\tau)}\Big)}\,, \\ \zeta^{(e)}(\omega,\omega') &= \frac{\Big(e^{-i\omega\tau}-1\Big)\Big(e^{i(\omega+\omega')\tau}-1\Big)}{\omega(\omega+\omega')(\omega\tau-2\pi)\Big((\omega+\omega')\tau-2\pi\Big)}\,. \end{aligned}$$

The phase $\varphi(\varepsilon)$ is the phase defined above in Eq.(4.29) with $\varepsilon = E - \mu$.

The current emitted by the source in the non-adiabatic regime

To calculate this current, we make use of the Residue theorem. For this, we expand the denominators of the functions j and ζ using the Breit-Wigner assumption $T_{\rm SES} \ll 1$. With the expression of the energies $\varepsilon_k \equiv E_k - \mu$ given by Eq.(4.30), we get:

$$\begin{aligned} \frac{1}{|1-\sqrt{R_{\rm SES}}e^{i\varphi(\varepsilon)}|^2} &= \sum_k \frac{\Delta^2/4\pi^2}{\Big(\varepsilon-\Delta(k-\frac{1}{2})\Big)^2+\gamma^2} = \frac{\Delta^2}{4\pi\gamma}\sum_k \delta\Big(\varepsilon-\Delta(k-\frac{1}{2})\Big)\,, \\ \frac{1}{1-\sqrt{R_{\rm SES}}e^{-i(\varphi(\varepsilon)+\omega\tau)}} &= \sum_l \frac{-i\Delta/2\pi}{\big[\varepsilon-\Delta(l-\frac{1}{2})\big]+\hbar\omega-i\gamma}\,, \\ \frac{1}{1-\sqrt{R_{\rm SES}}e^{i(\varphi(\varepsilon)+(\omega+\omega')\tau)}} &= \sum_m \frac{i\Delta/2\pi}{\big[\varepsilon-\Delta(m-\frac{1}{2})\big]+\hbar(\omega+\omega')+i\gamma} \end{aligned}$$

Here we have introduced the coefficient γ :

$$\gamma \equiv \frac{\Delta T_{\rm SES}}{4\pi}\,, \quad (4.40)$$

verifying $\lim_{T_{\rm SES}\to 0}\gamma = 0$. The integrals over ω, ω' and ε are done with the Residue theorem and we get the expression of the current $I^{(e)}_{\rm na}(t-t^-)$ emitted by the source in the non-adiabatic regime in the time interval $[-\mathcal{T}/2, 0]$:

$$I^{(e)}_{\rm na}(t) = \alpha^{(e)}\,\frac{e^{-(t-t^-)/\tau_D}}{\tau_D}\,\Theta(t-t^-)\,,$$

with :

$$\begin{aligned} \tau_D &= \frac{h}{T_{\rm SES}\,\Delta} \quad \text{being the dwell time of the particle inside the cavity and} \\ \alpha^{(e)} &= \sum_k \left(f\big(\Delta(k-\frac{1}{2})\big) - f\big(\Delta(k+\frac{1}{2})\big) \right) . \end{aligned}$$

The coefficient $\alpha^{(e)}$ is important as it implies that several levels of the mesoscopic capacitor may contribute to the transport at non-zero temperature. In the non-adiabatic regime (as in adiabatic regime), we assume zero temperature and for the electron emission, only the term corresponding to $k = 0$ does not vanish. Therefore, at zero temperature, only one level of the cavity contributes to the transport and $\alpha = 1$. The current $I^{(e)}_{\rm na}(t)$ in the first period of the potential, $t \in [-\mathcal{T}/2, 0]$, is then given by:

$$I^{(e)}_{\rm na}(t) = \frac{e}{\tau_D} e^{-(t-t^-)/\tau_D}\,\Theta(t-t^-) \quad \text{for} \quad -\mathcal{T}/2 < t < 0\,, \tag{4.41}$$

where Θ is the Heaviside function. Following exactly the same procedure for the step of the potential at time t^+ in the interval $[0, \mathcal{T}/2]$ during which a hole is emitted we get the current produced by the emission of holes $I^{(h)}_{\rm na}(t)$:

$$I^{(h)}_{\rm na}(t) = \alpha^{(h)}\,\frac{e^{-(t-t^+)/\tau_D}}{\tau_D}\,\Theta(t-t^+)\,,$$

with :

$$\alpha^{(h)} = \sum_k \left(f\big(\Delta(k-\frac{1}{2})\big) - f\big(\Delta(k-\frac{3}{2})\big) \right) .$$

By shifting k by 1, we obtain that $\alpha^{(h)} = -\alpha^{(e)}$ at any temperature. In the particular case of zero temperature, the only level which contributes to this current is the term corresponding to $k = 1$. The total current emitted by the cavity is the sum of the current produced by the electrons and the holes:

$$I_{\rm na}(t) = \frac{e}{\tau_D} e^{-(t-t^-)/\tau_D}\Theta(t-t^-) - \frac{e}{\tau_D} e^{-(t-t^+)/\tau_D}\Theta(t-t^+)\,. \tag{4.42}$$

The expression of the current in the non-adiabatic regime is in agreement with the experimental measurements as shown in Fig. 2.11 in the main text. The current exhibits an exponential behavior with a characteristic time corresponding to the dwell time of the particle inside the cavity, $\tau_D = h/(T_{\rm SES}\Delta)$.

Bibliography

[Abragam 85] A. Abragam, *Principles of Nuclear Magnetic Resonance*, Oxford University Press, Oxford (1985).

[Aharonov 59] Y. Aharonov and D. Bohm, *Significance of electromagnetic potentials in the quantum theory*, Phys. Rev. **115**, 485 (1959).

[Albert 10] M. Albert, C. Flindt and M. Büttiker, *Accuracy of the quantum capacitor as a single-electron source*, Phys. Rev. B **82**, 041407 (2010).

[Albert 11] M. Albert, C. Flindt, and M. Büttiker, *Distributions of waiting times of dynamic single-electron emitters*, Phys. Rev. Lett. **107**, 086805 (2011).

[Albert 12] M. Albert, G. Haack, C. Flindt and M. Büttiker, *Electron waiting times in mesocopic conductors*, Phys. Rev. Lett. **108**, 186806 (2012).

[Aleiner 02] I. L. Aleiner, P. W. Brouwer, and L. I. Glazman, *Quantum effects in Coulomb blockade*, Phys. Rep. **358**, 309 (2002).

[Altshuler 85] B. L. Altshuler, *Fluctuations in the extrinsic conductivity of disordered conductors*, Pis'ma Zh. Eksp. Teor. Fiz. **41**, 530 (1985) [JETP Lett. **41**, 648 (1985)].

[Ashcroft] N. W. Ashcroft and N. D. Mermin, *Solid State Physics*, Saunders College Publishing, Philadelphia (1976).

[Averin 91] D. Averin, A. Korotkov, and K. Likharev, *Theory of single-electron charging of quantum wells and dots*, Phys. Rev. B **44**, 6199 (1991).

[Averin 05] D. V. Averin and E. V. Sukhorukov, *Counting statistics and detector properties of quantum point contacts*, Phys. Rev. Lett. **95**, 126803 (2005).

[Avron 00] J. E. Avron, A. Elgart, G. M. Graf, and L. Sadun, *Geometry, statistics, and asymptotics of quantum pumps*, Phys. Rev. B **62**, R10618 (2000).

[Baranger 94] H. U. Baranger and P. A. Mello, *Mesoscopic transport through chaotic cavities: A random S-matrix theory approach*, Phys. Rev. Lett. **73**, 142 (1994).

[Barenco 95] A. Barenco, C. H. Bennett, R. Cleve, D. P. DiVincenzo, N. Margolus, P. Shor, T. Sleator, J. A. Smolin, and H. Weinfurter, Phys. Rev. A **52**, 3457 (1995).

[Battista 11] F. Battista and P. Samuelsson, *Proposal for nonlocal electron-hole turnstile in the quantum Hall regime*, Phys. Rev. B **83**, 125324 (2011).

[Beenakker 91] C. W. J. Beenakker and H. van Houten, *Quantum transport in semiconductor nanostructures*, Solid State Physics **44**, 1 (1991).

[Beenakker 97] C. W. J. Beenakker, *Random-matrix theory of quantum transport*, Rev. Mod. Phys. **69**, 731-808 (1997).

[Beenakker 04] C. W. J. Beenakker, D. P. DiVincenzo, C. Emary, and M. Kindermann, *Charge detection enables free-electron quantum computation*, Phys. Rev. Lett. **93**, 020501 (2004).

[Bennett 00] C. H. Bennett and D. P. DiVincenzo, *Quantum information and computation*, Nature **404**, 247 (2000).

[Bieri 09] E. Bieri, M. Weiss, O. Göktas, M. Hauser, C. Schönenberger, and S. Oberholzer, *Finite-bias visibility dependence in an electronic Mach-Zehnder interferometer*, Phys. Rev. B **79**, 245324 (2009).

[Blanter 00] Y. M. Blanter and M. Büttiker, *Shot noise in mesoscopic conductors*, Phys. Rep. **336**, 1 (2000).

[Bleszynski-Jayich 09] A. C. Bleszynski-Jayich, W. E. Shanks, B. Peaudecerf, E. Ginossar, F. von Oppen, L. Glazman, and J. G. E. Harris, *Persistent currents in normal metal rings*, Science **326**, 272 (2009).

[Blumenthal 07] M. D. Blumenthal, B. Kaestner, L. Li, S. Giblin, T. J. B. M. Janssen, M. Pepper, D. Anderson, G. Jones, and D. A. Ritchie, *Gigahertz quantized charge pumping*, Nat. Phys. **3**, 343 (2007).

[Bocquillon 12] E. Bocquillon, F. D. Parmentier, C. Grenier, J.-M. Berroir, P. Degiovanni, D. C. Glattli, B. Plaçais, A. Cavanna, Y. Jin, and G. FŔve, *Electron quantum optics: Partitioning electrons one by one*, to be published in Phys. Rev. Lett (2012).

[Bohigas 84] O. Bohigas, M. J. Giannoni, and C. Schmit, *Characterization of chaotic quantum spectra and universality of level fluctuation laws*, Phys. Rev. Lett. **52**, 1 (1984).

[Braginsky 92] V. D. Braginsky and F. Y. Khalili, *Quantum measurement*, Cambridge University Press, Cambridge (1992).

[Brandes 08] T. Brandes, *Waiting times and noise in single particle transport*, Ann. Phys. (Berlin) **17**, 477 (2008).

[Brouwer 97] P. W. Brouwer, *On the Random-Matrix Theory of Quantum Transport*, PhD thesis (1997).

[Brouwer 98] P. W. Brouwer, *Scattering approach to parametric pumping*, Phys. Rev. B **58**, 10135 (1998).

[Budini 11] A. A. Budini, *Large deviations of ergodic counting processes: A statistical mechanics approach*, Phys. Rev. E **84**, 011141 (2011).

[Buks 98] E. Buks, R. Schuster, M. Heiblum, D. Mahalu, and V. Umansky, *Dephasing due to which path detector*, Nature **391**, 871 (1998).

[Büttiker 83] M. Büttiker, Y. Imry, and R. Landauer, *Josephson behavior in small normal one-dimensional rings*, Phys. Lett. A **96**, 365 (1983).

[Büttiker 84] M. Büttiker, Y. Imry, and M. Ya. Azbel, *Quantum oscillations in one-dimensional normal-metal rings*, Phys. Rev. A **30**, 1982 (1984).

[Büttiker 88] M. Büttiker, *Absence of backscattering in the quantum Hall effect in multiprobe conductors*, Phys. Rev. B **38**, 9375 (1988).

[Büttiker 90] M. Büttiker, *Scattering theory of thermal and excess noise in open conductors*, Phys. Rev. Lett. **65**, 2901 (1990).

[Büttiker 92a] M. Büttiker, *Scattering theory of current and intensity noise correlations in conductors and wave guides*, Phys. Rev. B **46**, 12485 (1992).

[Büttiker 92] M. Büttiker, *Flux-sensitive correlations of mutually incoherent quantum channels*, Phys. Rev. Lett. **68**, 843 (1992).

[Büttiker 93a] M. Büttiker, H. Thomas, A. Prêtre, *Mesoscopic capacitors*, Phys. Lett. A **180**, 364 (1993).

[Büttiker 93b] M. Büttiker, A. Prêtre, H. Thomas, *Dynamic conductance and the scattering matrix of small conductors*, Phys. Rev. Lett. **70**, 4114 (1993).

[Büttiker 94] M. Büttiker, H. Thomas and A. Prêtre, *Current partition in multiprobe conductors in the presence of slowly oscillating external potentials*, Z. Phys. B **94**, 133 (1994).

[Büttiker 00a] M. Büttiker and A. M. Martin, *Charge relaxation and dephasing in Coulomb-coupled conductors*, Phys. Rev. B **61**, 2737 (2000).

[Büttiker 00b] M. Büttiker, Charge Fluctuations and Dephasing in Coulomb Coupled Conductors in *Quantum Mesoscopic Phenomena and Mesoscopic Devices in Microelectronics*, Kluwer Academic Publishers (Dordrecht-Boston-London, 2000), p.211-242.

[Calogero 69] F. Calogero, *Solution of a three-body problem in one dimension*, J. Math. Phys. **10**, 2191 (1969).

[Carmichael 89] H. J. Carmichael, S. Singh, R. Vyas, and P. R. Rice, *Photoelectron waiting times and atomic state reduction in resonance fluorescence*, Phys. Rev. A **39**, 1200 (1989).

[Caves 80] C. M. Caves, K. S. Thorne, R. W. P. Drever, V. D. Sandberg, and M. Zimmermann, *On the measurement of a weak classical force coupled to a quantum-mechanical oscillator*, Rev. Mod. Phys. **52**, 341 (1980).

[Chalker 09a] D. L. Kovrizhin and J. T. Chalker, *Exactly solved model for an electronic Mach-Zehnder interferometer*, Phys. Rev. B **80**, 161306 (2009).

[Chalker 09b] D. L. Kovrizhin and J. T. Chalker, *Multiparticle interference in electronic Mach-Zehnder interferometers*, Phys. Rev. B **81**, 155318 (2010).

[Chandrasekhar 91] V. Chandrasekhar, R. A. Webb, M. J. Brady, M. B. Ketchen, W. J. Gallagher, and A. Kleinsasser, *Magnetic response of a single, isolated gold loop*, Phys. Rev. Lett. **67**, 3578 (1991).

[Chang 08] D.-I. Chang, G. L. Khym, K. Kang, Y. Chung, H.-J. Lee, M. Seo, M. Heiblum, D. Mahalu and V. Umansky, *Quantum mechanical complementarity probed in a closed-loop Aharonov-Bohm interferometer*, Nat. Phys. **4**, 205 (2008).

[Chung 05] V. S .-W Chung, P. Samuelsson and M. Büttiker, *Visibility of current and shot noise in electrical Mach-Zehnder and Hanbury Brown Twiss interferometers*, Phys. Rev. B **72**, 125320 (2005).

[Clerk 03] A. A. Clerk, S. M. Girvin, and A. D. Stone, *Quantum-limited measurement and information in mesoscopic detectors*, Phys. Rev. B **67**, 165324 (2003).

[Clerk 10] A. A. Clerk, M. H. Devoret, S. M. Girvin, F. Marquardt, and R. J. Schoelkopf, *Introduction to quantum noise, measurement, and amplification*, Rev. Mod. Phys. **82**, 1155 (2010).

[Coish 06] W. A. Coish, V. N. Golovach, J. C. Egues, and D. Loss, *Measurement, control, and decay of quantum-dot spins*, Physica Status Solidi (b) **243**, 3658 (2006).

[Cox 62] D. R. Cox, *Renewal Theory*, Chapman and Hall, London (1962).

[Cronin 09] A. D. Cronin, J. Schmiedmayer, and D. E. Pritchard, *Optics and interferometry with atoms and molecules*, Rev. Mod. Phys. **81**, 1051 (2009).

[Delbecq 11] M. R. Delbecq, V. Schmitt, F. D. Parmentier, N. Roch, J. J. Viennot, G. Fève, B. Huard, C. Mora, A. Cottet, and T. Kontos, *Coupling a quantum dot, fermionic leads and a microwave cavity on a chip*, Phys. Rev. Lett. **107**, 256804 (2011).

[Devoret 04] M. H. Devoret, A. Wallraff, J. M. Martinis, *Superconducting Qubits: A Short Review*, arXiv:0411.174 (2004).

[Dubois 12] J. Dubois and D. C. Glattli, *Private communication* (2012).

[Engel 05] H.-A. Engel and D. Loss, *Fermionic Bell-state analyzer for spin qubits*, Science **309**, 586 (2005).

[English 06] B. P. English, W. Min, A. M. van Oijen, K. T. Lee, G. Luo, H. Sun, B. J. Cherayil, S. C. Kou, X. S. Xie, *Ever-fluctuating single enzyme molecules: MichaelisÐMenten equation revisited*, Nat. Chem. Biol. **2**, 87 (2006).

[Fève 06] G. Fève, *Quantification du courant alternatif : la boîte quantique comme source d'électrons uniques subnanoseconde*, PhD Thesis (2006).

[Fève 07] G. Fève, A. Mahé, J.-M. Berroir, T. Kontos, B. Plaçais, D. C. Glattli, A. Cavanna, B. Etienne and Y. Jin, *An on-demand coherent single-electron source*, Science **316**, 1169 (2007).

[Flagg 10] E. B. Flagg, A. Muller, S. V. Polyakov, A. Ling, A. Migdall, and G. S. Solomon, *Interference of single photons from two separate semiconductor quantum dots*, Phys. Rev. Lett. **104**, 137401 (2010).

[Flindt 09] C. Flindt, C. Fricke, F. Hohls, T. Novotny, K. Netocny, T. Brandes and R. J. Haug, *Universal oscillations in counting statistics*, Proc. Nat. Ac. Sc **106**, 10116 (2009).

[Frey 12] T. Frey, P. J. Leek, M. Beck, A. Blais, T. Ihn, K. Ensslin, and A. Wallraff, *Dipole coupling of a double quantum dot to a microwave resonator*, Phys. Rev. Lett. **108**, 046807 (2012).

[Fujiwara 08] A. Fujiwara, K. Nishiguchi and Y. Ono, *Nanoampere charge pump by single-electron ratchet using silicon nanowire metal-oxide-semiconductor field-effect transistor*, Appl. Phys. Lett **92**, 042102 (2008).

[Gabelli 06] J. Gabelli, G. Fève, J.-M. Berroir, B. Plaçais, A. Cavanna, B. Etienne, Y. Jin, and D. C. Glattli, *Violation of Kirchhoff's laws for a coherent RC circuit*, Science, **313**, 499 (2006).

[Gabelli 09] J. Gabelli and B. Reulet, *Full counting statistics of avalanche transport: an experiment*, Phys. Rev. B **80**, 161203(R) (2009).

[Gefen 84] Y. Gefen, Y. Imry, and M. Ya. Azbel, *Quantum oscillations and the Aharonov-Bohm effect for parallel resistors*, Phys. Rev. Lett. **52**, 129 (1984).

[Glauber 63a] R. J. Glauber, *Photon correlations*, Phys. Rev. Lett. **10**, 84 (1963).

[Glauber 63b] R. J. Glauber, *The quantum theory of optical coherence*, Phys. Rev. **130**, 2529 (1963).

[Glauber 63c] R. J. Glauber, *Coherent and incoherent states of the radiation field*, Phys. Rev. **131**, 2766 (1963).

[Gopich 06] I. V. Gopich and A. Szabo, *Theory of the statistics of kinetic transitions with application to single-molecule enzyme catalysis*, J. Chem. Phys. **124**, 154712 (2006).

[Grenier 11] C. Grenier, R. Hervé, E. Bocquillon, F. D. Parmentier, B. Plaçais, J.-M. Berroir, G. Fève, and P. Degiovanni, *Single electron quantum tomography in quantum Hall edge channels*, New J. Phys. **13**, 093007 (2011).

[Grynberg] G. Grynberg, A. Aspect, and C. Fabre, *Introduction aux lasers et à l'optique quantique*, Ellipses, Ecole Polytechnique, Paris (1997).

[Gurvitz 97] S. A. Gurvitz, *Measurements with a noninvasive detector and dephasing mechanism*, Phys. Rev. B **56**, 15215 (1997).

[Gustavsson 06] S. Gustavsson, R. Leturcq, B. Simovic, R. Schleser, T. Ihn, P. Studerus and K. Ensslin, D. C. Driscoll and A. C. Gossard, *Counting statistics of single electron transport in a quantum dot*, Phys. Rev. Lett. **96**, 076605 (2006).

[Haack 10] G. Haack, H. Förster, and M. Büttiker, *Parity detection and entanglement with a Mach-Zehnder interferometer*, Phys. Rev. B **82**, 155303 (2010).

[Haack 11] G. Haack, M. Moskalets, J. Splettstoesser, and M. Büttiker, *Coherence of single-electron sources from Mach-Zehnder interferometry*, Phys. Rev. B **84**, 081303(R) (2011).

[Haack 12] G. Haack, M. Moskalets, M. Büttiker, *Chiral single-electron source : Adiabatic versus non-adiabatic emission*, manuscript in preparation, (2012).

[Haake 10] F. Haake, *Quantum Signatures of Chaos*, Springer, Heidelberg (2010).

[Hackenbroich 00] G. Hackenbroich, *Phase coherent transmission through interacting mesoscopic systems*, Phys. Rep. **343**, 463-538 (2001).

[Halperin 82] B. I. Halperin, *Quantized Hall conductance, current-carrying edge states, and the existence of extended states in a two-dimensional disordered potential*, Phys. Rev. B **25**, 2185 (1982).

[Haroche 06] S. Haroche and J. M. Raimond, *Exploring the quantum*, Oxford University Press, Oxford (2006).

[Hashisaka 10] M. Hashisaka, A. Helzel, S. Nakamura, L. Litvin, Y. Yamauchi, K. Kobayashi, T. Ono, H.-P. Tranitz, W. Wegschneider, C. Strunk, *Temperature dependence of the visibility in an electronic Mach-Zehnder interferometer*, Physica E **42**, 1091 (2010).

[Hayashi 03] T. Hayashi, T. Fujisawa, H. D. Cheong, Y. H. Jeong, and Y. Hirayama, *Coherent manipulation of electronic states in a double quantum dot*, Phys. Rev. Lett. **91**, 226804 (2003).

[Hassler 08] F. Hassler, M. V. Suslov, G. M. Graf, M. V. Lebedev, G. B. Lesovik, and G. Blatter, *Wave-packet formalism of full counting statistics*, Phys. Rev. B **78**, 165330, (2008).

[Huynh 12] P-A. Huynh, F. Portier, H. le Sueur, G. Faini, U. Gennser, D. Mailly, F. Pierre, W. Wegscheider, and P. Roche, *Quantum coherence engineering in the integer quantum Hall regime*, arXiv:1202.3591 (2012).

[Imry 02] Y. Imry, *Introduction to Mesoscopic Physics*, Oxford University Press, Oxford, (2002).

[Ivanov 93] D. A. Ivanov, and L. S. Levitov, *Statistics of charge fluctuations in quantum transport in an alternating field*, JETP Lett. **58**, 461 (1993).

[Jalabert 94] R. A. Jalabert, J.-L. Pichard, and C.W.J. Beenakker, *Universal quantum signatures of chaos in ballistic transport*, Europhysics Lett. **27**, 255 (1994).

[Ji 03] Y. Ji, Y. Chung, D. Sprinzak, M. Heiblum, D. Mahalu, and H. Shtrikman, *An electronic Mach-Zehnder interferometer*, Nature **422**, 415 (2003).

[Jordan 06] A. N. Jordan and A. N. Korotkov, *Qubit feedback and control with kicked quantum nondemolition measurements: A quantum Bayesian analysis*, Phys. Rev. B **74**, 085307 (2006).

[Keller 96] M. W. Keller, J. M. Martinis, N. M. Zimmerman, and A. H. Steinbach, *Accuracy of electron counting using a 7-junction electron pump*, Appl. Phys. Lett. **69**, 1804 (1996).

[Keeling 06] J. Keeling, I. Klich and L. S. Levitov, *Minimal excitation states of electrons in one-dimensional wires*, Phys. Rev. Lett. **97**, 116403 (2006).

[Keeling 08] J. Keeling, A. V. Shytov, and L. S. Levitov, *Coherent particle transfer in an on-demand single-electron source*, Phys. Rev. Lett. **101**, 196404 (2008).

[Khlus 87] V. A. Khlus, *Current and voltage fluctuations in microjunctions between normal metals and superconductors*, Sov. Phys. JETP **66**, 1243 (1987).

[Khym 06] G. L. Khym, Y. Lee, and K. Kang, *Controlled dephasing and measurement efficiency via quantum dot detector*, Journal of the Phys. Soc. of Japan **75**, 063707 (2006).

[Kiraz 04] A. Kiraz, M. Atatüre, and A. Imamoglu, *Quantum-dot single-photon sources: Prospects for applications in linear optics quantum-information processing*, Phys. Rev. A **69**, 032305 (2004).

[Knill 01] E. Knill, R. Laflamme, and G. J. Milburn *A scheme for efficient quantum computation with linear optics*, Nature **409**, 46 (2001).

[Koch 05] J. Koch, M. E. Raikh, and F. von Oppen, *Full counting statistics of strongly non-ohmic transport through single molecules*, Phys. Rev. Lett. **95**, 056801 (2005).

[Kok 07] P. Kok, W. J. Munro, K. Nemoto, T. C. Ralph, J. P. Dowling, G. J. Milburn, *Linear optical quantum computing with photonic qubits*, Rev. Mod. Phys. **79**, 135 (2007).

[Korotkov 99] A. N. Korotkov, *Continuous quantum measurement of a double dot*, Phys. Rev. B **60**, 5737 (1999).

[Korotkov 01] A. N. Korotkov, *Selective quantum evolution of a qubit state due to continuous measurement*, Phys. Rev. B **63**, 115403 (2001).

[Korotkov 02] A. N. Korotkov, *Continuous measurement of entangled qubits*, Phys. Rev. A **65**, 052304 (2002).

[Kouwenhoven 91] L. P. Kouwenhoven, A. T. Johnson, N. C. van der Vaart, C. J. P. M. Harmans, and C. T. Foxon, *Quantized current in a quantum-dot turnstile using oscillating tunnel barriers*, Phys. Rev. Lett. **67**, 1626 (1991).

[Kovrizhin 09a] D. L. Kovrizhin and J. T. Chalker, *Exactly solved model for an electronic Mach-Zehnder interferometer*, Phys. Rev. B **80**, 161306 (2009).

[Kovrizhin 09b] D. L. Kovrizhin and J. T. Chalker, *Multiparticle interference in electronic Mach-Zehnder interferometers*, arXiv:0912.4840v1 (2009).

[Kravtsov 09] V. E. Kravtsov, *Random matrix theory: Wigner-Dyson statistics and beyond*, arXiv:0911.0639 (2009).

[Kumar 96] A. Kumar, L. Saminadayar, Y. Jin, B. Etienne, and D. C. Glattli, *Experimental test of the quantum shot noise reduction theory*, Phys. Rev. Lett. **76**, 2778 (1996).

[Landau 59] L. D. Landau and E. M. Lifshitz, *Statistical Physics*, Pergamon, Oxford, (1959).

[Landauer 87] R. Landauer, *Computation: A fundamental physical view*, Physica D **38**, 226 (1987).

[Laughlin 92] R. B. Laughlin, *Anomalous quantum Hall effect: an incompressible quantum fluid with fractional charge excitations*, Phys. Rev. Lett. **50**, 1395 (1982).

[Lee 85] P. A. Lee and A. D. Stone, *Universal conductance fluctuations in metals*, Phys. Rev. Lett. **55**, 1622 (1985).

[Lenard 64] A. Lenard, *Momentum distribution in the ground state of the one-dimensional system of impenetrable bosons*, J. Math. Phys. **5**, 930 (1964).

[Lesovik 89] G. B. Lesovik, *Excess quantum shot noise in 2D ballistic point contacts*, Sov. Phys. JETP **49**, 592 (1989).

[Lesovik 11] G. B. Lesovik and I. A. Sadovskyy, *Scattering matrix approach to the description of quantum electron transport*, Phys. Usp. **54**, 1007 (2011).

[Levinson 97] Y. Levinson, *Dephasing in a quantum dot due to coupling with a quantum point contact*, Europhys. Lett. **39**, 299 (1997).

[Levitov 93] L. S. Levitov and G. B. Lesovik, *Charge distribution in quantum shot noise*, JETP Lett. **58**, 230 (1993).

[Levitov 96] L. S. Levitov, H.-W. Lee, and G. B. Lesovik, *Electron counting statistics and coherent states of electric current*, J. Math. Phys. **37**, 4845 (1996).

[Levkivskyi 08] I. P. Levkivskyi and E. V. Sukhorukov, *Dephasing in the electronic Mach-Zehnder interferometer at filling factor* $\nu = 2$, Phys. Rev. B **78**, 045322 (2008).

[Lévy 90] L. P. Lévy, G. Dolan, J. Dunsmuir, and H. Bouchiat, *Magnetization of mesoscopic copper rings: Evidence for persistent currents*, Phys. Rev. Lett. **64**, 2074 (1990).

[Li 99] W. Li and L. E. Reichl, *Floquet scattering through a time-periodic potential*, Phys. Rev. B **60**, 15732 (1999).

[Litvin 07] L. V. Litvin, H.-P. Tranitz, W. Wegscheider and C. Strunk, *Decoherence and single electron charging in an electronic Mach-Zehnder interferometer*, Phys. Rev. B. **75**, 033315 (2007).

[Litvin 08] L. V. Litvin, A. Helzel, H.-P. Tranitz, W. Wegscheider, and C. Strunk, *Edge-channel interference controlled by Landau level filling*, Phys. Rev. B **78**, 075303 (2008).

[Loudon] R. Loudon, *The Quantum Theory of Light*, 3rd edition, Oxford Science Publications, Oxford (2000).

[Lounis 05] B. Lounis and M. Orrit, *Single-photon sources*, Rep. Prog. Phys. **68**, 1129 (2005).

[Lutchyn 10] R. M. Lutchyn, J. D. Sau, and S. Das Sarma, *Majorana fermions and a topological phase transition in semiconductor-superconductor heterostructures*, Phys. Rev. Lett. **105**, 077001 (2010).

[Mahé 10] A. Mahé, F. D. Parmentier, E. Bocquillon, J.-M. Berroir, D. C. Glattli, T. Kontos, B. Plaçais, G. Féve, A. Cavanna, and Y. Jin, *Current correlations of an on-demand single-electron emitter*, Phys. Rev. B **82**, 201309 (2010).

[Maire 08] N. Maire, F. Hohls, B. Kaestner, K. Pierz, H. W. Schumacher, and R. J. Haug, *Noise measurement of a quantized charge pump*, Appl. Phys. Lett **92**, 082112 (2008).

[Mandel 99] L. Mandel, *Quantum effects in one-photon and two-photon interference*, Rev. Mod. Phys. **71**, S274 (1999).

[Mao 04] W. Mao, D. V. Averin, R. Ruskov, and A. N. Korotkov, *Mesoscopic quadratic quantum measurements*, Phys. Rev. Lett. **93**, 056803 (2004).

[Martin 92] T. Martin and R. Landauer, *Wave-packet approach to noise in multichannel mesoscopic systems*, Phys. Rev. B **45**, 1742 (1992).

[Martin 00] A. M. Martin and M. Büttiker, *Coulomb-induced positive current-current correlations in normal conductors*, Phys. Rev. Lett. **84**, 3386-3389 (2000).

[McClure 09] D. T. McClure, Y. Zhang, B. Rosenow, E. M. Levenson-Falk, C. M. Marcus, L. N. Pfeiffer, and K. W. West, *Edge-state velocity and coherence in a qantum Hall Fabry-Pérot interferometer*, Phys. Rev. Lett. **103**, 206806 (2009).

[Messiah] A. Messiah, *Quantum Mechanics*, North-Holland, Amsterdam (1961).

[Metha 04] M. L. Metha, *Random Matrices*, Elsevier, Amsterdam (2004).

[Michler 00] P. Michler, A. Imamoglu, M. D. Mason, P. J. Carson, G. F. Strouse, and S. K. Buratto, *Quantum correlation among photons from a single quantum dot at room temperature*, Nature **406**, 968 (2000).

[Milburn 01] H-S. Goan and G. J. Milburn, *Dynamics of a mesoscopic charge quantum bit under continuous quantum measurement*, Phys. Rev. B **64**, 235307 (2001).

[Moskalets 02] M. Moskalets and M. Büttiker, *Floquet scattering theory of quantum pumps*, Phys. Rev. B **66**, 205320 (2002).

[Moskalets 08] M. Moskalets, P. Samuelsson, and M. Büttiker, *Quantized dynamics of a coherent capacitor*, Phys. Rev. Lett **100**, 086601 (2008).

[Moskalets 11] M. Moskalets, *Scattering matrix approach to non-stationary quantum transport*, Imperial College Press, London (2011).

[Mourik 12] V. Mourik, K. Zuo, S. M. Frolov, S. R. Plissard, E. P. A. M. Bakkers, and L. P. Kouwenhoven, *Signatures of Majorana fermions in hybrid superconductor-semiconductor nanowire devices*, Science **1126**, 1222360 (2012).

[Nazarov 03] Yu. V. Nazarov (ed.), *Quantum Noise in Mesoscopic Physics*, NATO Science Series, Kluwer, Dordrecht (2003).

[Neder 06] I. Neder, M. Heiblum, Y. Levinson, D. Mahalu, and V. Umansky, *Unexpected behavior in a two-path electron interferometer*, Phys. Rev. Lett. **96**, 016804 (2006).

[Neder 07] I. Neder, N. Ofek, Y. Chung, M. Heiblum, D. Mahalu, and V. Umansky, Nature **448**, 333 (2007).

[Neuenhahn 08] C. Neuenhahn and F. Marquardt, *Dephasing by electron-electron interactions in a ballistic Mach-Zehnder interferometer*, New J. Phys. **10**, 115018 (2008).

[Nielsen 00] M. A. Nielsen and I. L. Chuang, *Quantum Computation and Quantum Information*, Cambridge University Press, Cambridge (2000).

[Oberholzer 00] S. Oberholzer, M. Henny, C. Strunk, C. Schönenberger, T. Heinzel, K. Ensslin, and M. Holland, *The Hanbury Brown and Twiss experiment with fermions*, Physica E **6**, 314 (2000).

[Ol'khovskaya 08] S. Ol'khovskaya, J. Splettstoesser, M. Moskalets, and M. Büttiker, *Shot noise of a mesoscopic two-particle collider*, Phys. Rev. Lett. **101**, 166802 (2008).

[Oreg 10] Y. Oreg, G. Refael, and F. von Oppen, *Helical liquids and Majorana bound states in quantum wires*, Phys. Rev. Lett. **105**, 177002 (2010).

[Parmentier 12] F. D. Parmentier, E. Bocquillon, J.-M. Berroir, D. C. Glattli, B. Plaçais, M. Albert, C. Flindt, M. Büttiker, and G. Fève, *Current noise spectrum of a single-particle emitter: Theory and experiment*, Phys. Rev. B **85**, 165438 (2012).

[Picciotto 97] R. de-Picciotto, M. Reznikov, M. Heiblum, V. Umansky, G. Bunin, and D. Mahalu, *Direct observation of a fractional charge*, Nature **389**, 162 (1997).

[Pilgram 02] S. Pilgram and M. Büttiker, *Efficiency of mesoscopic detectors*, Phys. Rev. Lett. **89**, 200401 (2002).

[Pilgram 04] S. Pilgram, *Statistics of fluctuations in transport through interacting mesoscopic conductors*, PhD thesis, Université de Genève (2004).

[Polianski 01] M. L. Polianski and P. W. Brouwer, *Pumped current and voltage for an adiabatic quantum pump*, Phys. Rev. B **64**, 075304 (2001).

[Pothier 92] H. Pothier, P. Lafarge, C. Urbina, D. Esteve, and M. H. Devoret, *Single-electron pump based on charging effects*, Europhys. Lett. **17**, 249 (1992).

[Prêtre 96] A. Prêtre, H. Thomas, M. Büttiker, *Dynamic admittance of mesoscopic conductors: Discrete-potential model*, Phys. Rev. B **54**, 8130 (1996).

[Reznikov 95] M. Reznikov, M. Heiblum, Hadas Shtrikman, and D. Mahalu, *Temporal correlation of electrons: Suppression of shot noise in a ballistic quantum point contact*, Phys. Rev. Lett. **75**, 3340 (1995).

[Roche] P. Roche and F. Portier, *private communication* (2012).

[Roulleau 07] P. Roulleau, F. Portier, D. C. Glattli, and P. Roche, A. Cavanna, G. Faini, U. Gennser, and D. Mailly , *Finite bias visibility of the electronic Mach-Zehnder interferometer*, Phys. Rev. B **76**, 161309 (2007).

[Roulleau 08] P. Roulleau, F. Portier, P. Roche, A. Cavanna, G. Faini, U. Gennser, and D. Mailly, *Direct measurement of the coherence length of edge states in the integer quantum Hall regime*, Phys. Rev. Lett. **100**, 126802 (2008).

[Roulleau 09] P. Roulleau, F. Portier, P. Roche, A. Cavanna, G. Faini, U. Gennser, and D. Mailly, *Tuning Decoherence with a Voltage Probe*, Phys. Rev. Lett. **102**, 236802 (2009).

[Ruskov 03] R. Ruskov and A.N. Korotkov, *Entanglement of solid-state qubits by measurement*, Phys. Rev. B **67**, 241305(R) (2003).

[Ruskov 06] R. Ruskov, A.N. Korotkov, and A. Mizel, *Quantum Zeno stabilization in weak continuous measurement of two qubits*, Phys. Rev. B **73**, 085317 (2006).

[Saminadayar 97] L. Saminadayar, Y. Jin, B. Etienne, and D. C. Glattli, *Observation of the e/3 fractionally charged Laughlin quasiparticle*, Phys. Rev. Lett. **79**, 2526 (1997).

[Santori 02] C. Santori, D. Fattal, J. Vukovi, G. S. Solomon, and Y. Yamamoto, *Indistinguishable photons from a single-photon device*, Nature **419**, 594 (2002).

[Seelig 01] G. Seelig and M. Büttiker, *Charge-fluctuation-induced dephasing in a gated mesoscopic interferometer*, Phys. Rev. B **64**, 245313 (2001).

[Schottky 18] W. Schottky, *Über spontane Stromschwankungen in verschiedenen Elektrizitätsleitern*, Ann. Phys. (Leipzig) **57**, 541 (1918).

[Schriefl 05] J. Schriefl, M. Clusel, D. Carpentier, and P. Degiovanni, *Dephasing by a nonstationary classical intermittent noise*, Phys. Rev. B **72**, 035328 (2005).

[Sherkunov 09] Y. Sherkunov, J. Zhang, N. d'Ambrumenil and B. Muzykantskii, *Optimal electron entangler and single-electron source at low temperatures*, Phys. Rev. B **80**, 041313 (2009).

[Splettstoesser 09] J. Splettstoesser, M. Moskalets and M. Büttiker, *Two-particle nonlocal Aharonov-Bohm effect from two single-particle emitters*, Phys. Rev. Lett. **103**, 076804 (2009).

[Sukhorukov 07] E. V. Sukhorukov and V. V. Cheianov, *Resonant Dephasing in the Electronic Mach-Zehnder Interferometer*, Phys. Rev. Lett. **99**, 156801 (2007).

[Sutherland 70] B. Sutherland, *Quantum many-body problem in one dimension: Ground state*, J. Math. Phys. **12**, 246 (1971).

[Tannoudji 86] C. Cohen-Tannoudji and J. Dalibard, *Single-atom laser spectroscopy. Looking for dark periods in fluorescence light*, Europhys. Lett. **1**, 441 (1986).

[Trauzettel 06] B. Trauzettel, A. N. Jordan, C. W. J. Beenakker, and M. Büttiker, *Parity meter for charge qubits: An efficient quantum entangler*, Phys. Rev. B **73**, 235331 (2006).

[Turchette 95] Q. A. Turchette, C. J. Hood, W. Lange, H. Mabuchi, and H. J. Kimble, *Measurement of conditional phase shifts for quantum logic*, Phys. Rev. Lett **75**, 4710 (1995).

[Ubbelohde 12] N. Ubbelohde, C. Fricke, C. Flindt, F. Hohls, and R. J. Haug, *Measurement of finite-frequency current statistics in a single-electron transistor*, Nat. Commun. **3**, 612 (2012).

[Umbach 84] C. P. Umbach, S. Washburn, R. B. Laibowitz, and R. A. Webb, *Magnetoresistance of small, quasi-one-dimensional, normal-metal rings and lines*, Phys. Rev. B **30**, 4048 (1984).

[Van der Vaart 94] N. C. van der Vaart, M. P. de Ruyter van Steveninck, L. P. Kouwenhoven, A. T. Johnson, Y. V. Nazarov, and C. J. P. M. Harmans, *Time-resolved tunneling of single electrons between Landau levels in a quantum dot*, Phys. Rev. Lett. **73**, 320 (1994).

[Van Kampen 07] N. G. van Kampen, *Stochastic processes in physics and chemistry* Elsevier, Amsterdam (2007).

[Van Wees 88] B. J. van Wees, H. van Houten, C. W. J. Beenakker, J. G. Williamson, L. P. Kouwenhoven, D. van der Marel, and C. T. Foxon, *Quantized conductance of point contacts in a two-dimensional electron gas*, Phys. Rev. Lett. **60**, 848 (1988).

[Vyas 99] R. Vyas and S. Singh, *Antibunching and photoemission waiting times*, J. Opt. Soc. Am. B **17**, 634 (1999).

[Walls 94] D. F. Walls and G. J. Millburn, *Quantum Optics*, First edition Springer-Verlag, Berlin (1994).

[Webb 85] R. A. Webb, S. Washburn, C. P. Umbach, and R. B. Laibowitz, *Observation of h/e Aharonov-Bohm oscillations in normal-metal rings*, Phys. Rev. Lett. **54**, 2696 (1985).

[Welack 08] S. Welack, M. Esposito, U. Harbola, and S. Mukamel, *Interference effects in the counting statistics of electron transfers through a double quantum dot*, Phys. Rev. B **77**, 195315 (2008).

[Welack 09] S. Welack, S. Mukamel, and Y. Yan, *Waiting time distributions of electron transfers through quantum dot Aharonov-Bohm interferometers*, Europhys. Lett. **85**, 57008 (2009).

[Wharam 88] D. A. Wharam, T. J. Thornton, R. Newbury, M. Pepper, H. Ahmed, J. E. F. Frost, D. G. Hasko, D. C. Peacock, D. A. Ritchie and G. A. C. Jones, *One-dimensional transport and the quantization of the ballistic resistance*, J. Phys. C **21**, L209 (1988).

[Williams 08] N. S. Williams and A. N. Jordan, *Entanglement genesis under continuous parity measurement*, Phys. Rev. A **78**, 062322 (2008).

[Yamamoto 99] Y. Yamamoto and A. Imamoglu, *Mesoscopic Quantum Optics*, John Wiley and Sons, New York (1999).

[Young 10] C. E. Young and A. A. Clerk, *Inelastic backaction due to quantum point contact charge fluctuations*, Phys. Rev. Lett. **104**, 186803 (2010).

[Zakka-Bajjani 10] E. Zakka-Bajjani, J. Dufouleur, N. Coulombel, P. Roche, D.C. Glattli, and F. Portier, Phys. Rev. Lett. **104**, 206802 (2010).

[Zilberberg 08] O. Zilberberg, B. Braunecker, and D. Loss, *Controlled-NOT gate for multiparticle qubits and topological quantum computation based on parity measurements*, Phys. Rev. A **77**, 012327 (2008).

[Zoller 87] P. Zoller, M. Marte, and D. F. Walls, *Quantum jumps in atomic systems*, Phys. Rev. A **35**, 198 (1987).

List of abbreviations

AB	Aharonov-Bohm
DQD	Double quantum dot
HBT	Hanbury-Brown and Twiss
MZI	Mach-Zehnder interferometer
QIP	Quantum information processing
QND	Quantum non demolition
QPC	Quantum point contact
SES	Single-electron source
WTD	Waiting times distribution

List of publications

1. M. Albert, G. Haack, C. Flindt and M. Büttiker, *Electron waiting times in mesocopic conductors*, Phys. Rev. Lett. **108**, 186806 (2012).

2. G. Haack, M. Moskalets, J. Splettstoesser, and M. Büttiker, *Coherence of single-electron sources from Mach-Zehnder interferometry*, Phys. Rev. B **84**, 081303(R) (2011).

3. G. Haack, H. Förster, and M. Büttiker, *Parity detection and entanglement with a Mach-Zehnder interferometer*, Phys. Rev. B **82**, 155303 (2010).

4. G. Haack, F. Helmer, M. Mariantoni, F. Marquardt, and E. Solano, *Resonant quantum gates in circuit quantum electrodynamics*, Phys. Rev. B **82**, 024514 (2010).

Résumé

Cette thèse est consacrée à l'étude des propriétés de cohérence d'états à électron unique ou à plusieurs électrons dans des systèmes mesoscopiques. Bien que ces systèmes comportent généralement un grand nombre d'atomes, ils sont suffisamment petits pour permettre une propagation cohérente des électrons. La cohérence de phase des électrons a permis d'observer divers effets quantiques comme par exemple les courants persistants ou la mesure de fluctuations universelles de la conductance. Depuis le début de la physique mésoscopique, d'énormes progrès expérimentaux ont été faits, ce qui permet aujourd'hui d'étudier de manière beaucoup plus précise les propriétés quantiques de conducteurs mésoscopiques. Dans cette thèse, nous avons considéré en particulier l'interféromètre de Mach-Zehnder électronique qui a été réalisé pour la première fois en 2003 au Weizmann Institute en Israël ainsi qu'une source qui permet d'injecter des électrons uniques, un par un, tout en contreôlant le temps d'émission de ces états à une particule. Cette source a été réalisée dans le Laboratoire Pierre Aigrain à Paris en 2007 pour la première fois. Elle constitue une avancée majeure pour la physique mesoscopique car elle permet de contrôler l'information quantique contenue dans chaque électron, de manière individuelle.

Dans le premier chapitre de cette thèse, nous avons considéré l'interferomètre de Mach-Zehnder comme détecteur de parité pour deux qubits (bits quantiques) couplés aux bras de l'interféromètre. La mesure de parité est une source d'intrication, indispensable pour le traitement de l'information quantique. Nous avons tout d'abord donné les conditions sous lesquelles cet interéromètre peut être utilisé comme détecteur de parité et, en utilisant les propriétés de cohérence des électrons dans ce dispositif, nous avons montré que le Mach-Zehnder fonctionne comme détecteur idéal, dans le sens où celui-ci ne va pas déphaser les qubits plus vite que le temps nécessaire à l'acquisition de l'information concernant leur parité. Cette propriété permet d'augmenter de manière significative la probabilité de générer des états intriqués à deux qubits, par exemple les fameux états de Bell.

Dans le chapitre 2, nous avons caractérisé les propriétés de cohérence des électrons émis par la source à électrons uniques à l'aide de leur longueur de cohérence. Celle-ci est fondamentale car elle définit la distance sur laquelle une particule unique peut interférer avec elle-même à la sortie d'un interferomètre. Pour la déterminer, nous avons donc naturellement considérer une expérience d'interférométrie faisant

intervenir le Mach-Zehnder. A partir de l'expression du courant à la sortie de l'interféromètre calculée à l'aide de la matrice de diffusion du système, nous avons extrait la fonction de corrélation au premier ordre $G^{(1)}$ des électrons uniques émis par la source. La décroissance de $G^{(1)}$ en fonction de la différence de marche de l'interféromètre est caractérisée par la longueur de cohérence. Dans notre modèle où des sources additionnelles de déphasage ne sont pas prises en compte (par exemple des effets de température finie ou des interactions des électrons avec la mer de Fermi), nous avons montré que cette source émet des états à particule unique dont la longueur de cohérence est entièrement déterminée par la longueur de relaxation de la source. Cette propriété est prometteuse pour manipuler de manière cohérente des états quantiques à une particule.

Finalement, dans le chapitre 3, nous avons développé une théorie quantique de la distribution des temps d'attente entre deux électrons consécutifs dans un conducteur mésoscopique. La distribution des temps d'attente fournit des informations complémentaires sur le transport de charges par rapport au courant moyen et à ses fluctuations mesurées généralement dans les expériences de transport électronique. En effet, cet outil statistique permet d'obtenir des informations sur la statistique quantique des électrons se propageant dans le conducteur, et par là, permet de caractériser les propriétés de cohérence de l'état incident à plusieurs électrons. Nous avons illustré ce formalisme en calculant la distribution de temps d'attente pour des électrons émis par une source dc et qui sont diffusés par un point contact quantique. L'état incident est décrit par un déterminant de Slater. De manière remarquable, nous avons trouvé que cette distribution correspond à la distribution de Wigner-Dyson pour une transmission parfaite à travers le point contact quantique, alors que la distribution est poissonnienne pour un point contact quantique presque totalement fermé. Cela a permis de mettre en évidence, entre autres, le fait que les électrons ne sont pas séparés en temps de manière uniforme (il existe des fluctuations) du fait des interactions à courte distance induites par le principe de Pauli. La distribution des temps d'attente, dérivée en tenant compte des propriétés quantiques des électrons, constitue donc un outil riche et efficace pour caractériser la cohérence d'états à plusieurs particules, comme ceux émis par une source dc par exemple.